SUBSEA BOP STACK SHEAR/SEAL CAPABILITY MODELING TOOL

FINAL REPORT

SwRI® Project No. 18.21614
BSEE Contract No. E15PC00006

Prepared for:

Department of Interior
Bureau of Safety and Environmental Enforcement (BSEE)
Acquisition Operations Branch
45600 Woodland Road, Mailstop VAE-AMD
Sterling, Virginia 20166

April 20, 2017

THIS REPORT IS AUTHORIZED FOR PUBLIC RELEASE.

SwRI® **SOUTHWEST RESEARCH INSTITUTE**®

SUBSEA BOP STACK SHEAR/SEAL CAPABILITY MODELING TOOL

FINAL REPORT

SwRI® Project No. 21614
BSEE Contract No. E15PC00006
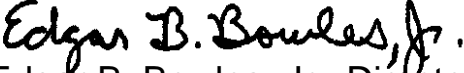
Prepared for:

Department of Interior
Bureau of Safety and Environmental Enforcement (BSEE)
Acquisition Operations Branch
45600 Woodland Road, Mailstop VAE-AMD
Sterling, Virginia 20166

Prepared by:

Steven T. Green
Nicholas Mueschke, Ph.D.
Amy McCleney, Ph.D.
Sidney Chocron, Ph.D.

THIS REPORT IS AUTHORIZED FOR PUBLIC RELEASE.

Approved:

Edgar B. Bowles, Jr.

Edgar B. Bowles, Jr., Director
Fluids and Machinery Engineering Department

ADVERTISING, CONFIDENTIALITY, AND RECORD RETENTION POLICY

All work related to this project is subject to the Southwest Research Institute® Advertising, Confidentiality, and Record Retention Policy. This policy specifically addresses the distribution of abridged versions of SwRI® reports (including excerpts) and also restricts the use of the SwRI name, logo, and test results for advertising purposes. SwRI policies specifically prohibit the use in advertising of its name, logo, and results provided by our studies. The following paragraph, extracted verbatim from SwRI contractual documents clarifies this point:

"SwRI shall not publish or make known to others the subject matter or results of the Project or any information obtained in connection therewith which is proprietary and confidential to Client without Client's written approval. No advertising or publicity containing any reference to SwRI, or any of their employees, either directly or by implication shall be made use of by Client or on Client's behalf without SwRI's written approval. In the event Client distributes any report issued by SwRI on this Project outside its own organization, such report shall be used in its entirety, unless SwRI approves a summary of abridgment for distribution."

SwRI will retain a record copy of the report for a period of ten (10) years. This permits us to answer questions that may be raised after a report has been mailed and provides a basis for additional work, if required. The contents of the report and any information that comes into our possession during the course of a study are held confidential to the company conducting the study and are not disclosed to anyone without client's prior permission.

TABLE OF CONTENTS

TABLE OF CONTENTS (cont'd)

LIST OF FIGURES

LIST OF FIGURES (cont'd)

LIST OF FIGURES (cont'd)

LIST OF TABLES

EXECUTIVE SUMMARY

Blowout preventers (BOPs) are devices that are required to be installed on all subsea wells to provide operators with a means of closing off the well in the event that fluid with a higher than expected pressure or gas content reaches the wellhead or even the platform. These so-called "kick" events pose a serious risk to the safe operation of the well. Blowouts have cost many lives, severely damaged equipment, and adversely impacted the marine environment.

BOP stacks are actually large assemblies comprised of different types of blowout prevention mechanisms. Blind shear rams are included in stacks for emergency cases requiring sealing of the wellbore via severing the drill pipe or production tubing. The reliability of the shear rams when severing drill strings or tubing and effectively sealing the wellbore under all expected operating conditions is critical for safe, dependable, and environmentally conscious operations. U.S. government regulations require independent third-party verification of BOP blind shear ram capability under all expected operating conditions. To date, however, no uniform methodology for analysis of shear ram performance has been adopted as an accepted approach to this verification requirement.

Under contract to the Bureau of Safety and Environmental Enforcement (BSEE), Southwest Research Institute (SwRI) conducted a project to develop a validated methodology for computing the forces acting on BOP blind shear rams using commercially available software packages. The overarching objective for this project was to provide a tool that will allow BSEE to reliably assess BOP ram force requirements under potential flowing conditions.

There are many interacting physical processes that occur during the operation of a shear ram to sever and seal a drill pipe. The accurate simulation of these processes requires the combination of a structural finite element analysis (FEA) of the shear rams deforming and shearing the drill pipe and a computational fluid dynamics (CFD) analysis of the changing fluid flow field to compute the pressures acting on the pipe and rams. A representative scenario of a high-pressure, high-flow well in the Gulf of Mexico was used in this project to investigate the performance of combined FEA/CFD methodologies having varying degrees of complexity.

A methodology of combining commercially available FEA and CFD software packages was successfully developed that offers high-fidelity simulations that converge to a solution within a reasonable time frame. The methodology was applied to a set of parametric cases to investigate the sensitivity of the ram closure forces and axial hydrodynamic pressure forces with respect to variations in the well pressure, flow rate, ram closure speed, fluid properties, and the drill pipe size.

Finally, all of the simulation results were collected into a database tool entitled BOP Shear Ram Simulation Database (BSRSD). The database records include the pertinent operating conditions for each scenario and the three components of the total ram actuator force corresponding to the drill pipe shear force, hydrostatic pressure force, and the hydrodynamic pressure force. The database can interpolate between the operating conditions listed in the records to estimate the shear ram forces for conditions other than those specifically catalogued in the database.

It is intended that the FEA/CFD analysis methodology and database tool developed here serve as the foundation for assessing BOP shear ram closure forces over the complete BOP designs and operational scenarios found in the offshore oil industry.

1. INTRODUCTION

The installation of a blowout preventer (BOP) stack is used as a precautionary method for preventing blowouts from subsea wells. A BOP may be actuated to close off a well in imminent danger after detection of a formation kick. Although a BOP stack may be comprised of a series of different types of blowout prevention mechanisms, blind shear rams are included in stacks for emergency cases requiring severing of the drill pipe and sealing of the wellbore. Reliability of the shear rams to seal the wellbore effectively under all expected operating conditions is critical for safe, dependable, and environmentally conscious operations.

A simplified view of a blind shear ram assembly in a BOP is shown in Figure 1-1. The closure of blind shear rams under high flow rate conditions is a highly complicated process. There are interactions among the movements of the rams, the high-velocity flow of drilling and production fluids past the rams, and the deformations and eventual fracture of the central pipe that occur during the closure of the well.
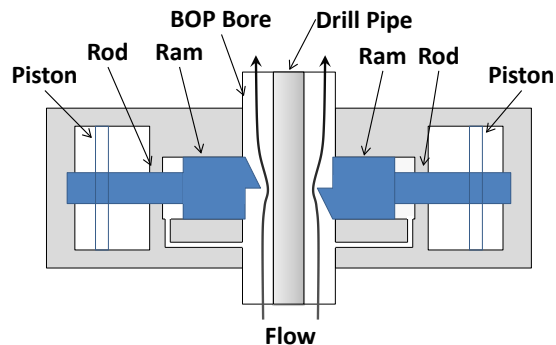
Figure 1-1. Simplified Diagram of a Blind Shear Ram
To close a wellbore, hydraulic pistons are actuated to drive the rams together. Large forces are needed to close the rams against the well pressure, shear the drill pipe, and seal the well.

There are three components of the overall force acting on the shear ram. These arise from 1) the mechanical forces required to shear the drill pipe, 2) the net hydrostatic force of the annulus fluid pressure acting on the actuator piston, and 3) hydrodynamic forces resulting from the complicated flow over the shear ram faces. Computational simulations with high-fidelity physical and material models are required to accurately assess the operation of the rams and the forces required to close the rams against the flowing fluid and to sever the drill pipe.

There is no flow-testing facility that can provide the high flow rate and high-pressure conditions that exist in most offshore oil wells. So, the careful selection and application of accurate and validated computational simulations for analyzing BOP ram closure forces is critical to the overall BOP design analysis. BOPs cannot currently be tested under full-scale conditions.

Under contract to the Bureau of Safety and Environmental Enforcement (BSEE), Southwest Research Institute (SwRI) conducted a project to develop a validated methodology for computing the forces acting on BOP blind shear rams using commercially available software packages. The overarching objectives for this project were to (1) research the optimal simulation approach that may be used to include hydrodynamic forces in the estimation of ram closure force requirements and (2) provide a tool that will allow BSEE to reliably assess BOP ram force requirements under potential flowing conditions. To that end, SwRI developed the BOP Shear

Ram Simulation Database (BSRSD). This database stores simulation analysis results, but has interpolation capabilities so that the user can estimate BOP actuator force requirements for conditions not specifically matching those catalogued in the database.

This document describes and discusses all of the work performed in the execution of this project.

1.1 Technical Approach

The stated objectives for the project were to develop a BOP shear ram FEA/CFD simulation methodology and provide a tool that allows BSEE to reliably assess the forces acting on BOP shear rams under their potentially realizable operating conditions. The technical approach adopted by SwRI for achieving these objectives is summarized as follows.

1. Define a baseline scenario for the composition, pressure, and flow rate of a well of interest. Specifically, the scenario of interest in this work is the worst-case discharge (WCD) event that may occur while a well is being actively drilled. Use the baseline case to perform a finite element analysis (FEA) simulation to analyze shear forces and deformation of the drill pipe under the loads imposed by shear rams. Use the baseline case to also perform a computational fluid dynamics (CFD) simulation for the fluid flowing through the BOP annulus as the shear rams close.
2. Explore a range of potential methods for combining the mechanical shearing simulations with fluid dynamics simulations. Develop an optimized and validated methodology to combine the mechanical displacement and deformations from FEA simulations and hydrostatic and hydrodynamic pressures measured in CFD simulations to analyze the fluid-structure interaction (FSI) during the BOP closure event.
3. Use the optimized FEA/CFD combination methodology to explore the effects of a series of parametric variations of the baseline conditions on the shear ram forces.
4. Compile the results of the baseline and parameter variation simulations into a database tool with the ability to interpolate the ram force within the ranges of the different simulated scenarios.

1.2 Document Organization

Section 2 describes the baseline operational case and the investigation into four levels of complexity for combining structural and dynamics analysis of BOP shear ram forces. The investigation showed that there is a clearly distinct recommendation for a preferred methodology for a combined FEA/CFD analysis of the shear ram forces.

Section 3 describes 13 case studies used to investigate the sensitivity of the ram forces to variations in several of the operating conditions of the baseline case.

The results of the baseline and parametric cases were compiled into the database, BSRSD, introduced above. Section 4 briefly describes this database. The BSRSD user manual and a description of the steps required to execute the combined BOP FEA/CFD analysis procedure are the subject of a separate project document, Database and Resource Documentation.

Finally, the conclusions of this project and recommendations for possible future work are presented in Section 5.

2. NUMERICAL STUDY OF BOP FLUID-STRUCTURE INTERACTION

A goal of this project was to determine an optimum simulation strategy to capture the required force to close BOP shear rams under flowing conditions. In general, shear rams use a piston arrangement, such as that depicted in Figure 2-1. The forces acting on the ram faces exposed to well conditions outside of sealed doors must be exceeded by the closing forces applied by the BOP hydraulic pump/accumulator equipment. The three forces acting on the ram piston rods include a mechanical force, a net hydrostatic force, and hydrodynamic force components. The mechanical force is the force required to mechanically deform and shear the drill pipe. The net hydrostatic force is due to the ambient pressure of the fluid within the BOP cavity. The hydrodynamic force is due to the local inertia from the fluid impinging upon and flowing around the different angled surfaces of the shear rams. The lateral hydrodynamic force component acts in the same direction as the mechanical force and net hydrostatic force. The axial hydrodynamic force acts in the fluid flow direction (transverse to the piston rod). The focus of the numerical simulation effort is the calculation of the three forces from the drill pipe and annulus fluid that act in the direction opposing the travel of the piston and the axial hydrodynamic force. The hydraulic system pressure required to overcome these forces is not considered in this investigation. This section of the report presents results from four different numerical simulation methodologies applied to a baseline set of geometry and well conditions. The baseline setup conditions are outlined in the following subsection.
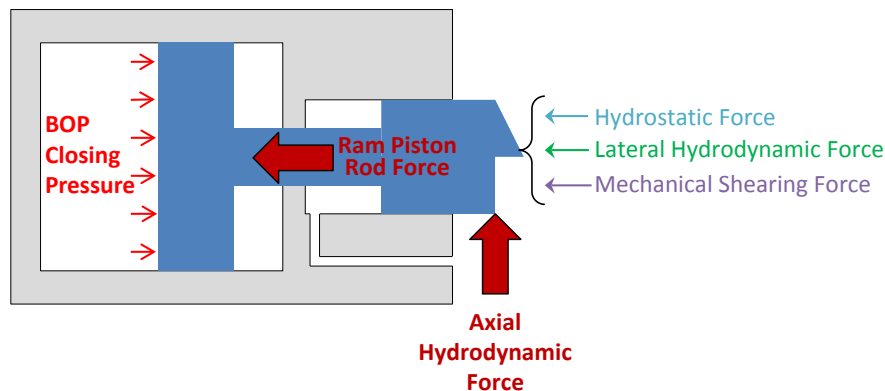
Figure 2-1. Schematic of BOP Ram Force Action
Three separate physical forces must be overcome in the closing of BOP rams, including hydrostatic, hydrodynamic, and mechanical forces from the annulus.

2.1   Baseline Case Conditions

BSEE provided SwRI with a partial list of data defining the representative well conditions to be used as baseline simulation conditions. These data included the following items: nominal BOP size, BOP blind shear ram manufacturer and model (but no geometry information), water depth, true vertical depth (TVD) and measured depth (MD), maximum surface pressure, maximum required BOP operating pressure, drill pipe dimensions (OD and pipe wall thickness), and the annular flow rate. Additional parameters required to fully define a baseline simulation case were provided by SwRI, including the details of the assumed shear ram geometry, shear ram closing time, drill pipe axial stress state, fluid properties, and

pressure/temperature conditions at the BOP stack under flowing conditions. A summary of the baseline conditions is provided in Table 2.1.

At the time the baseline investigation was conducted, no geometry information exchange agreement had been reached between BSEE, SwRI, and the original equipment manufacturers (OEMs). Thus, shear ram geometry for the baseline investigations was approximated based upon publically available images and dimensional information from OEM datasheets describing actual BOP shear ram models. Figure 2-2 shows an image of the baseline ram geometry. It is noted here that the approximated ram geometry contained a sharp edge on its front face.

Table 2.1. Baseline Conditions
The conditions provided below define the baseline scenario examined for all analysis tiers in Task 2.

PARAMETER	VALUE	NOTES
Shear Ram Geometry	18.75-inch BOP with Baseline Ram Geometry	BSEE-specified, approximate geometry reproduced by SwRI, see Figure 2-2.
Shear Ram Closing Time	45 s	Specified by API Standard 53
Wellbore Dimensions	18.75 in	Representative Rig 49580
Well Depth	30,788 ft TVD 30,790 ft MD	BSEE-specified, representative Rig 49580
Maximum Anticipated Surface Pressure	14,177 psi	BSEE-specified, representative Rig 49580
Drill Pipe Dimensions	6.625-inch, 0.813-inch wall thickness , 50 lbs/ft	BSEE-specified, representative Rig 49580
Drill Pipe Material	S-135 Grade Drill Pipe	BSEE-specified, representative Rig 49580
Drill Pipe Axial Stress State	Neutral	Assumed conservative state
Produced Fluid Properties	API 35 GOR 1,397 scf/stb	Assumed representative GOM crude oil (Petrosky and Farshad 1993, 1995; BSEE 2016)
Annular Flow Rate	100,000 stb/d	BSEE-specified
Annular Flowing Pressure and Temperature at BOP Stack	11,000 psia 300°F	Calculated based upon representative reservoir conditions, see Figure 2-3.
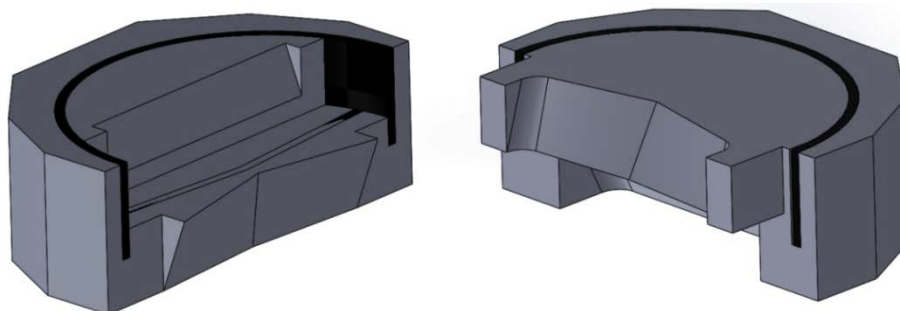
Figure 2-2. Baseline Blind Shear Ram Geometry
This image shows ram geometry used for baseline numerical simulations. This ram geometry is not an actual design, but was generated to approximate the main features of the baseline ram geometry specified by BSEE for the baseline simulation case.
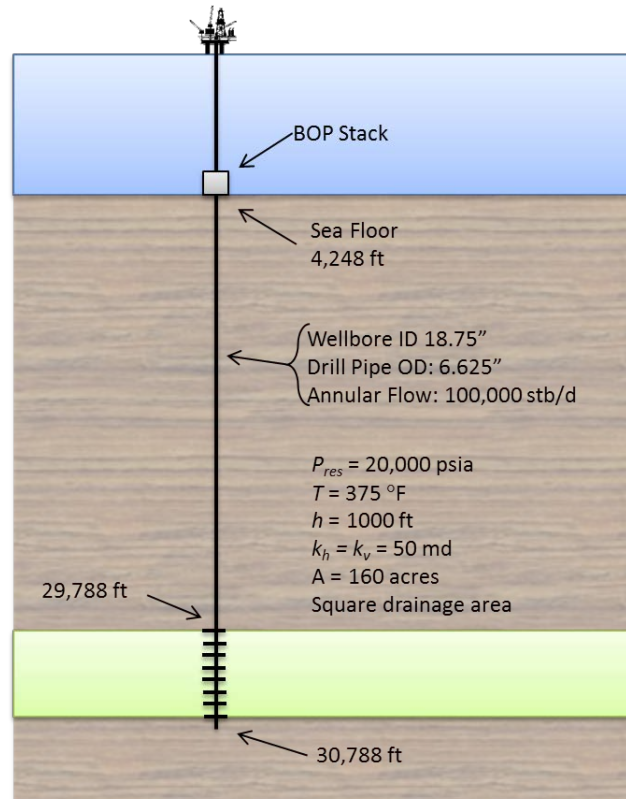
Figure 2-3. Representative Reservoir Conditions

A representative set of reservoir conditions was defined in conjunction with the specified well trajectory, wellbore diameter, drill pipe, and seafloor depth. These conditions are then used to determine the flowing pressure and temperature at the BOP stack for the different simulation models.

The flowing pressure and fluid properties at the BOP were estimated from black oil models representative of outer continental shelf (OCS) Gulf of Mexico (GOM) conditions. Specifically, the produced crude oil properties were selected based upon the average API gravity (Petrosky and Farshad 1993, 1995) and gas/oil ratio (GOR) (BSEE 2016) of OCS GOM reservoirs. Fluid properties, such as bubble point, density, and viscosity were calculated using the black oil models of Petrosky and Farshad (1993, 1995) developed specifically for GOM crude oils. The density and viscosity of the representative crude oil are shown in Figure 2-4 for a range of temperatures.

The operating pressure and temperature at the BOP stack were determined by performing a steady-state nodal analysis calculation based upon an assumed set of reservoir and lower completion conditions (Beggs 1991; Brill and Mukherjee 1999). The assumed reservoir state is shown in Figure 2-3. For the assumed crude oil, well and equipment dimensions, and reservoir conditions, the pressure and temperature loss between the production zone near the bottom of the well and the BOP stack may be calculated. The flowing pressures and temperatures in the wellbore from these calculations are shown in Figure 2-5. For these conditions, the resulting pressure and temperature at the BOP stack are approximately 11,000 psia and 250-350°F, depending on the thermal losses to the ambient environment. For the sake of defining baseline conditions, the middle value of 300°F was selected. At the flowing conditions of 11,000 psia and 300°F, the crude oil is expected to be single phase (above the bubble point) with a density of 38.88 lb/ft^3 [622.8 kg/m^3] and a viscosity of 0.344 cP.
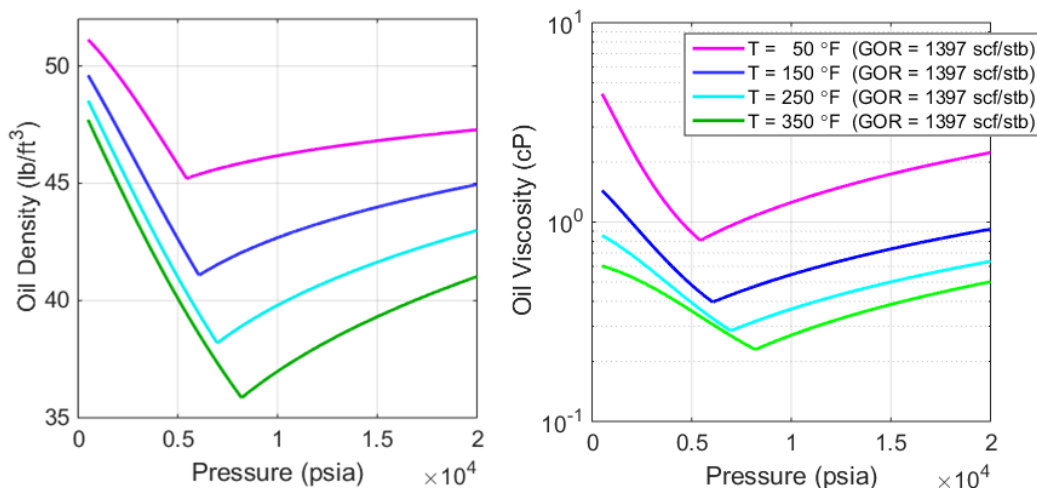
Figure 2-4. Fluid Density and Viscosity for Baseline Crude Oil

The fluid properties for the baseline scenario are based upon a representative Gulf of Mexico crude oil (API 35, 1,397 scf/sbbl GOR). The fluid properties, such as density and viscosity required by the different simulations, will be calculated by analytical black oil model forms as a function of pressure and temperature using the API gravity and GOR as inputs.
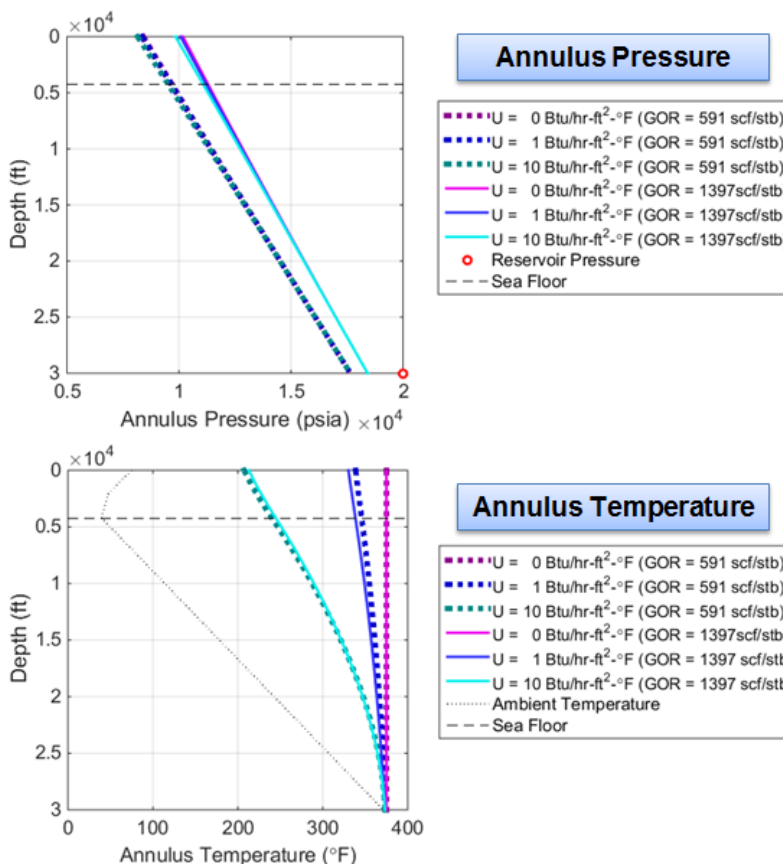
Figure 2-5. Calculated Pressure and Temperature Loss in the Wellbore

For the given flow rate of 100,000 stb/d, a steady-state nodal analysis was performed to estimate the flowing pressure, temperature, and fluid properties at the BOP stack (depth of 4,248 ft). This analysis uses the assumed reservoir conditions, rock properties, well trajectory, and analytical fluid property models to calculate pressure and temperature losses due to flow up the wellbore annulus.

2.2   FEA Model Development

Tier 1 analyses focus on the FEA modeling of drill pipe shearing without including any hydrodynamic effects. These simulations provide a baseline for Tier 2-4 analyses, which include the downhole hydrodynamic effects. These simulations were performed using the LS-DYNA® FEA code developed by Livermore Science Technology Corporation.   LS-DYNA is a Lagrangian structural FEA code capable of performing explicit, transient FEA analyses of materials undergoing large deformations, damage, and failure. An overview of the model development is provided here.

Tier 1 simulations do not include any effects of the surrounding fluid within the drill string or annulus and, thus, the computational domain was simplified to the two shear rams and a 15-ft section of drill pipe. The simulations were started with the shear rams almost in contact with the centrally located drill pipe, corresponding to 29.8% area open to flow. An image of the full FEA domain and computational mesh is shown in Figure 2-6.
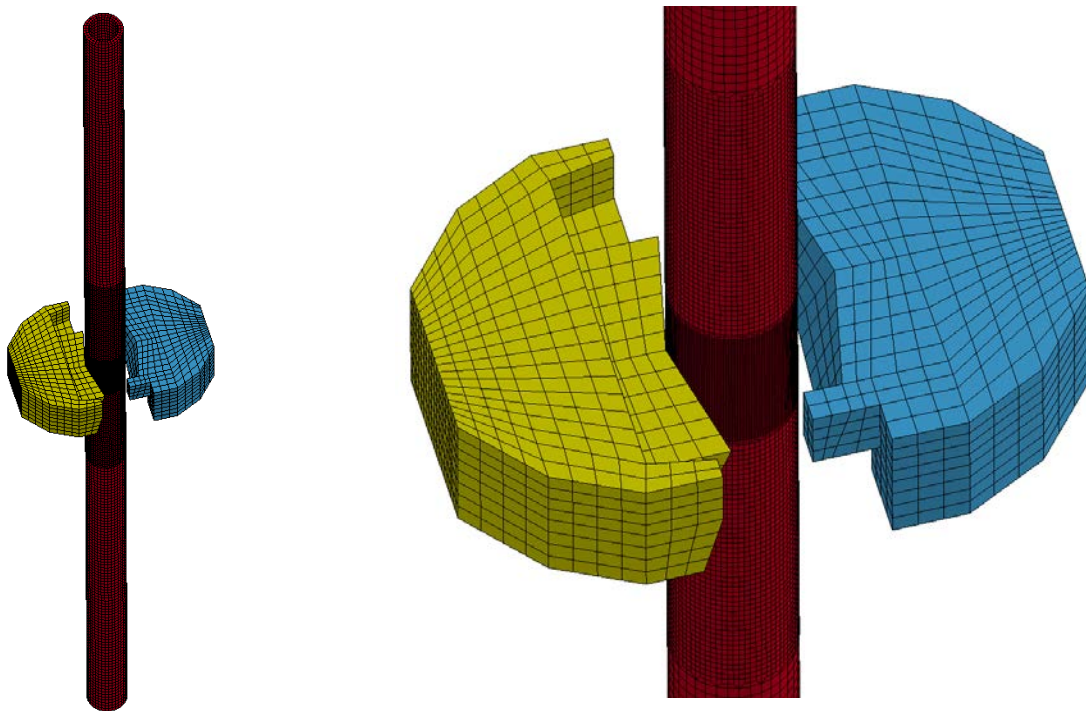
Figure 2-6. Images of the Tier 1 FEA Simulation Domain
The Tier 1 FEA simulation domain does not include casing or fluid effects. A refined grid resolution of the drill pipe can be seen around the region where the shear rams interact with the pipe.

In order to verify the proper operation of the FEA model, a series of solution-sensitivity tests were performed to determine which numerical parameters had the greatest effect on the results. An overview of the parameters varied and the final parameter selections are listed in Table 2.2. For each parameter listed, simulations were performed with different settings to ensure that the FEA model was functioning properly and that additional model refinement was not required.

Table 2.2. FEA Simulation Parameters

A set of FEA modeling options was examined to confirm the proper operation of the simulations. The final parameters and modeling options selected are listed here.

PARAMETER	PRODUCTION RUN MODEL PARAMETER
Drill pipe material model	Full Johnson-Cook strength and damage model
Drill pipe far-field boundary conditions	Drill pipe boundaries were constrained and not allowed to translate in the y (transverse) and z (wellbore) axis directions, but allowed to translate in x direction (axis of shear ram travel). Also, drill pipe boundaries were constrained and not allowed to rotate in any direction.
Length of the drill pipe included in the model	Total of 15 ft of drill pipe included (7.5 ft on either side of the shear rams)
Computation mesh resolution of the drill pipe	8 grid cells across the pipe wall thickness: Nominally 0.1-inch × 0.14-inch × 0.12-inch grid cells
Computation mesh resolution of the shear rams	Nominally 1-inch × 1-inch × 1-inch grid cells
Metal-on-metal contact detection algorithms	Two algorithms used (in combination): Algorithm #1: Eroding surface-to-surface Algorithm #2: Nodes-to-surface
Computational element integration method	Single-point integration elements
Metal-on-metal friction	Static friction factor based on normal force at contact points: $\mu_f = 0.5$
Ram travel speed	Examined range of ram velocities: 0.4667 in/s (1×) to 7.467 in/s (16×)

2.3 Drill Pipe Material Model

The choice of material strength and failure models used to characterize the drill pipe was found to be a particularly crucial aspect of the simulation, and changes to these models could result in significant variations in shear force computed in the simulations. The material models, also called the constitutive models, are an essential part of the computer simulations because they provide the stress in the materials as a function of the deformation. Depending on the material and the application, the constitutive model might be as simple as a linear elastic material or a sophisticated model describing the elastic, plasticity, and failure behaviors.

Ideally, the parameters for the constitutive model should come from laboratory mechanical testing of specimens. A simple model, e.g., elastic or elastic-plastic, can use information solely from a tensile test of a dog-bone specimen. More comprehensive and accurate models require testing the specimens in tension, compression, torsion (shear), high and low temperatures, high and low strain rates, etc. If the constants are properly determined, then the computer model should be able to predict the behavior of the material under complex states of stress or pressures, and a range of temperature and strain rates.

When laboratory tests are not available, the constants for the model can come from other sources: 1) the literature, if available, 2) "tuning" the material constants to a reference experiment, usually similar to the problem of interest, 3) engineering judgment, or 4) a "smart" combination of any or all of the above. All of these methods have risks and should be used with care because the validity of the material constants will be much more restricted. For example, if

a material is a "well-behaved" von Mises material, a tensile test may provide enough data to predict plasticity and failure in shear. But many materials, including some steels, are not well-behaved and, hence, the material needs to be tested in both conditions to accurately represent both stress states.

Summarizing, the prediction of the computer models is only as accurate as the material models used in the computation. For this reason, it is important to trace back how the material model was generated. The two primary sources of information used to construct an S-135 material model are reported here. Data are used from the BSEE report on BOP Stack Sequencing and Shear Ram Design (MCS Kenny 2013) and the paper by Miscow et al. (2004).

The MCS Kenny (2013) report quotes the true stress–true strain curve for a drill pipe material from a "quality documentation package;" however, that document is inaccessible. The curve is shown in the report and was digitally scanned (see Figure 2-7) so it could be used to determine the appropriate material constants. Unfortunately, since the report with the original data were not available, it is not possible to know exactly how the true strain was measured. From the MCS Kenny report (2013), it appears that the true strain is probably a longitudinal strain that was "corrected" for the change in cross-sectional area, due to plastic deformation, with the equation:

$$\varepsilon_{true} = \ln(1 + \varepsilon_{eng}),$$
[1]

where ε_{eng} is the engineering strain (increase in length divided by initial length) and ε_{true} is the true strain. Note that this correction is only valid until necking appears in the specimen. Figure 2-7 does not show any maximum and the ensuing slope downwards, which usually appears when the neck starts forming. So, it is speculated that the curve may not be complete.

The other way to measure the true strain in the specimen is by tracking the diameter of the specimen using either a diametral extensometer or digital image correlation. When the specimen necks, if the diametral extensometer is properly placed, it provides the instantaneous cross section, which allows computing both the true stress and the true strain. MCS Kenny reports a longitudinal strain (maximum elongation) to failure of 19.5%, see Table 6.3 in MCS Kenny (2013), which is very similar to the maximum true strain seen in Figure 2-7. Usually true strains in the necking region are much larger than the longitudinal strain, so it is thought that the true strain reported in Figure 2-7 does not come from a direct measurement of the diameter of the neck in the specimen.
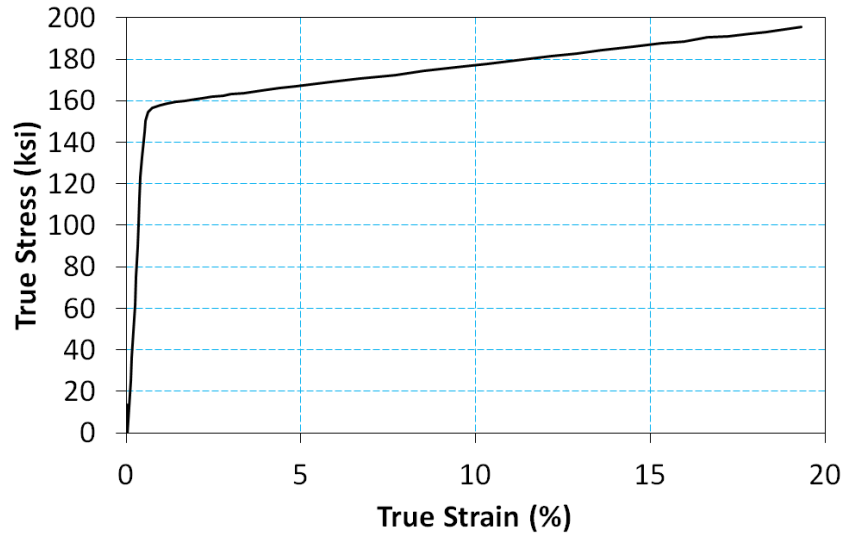
Figure 2-7. True Stress–True Strain Curve for S-135 Pipe Material from MCS Kenny (2013)
This figure shows the true stress–true strain curve for the drill pipe as it appears in the BSEE report on BOP Stack Sequencing and Shear Ram Design (MCS Kenny 2013). This information is used to aid the development of the material model used in this work, but is not directly incorporated verbatim.

Miscow et al. (2004) reported data measured from API S-135 steel pipe samples, see Table 2.3 in Miscow et al. (2004). The strength measured (149.1 ksi, 1,028 MPa) is very similar to the one reported by MCS Kenny (2013). The small difference may simply be coincidence as the accepted range for S-135 pipe ranges from 135-165 ksi (930.8-1,137.6 MPa). On the other side, the failure strain measured by Miscow et al. (2004) is quite different. Miscow et al. (2004) also reported the reduction of area of the tensile specimen, which allows for a true strain to be computed:

$$r = \frac{A - A_0}{A_0},$$ [2]

where r is the reduction in area, A the final cross section, and A_0 is the initial cross section. The true strain can also be computed as:

$$\varepsilon_{true} = \ln\left(\frac{A_0}{A}\right)$$ [3]

So, it is straightforward to calculate the true strain given the reduction of area.

The failure model reported by MCS Kenny (2013) is not well documented as it is claimed that a peer-reviewed journal article by Dzugan et al. (2012) was used for ductile damage initiation, but no data were found for shear damage initiation. Note that the steel reported by Dzugan et al. (2012) has very different properties and seems to yield around 43.5 ksi (300 MPa). MCS Kenny (2013) also reported using aluminum data from a different journal article (Hooputra 2004) because of the lack of data in shear.

Table 2.3. Comparison of Open Literature S-135 Data

Measured properties of S-135 pipe from different sources have been used to construct a material model for S-135 pipe.

PARAMETER	MCS KENNEY (2013)	MISCOW et al. (2004)
Yield Stress (ksi)	155.3	149.1
Ultimate Tensile Stress (ksi)	164.6	157.8
Longitudinal Failure Strain (%)	19.5	21.0
Reduction of Area (%)	*Unreported*	33

The material model proposed by SwRI for this project is the strength and failure model developed by Johnson and Cook (1985). The strength part of the model accounts for the following effects: 1) material hardening because of deformation, 2) high strain-rate hardening, and 3) high-temperature softening. These effects are decoupled and affect the strength in a multiplicative way:

$$Y = \left[A + B\varepsilon_p^n\right]\left[1 + C\,ln\dot{\varepsilon}^*\right]\left[1 - (T^*)^m\right] \tag{4}$$

where Y is the strength, ε_p is the equivalent plastic strain, ε is the total strain, $\dot{\varepsilon}^* = \dot{\varepsilon}^*/\dot{\varepsilon}_0^*$ is the dimensionless strain rate (usually $\dot{\varepsilon}_0^* = 1$ s^{-1}), and $T^* = (T - T_{ref}) / (T_{melt} - T_{ref})$ is the homologous temperature, T is the current temperature on the material, T_{ref} is a reference temperature and T_{melt} is the melting temperature for the material. The five material constants to be determined, usually with mechanical tests, are *A, B, n, C,* and *m.*

The failure part of the model also accounts for temperature and strain rate effects, but, additionally, accounts for pressure effects on the failure strain; i.e., it is well known that under high pressures, the strain to failure of a material increases:

$$\varepsilon_p^f = \left[D_1 + D_2\,e^{D_3\sigma^*}\right]\left[1 + D_4\,ln\dot{\varepsilon}^*\right]\left[1 + D_5 T^*\right] \tag{5}$$

where ε_f is the failure strain, D_1 through D_5 are material constants to be evaluated with the mechanical tests, $\sigma^* = \sigma_m/\bar{\sigma}$ is the triaxiality (σ_m mean stress and $\bar{\sigma}$ equivalent stress), $\dot{\varepsilon}^*$ is the dimensionless strain rate, and T* is the homologous temperature, the last two are as defined above.

There is no "perfect material model," but it is thought that the Johnson-Cook model strikes the right balance between complexity, accuracy, and testing volume. Ideally, the ten constants of the model are obtained directly from approximately 50 to 80 laboratory tests, including tensile, compression, shear, etc. tests at low and high temperatures and rates. The Johnson-Cook model does not take into account, for example, the third invariant effect; i.e., that some materials yield or fail at different stresses in compression and in tension. Similarly, the model cannot account for coupling effects between strain rate and temperature, very high-rate effects, etc. The literature is very extensive in modifications to the model to "improve" it, but the modified models rarely make it to the mainstream simulation codes.

Due to the lack of material tests that could provide the ten constants required for the material model, a clever combination of literature data, calibration through one of the tests reported by MCS Kenny (2013), and engineering judgment were used to obtain the Johnson-Cook constants.

The yield stress from both the report by MCS Kenny (2013) and Miscow et al. (2004) were very similar; therefore, it was assumed that the true stress–true strain curve provided in the report was realistic and a Johnson-Cook curve fit was performed through the data, as shown in Figure 2-8. The fit (blue continuous curve) properly goes through MCS Kenny data (black squares). Additionally, the adiabatic curve (red dashed) is provided as a reference. The adiabatic curve describes how the material behaves when it is deformed quickly and the heat generated by plastic deformation does not have the time to dissipate. The temperature of the material increases during plastic deformation and, consequently, its strength decreases as seen in Figure 2-8.
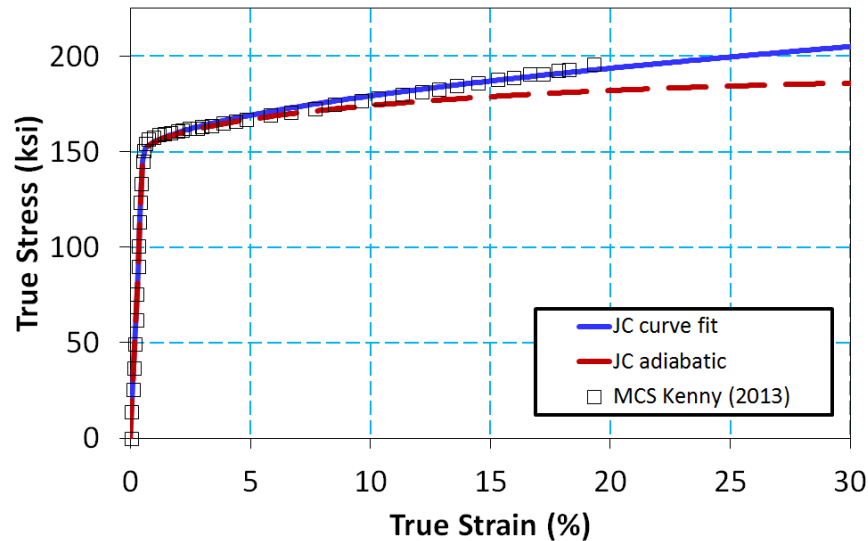
Figure 2-8. True Stress–True Strain Curve for S-135 Material Model
This figure shows the Johnson-Cook curve fit through the data (MCS Kenny 2013).

The curve fit described above allowed for the constants A, B, and n to be determined. These values are provided in Table 2.4. Lacking laboratory tests, the adiabatic curve was obtained assuming a typical value of the temperature constant $m = 1.0$, similar to the one used, for example, by Beissel et al. (2011) on 4340 steel. Note that the forensic simulation analysis of the Deepwater Horizon BOP (Det Norske Veritas 2011) also used properties from 4340 steel to populate parameters needed for a Johnson-Cook material model for S-135 pipe.

Table 2.4. Johnson-Cook Strength and Damage Model Parameters
Material model parameters used to fully define the Johnson-Cook strength and damage material model for S-135 grade drill pipe.

PARAMETER	CONSTANT(S)	VALUES
Flow Stress	A	149.4 ksi
Strain Hardening	B, n	108.8 ksi, 0.55
Strain Rate (plastic flow)	C	0.0
Thermal (plastic flow)	m, T_{melt}, T_{ref}	1.0, 1,520°C, 25°C
Pressure	D_1, D_2, D_3	0.0 , 0.5, -0.5
Strain Rate (failure)	D_4	0.0
Thermal (failure)	D_5	0.0
Reference Strain Rate $\dot{\varepsilon}^* = \dot{\varepsilon}/\dot{\varepsilon}_0$	$\dot{\varepsilon}_0$	0.001 1/s

The elastic-plastic properties of some steel alloys are strain-rate dependent, i.e., the strain-rate constant C might be positive, with typical values of 0.014, see Beissel et al. (2011). This value was used in simulations aimed at reproducing the benchmark shear test described in the report by MCS Kenny (2013), section 6.2. In this test, the shear ram was used to shear an S-135 drill pipe with an outer diameter of 3.5 inches (8.89 cm) in a non-flow condition with the objective of obtaining the force needed to push the ram. The pipe wall thickness was 0.368 inches (0.935 cm). The two tests performed provided a maximum force needed for the shear of 280,000 and 313,600 lbs. The final shape of the pipe's upper fish was similar to an ellipse with the major axis size being 4.5 inches (11.43 cm) and the minor axis 2.06 inches (5.24 cm). Both the force needed in the shears and the final shape of the pipe are key experimental results to properly calibrate the unknown material constants. For the strength model, only the strain-rate constant is considered unknown, because the other four constants are taken from reliable sources in the literature.

Simulations of the benchmark validation shear tests reported in MCS Kenny (2013) were performed by SwRI, see for example Figure 2-9. These simulations can be considered, in part, as calibration simulations because they were used to determine the strain-rate constant from the strength model. But they can also be considered validation simulations because, as the discussion on the failure model shows below, the simulations are able to reproduce the complex failure and deformation seen in the tests without having directly calibrated the failure constants.

(a) (b)
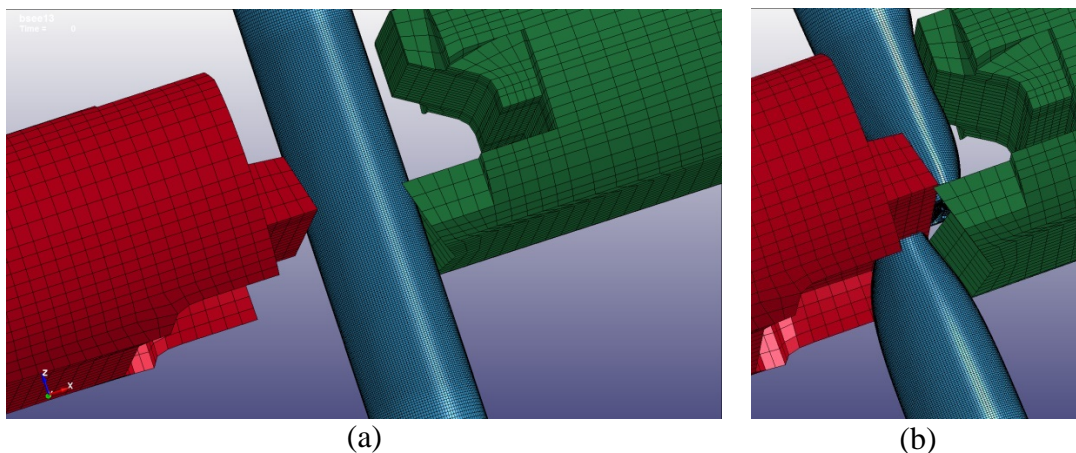
Figure 2-9. Simulation of Shearing Experiments Reported in MCS Kenny (2013)
These figures show a simulation of the benchmark shear test showing (a) the initial configuration before contact with the drill pipe and (b) the post-shear failure of the pipe.

The initial configuration of the shear rams and the pipe is shown in Figure 2-9a, and the pipes after being sheared can be seen in Figure 2-9b. The force history from the simulations is shown in Figure 2-10. This force history was obtained using the constants from Table 2.4, i.e., with a strain-rate constant value of zero. A value of *C=0.014* was used in preliminary simulations, but the maximum force was being overpredicted. Given that the constants *A*, *B*, *n*, and *m*, are well determined from the literature, it was assumed that the only "unknown" constant was *C*, and the best match with the benchmark test was obtained assuming a value of zero. The *C* constant is usually determined using Hopkinson Bar compression tests to evaluate the strength of the material at high rates. Note that, as it will be explained in the failure model section, the

failure constants were determined from data in the literature, i.e., they were not calibrated to match the data from the test.
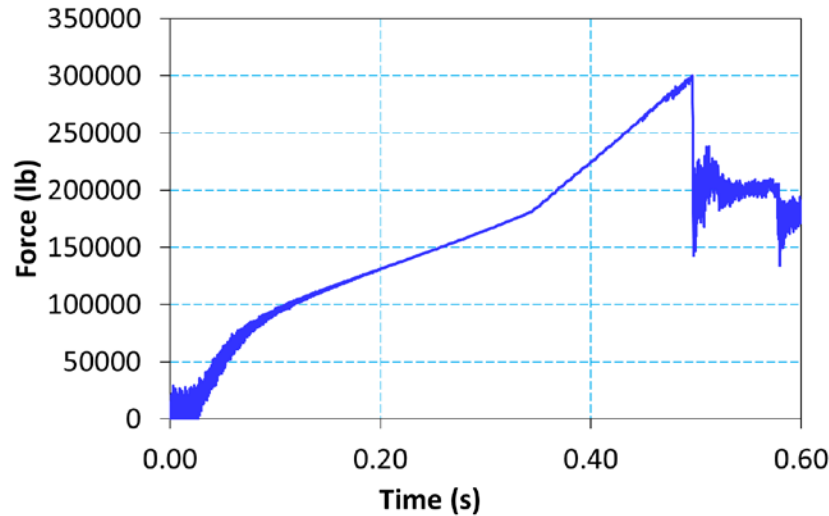
Figure 2-10. Representative Force on Rams during the Shearing Process
The force history obtained during the simulations of the validation shearing experiments reported by MCS Kenny (2013) is shown.

Figure 2-11 shows a graphical form representing Eq. 5. The *y*-axis is the equivalent plastic strain to failure and the *x*-axis is the triaxiality, as previously defined. Larger triaxiality means larger hydrostatic pressure in tension on the material (more "tension") which, see for example the Bridgman (1952) experiments, implies a decrease in the failure strain. There are three sets of data in Figure 2-11.
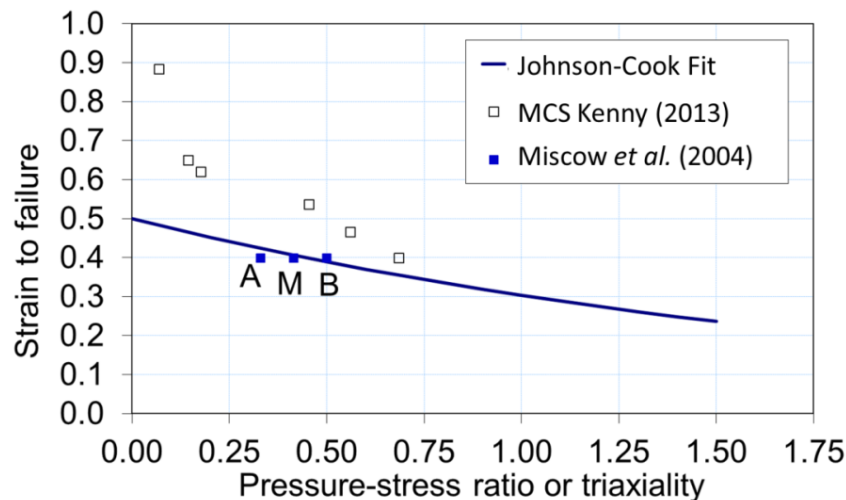
Figure 2-11. Strain-to-Failure for S-135 Drill Pipe Material Model
The failure model implemented by SwRI (blue curve) is compared to the data from Miscow et al. (2004) (blue full squares) and data from MCS Kenny (2013) (black hollow squares).

The first set is the data scanned from Figure 6.28 of MCS Kenny (2013). As the data seem to be coming from a source (Dzugan 2012) that used a material softer than S-135, these data were ignored. The second set of data on Figure 2-11 is the equivalent strain to failure calculated from the reduction in area published by Miscow et al. (2004). The reduction in area

reported is 33%. It is straightforward to calculate the plastic strain to failure as 40% from Eq. 2 and Eq. 3. For a tensile test, the triaxiality is 1/3 at the beginning; so, the point A = 0.4 is represented in the plot. During the tensile test, the triaxiality increases because of the specimen necking. LS-DYNA computations were performed on the tensile specimen used by Miscow et al. (2004) to measure the triaxiality change during the test up to the time of failure. The result from the computation was that, at failure, the triaxiality in the center of the specimen was close to 0.5 at the end of the test, which is point B = 0.4 in the plot. The point M is just the middle point between A and B, i.e., an average triaxiality during the tensile test.

The third set of data in Figure 2-11 is the blue curve, a representation of Eq. 5, where the following considerations were made to evaluate the material constants: 1) D_1 can be set to zero without loss of generality, 2) D_2 was calibrated to match the data from Miscow et al. (2004), i.e., approximately going through point M, 3) D_3 was set to the same value as that of steel 4340 (Beissel et al. 2011; Det Norske Veritas 2011) because of the lack of material test data, and 4) D_4 and D_5, strain-rate and temperature effects, were set to zero because of the lack of material test data. A summary of all of the failure constants for the material is show in Table 2.4.

Figure 2-12 compares the upper fish of the steel S-135 pipe geometry for the computation with the one obtained in the test after shearing the pipe. The computation result for the major axis of the "ellipse" is 4.44 inches, which compares very well with the 4.5 inches from the tests. The minor axis predicted by the computation is 1.76 inches, slightly smaller than the 2.06 inches measured in the test. These computational results are considered very satisfactory given that there is not a consistent set of constants available in the literature.
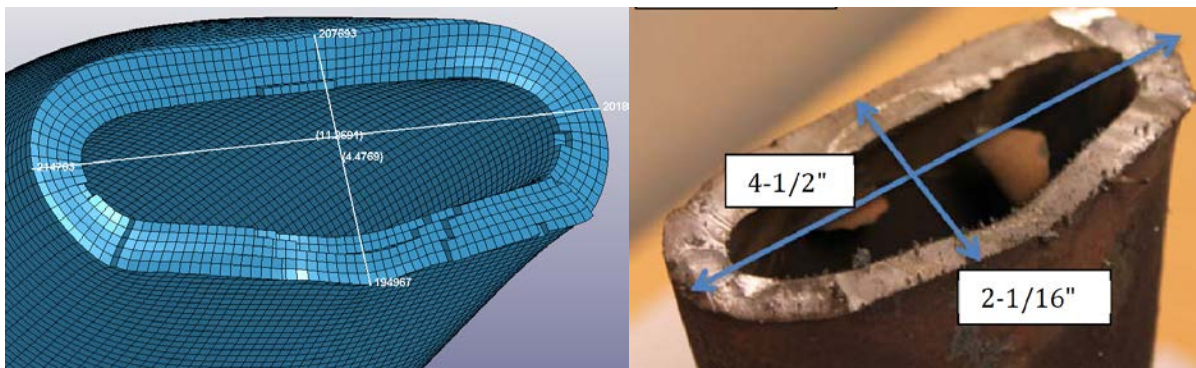
Figure 2-12. Upper S-135 Drill Pipe Dimensions Following a Shear Event
The dimensions of the pipe after being sheared from the FEA simulation (left) and experiment (right, MCS Kenny 2013).

In summary, a Johnson-Cook strength and failure material model was developed using data from MCS Kenny (2013), Miscow et al. (2004), and Beissel et al. (2011) due to the lack of a consistent set of material laboratory data. MCS Kenny (2013) provided the stress-strain curve that allowed fitting of the yield and hardening constants (*A*, *B*, *n*). The temperature constant *m* used was that typical for steel. The strain-rate constant was determined to be zero, based on the force measured in the shear test performed by MCS Kenny (2013). The failure constant D_1 can be zero without losing generality, while D_4 and D_5 were left as zero because of lack of temperature and high-rate effects of failure of this material. As a side note, D_4 and D_5 have only a second-order effect on the material behavior and are considered non-essential in this analysis.

The constants D_2 and D_3, were determined using the data from Miscow et al.(2004) and the "shape" of the 4340 steel curve.

The constants are presented in Table 2.4, where the reference strain rate is 0.001 s^{-1}. The reason this is provided is because some FEA software packages (including LS-DYNA) use the reference strain rate as a cutoff for strain-rate effects. Nevertheless, since the strain-rate constant was finally chosen as zero, a different reference strain rate should not make any difference.

It is noted that the material model presented in this work is intended to be representative of a single S-135 pipe; however, API 5D (2001) specifications allow for a broad range of material properties variations. Specifically, the API standard calls for S-135 pipe to have a yield strength in the range of 135-165 ksi and a minimum ultimate tensile strength of 145 ksi. Such a specification allows for a significant range of material strength and ductility parameters, and accordingly, a broad range of potential mechanical force requirements. A simulated tensile test of the S-135 material used in this study is presented here to allow for more effective comparison between the work presented here and other studies of experimental shear test data. A 2-inch long, 0.5-inch diameter specimen was pulled in tension and the specimen strain was recorded. An image from the numerical tensile test simulation is shown in Figure 2-13. The engineering stress versus engineering strain curve is shown in Figure 2-14. For the S-135 model used in this study, the yield strength (at 0.2% strain) is 149.4 ksi and the ultimate tensile strength is 162.7 ksi.
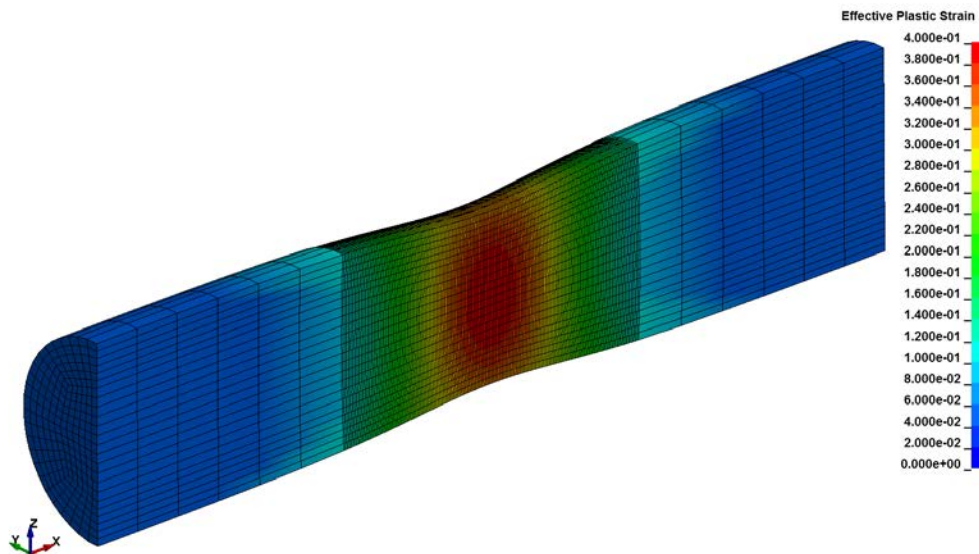
Figure 2-13. Numerical Tensile Test Simulation
The material model requires input parameters that are not standard material properties measured by drill pipe manufacturers. Thus, tensile test simulations were performed to measure equivalent parameters.
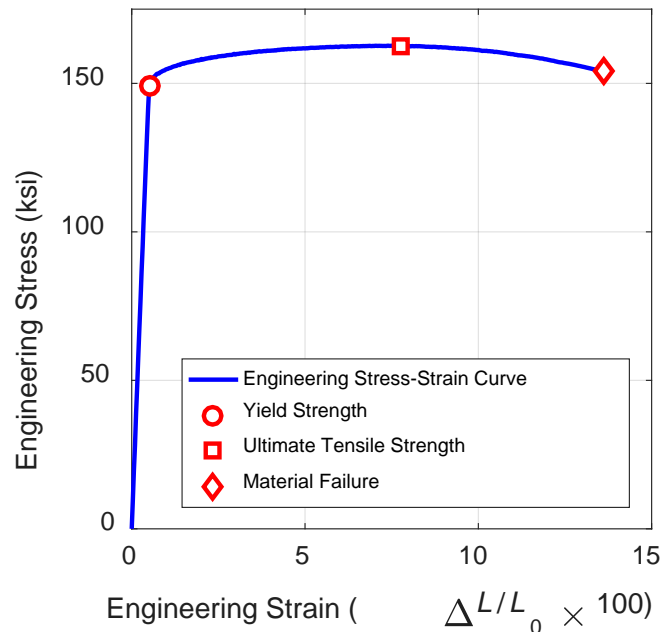
Figure 2-14. Engineering Stress-Strain Curve for S-135 Model
The yield strength (at 0.2% strain) is a supplied input to the material model, but ultimate tensile strength and strain-to-failure are not. The simulated tensile strength provides a measure of the ultimate tensile strength and failure point for comparison with other experimental measurements.

In order to validate the FEA model and material model formulation, simulations were performed to match the lab-scale experiments performed by MCS Kenny (2013). These experiments sheared a 3.5-inch S-135 grade drill pipe (0.368-inch wall thickness, 13.3 lb/ft) in a 13.625-inch Cameron blind shear ram BOP. Images from the final validation simulation are shown in Figure 2-15. Experimental measurements of the force required to shear the pipe were obtained by MCS Kenny (2013). Two repeat experiments were performed. Measured shearing forces of 280,000 and 313,600 lbs were recorded. Figure 2-16 shows the time history of the shearing force applied to the shear rams for the current FEA and material model combinations. The final shearing for this simulation was 295,200 lbs, which falls between the two experimental measurement points.
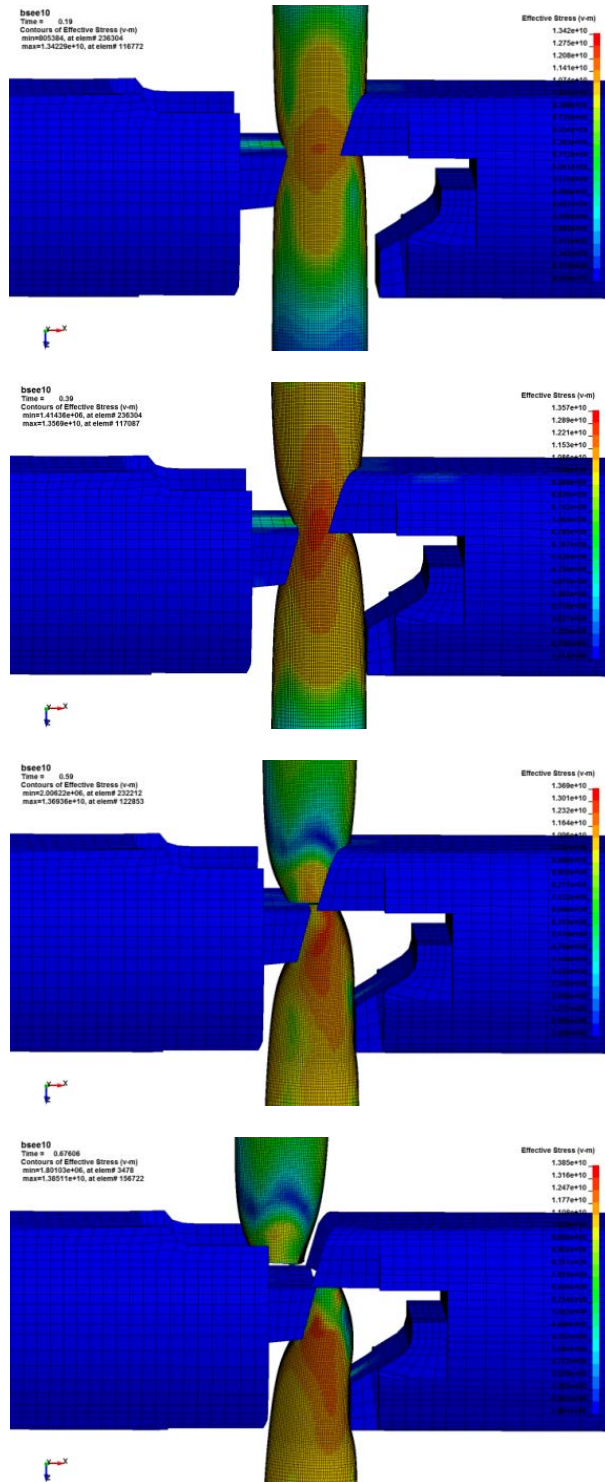
Figure 2-15. Images of the FEA Validation Simulation

The shearing of a 3.5-inch 13.3 lbs/ft S-135 grade drill pipe is shown. The color scale indicates local Von Mises stress on the surface of the drill pipe.
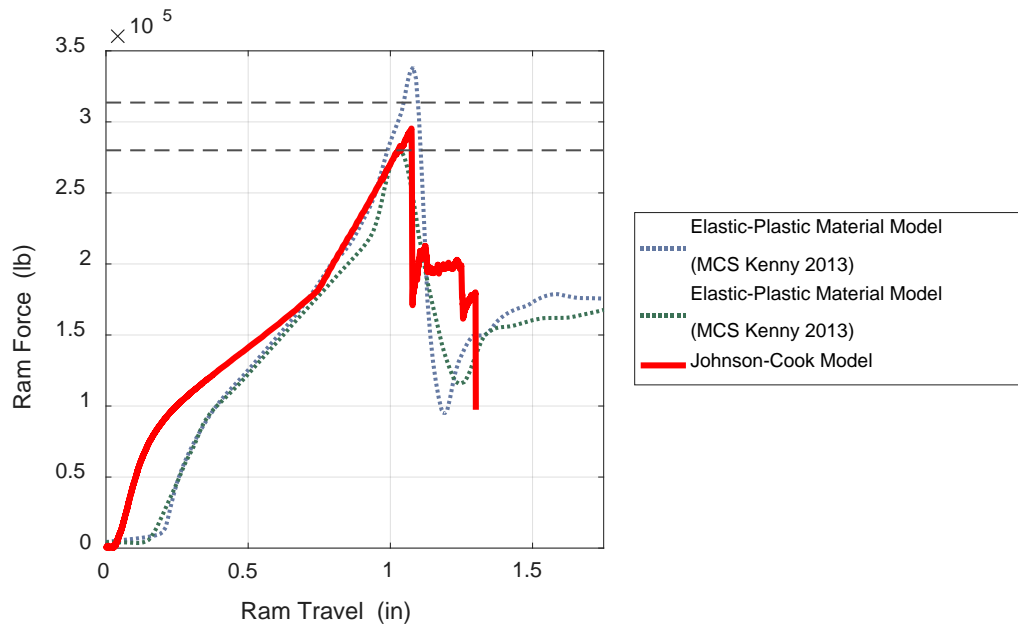
Figure 2-16. FEA Model Validation Test Results

The red curve indicates FEA and the material model developed in this work. The distance on the x-axis is measured from the initial contact of the shear rams with the drill pipe. Previous FEA simulations presented by MCS Kenny (2013), using a simplified elastic-plastic material model, are also shown in dotted lines. Horizontal dashed lines indicate measured shearing forces from two repeated shear test experiments.

2.4   Fluid Structure Analysis Methods

The baseline case was investigated with four tiers of complexity in the fluid-structure coupling to evaluate sensitivity of results to the FEA/CFD coupling methodology.   Each successive tier adds an additional layer of physics to the fluid-structure interaction (FSI) calculation. However, as the physical fidelity of the model increases, so does the computational complexity and cost (i.e., simulation run time and stability).   The four tiers are described as follows.

Tier 1: This first tier will serve as a benchmark analysis method, where FEA of the shear rams and tubing geometry will be considered with no hydrodynamic forces included. Simulations from Tiers 2-4 will be compared with Tier 1 to determine the effects and significance of the hydrodynamic forces on the shear ram operation. It should be noted that this approach should yield results closest to predictions from simple shear force equations.

Tier 2: The second tier simulation will use the deformed geometry from the Tier 1 simulation. In this analysis, CFD simulations will be run at different points of shear ram travel. At each predefined point of shear ram travel, the deformed tubing geometry will be discretized and gridded in preparation for CFD analysis. CFD simulations will then be used to determine the hydrodynamic forces on the tubing and shear rams. These forces will then be linearly added to the shear ram forcing values calculated in the Tier 1 analysis.

Tier 3: The third tier analysis is similar to the second tier, except that nonlinear interactions between the hydrodynamic forces and the tubing deformation will be considered. For this analysis methodology, CFD simulations will be performed to determine the hydrodynamic loads on the shear rams and tubing. Then, those loads will be discretized and applied to the FEA model for a set portion of the shear ram travel. Note that hydrodynamic loads will be held constant during FEA simulations where shear rams are translating and deforming tubing. At the end of the FEA simulation, the deformed geometry will be passed back to the CFD simulations so that the hydrodynamic loads on the tubing and shear rams may be updated.

Tier 4: The final analysis methodology will dynamically couple the FSI interactions by fully simulating the shear ram travel, material deformation, fluid flow, and fluid-structure interaction within a single simulation code.

Thus, the objective of this investigation was to compare the performance of all four of the proposed simulation tiers for the baseline BOP/shear ram configuration. The metrics of the comparison included the predicted shear ram force requirement, modeling complexity, overall computational efficiency, and solution stability for all the simulation tiers. The following sections describe the result obtained with each FEA/CFD analysis tier.

2.5 Tier 1 Analysis, FEA Modeling

Given the validated FEA and material model described in Section 2.3, a series of simulations were performed for the baseline geometry. These simulations examined the baseline shear ram geometry (18.75-inch BOP with approximated ram geometry models) and 6.625-inch diameter S-135 grade drill pipe with a 0.813-inch wall thickness (nominally 50 lbs/ft). Images from these simulations are shown in Figure 2-17 through Figure 2-19. These simulations show the initial tearing of the pipe at the ram edge followed by a more pronounced failure of the pipe. As the shear rams close, the crimping of the drill pipe ends can also be seen. This analysis does not account for any potential elastic recoil of the drill pipe after a shear event and, thus, the severed ends of the pipe remain in place as the rams move to a fully closed state.

To ensure that the numerical model is fully converged and the measured force does not depend upon the number of computational grid cells, a series of simulations were performed using different grid resolutions. These simulations used grids with two, four, and eight cells across the drill pipe thickness in the region of the shear rams. Also, due to the additional computational overhead imposed by the full Johnson-Cook material strength and damage model and the metal-on-metal contact algorithm, the potential to perform simulations with a ram travel speed faster than $U_{ram} = 0.4465$ in/s was explored. Simulations were performed at 1×, 2×, 4×, 8×, and 16× the baseline speed of 0.4465 in/s.
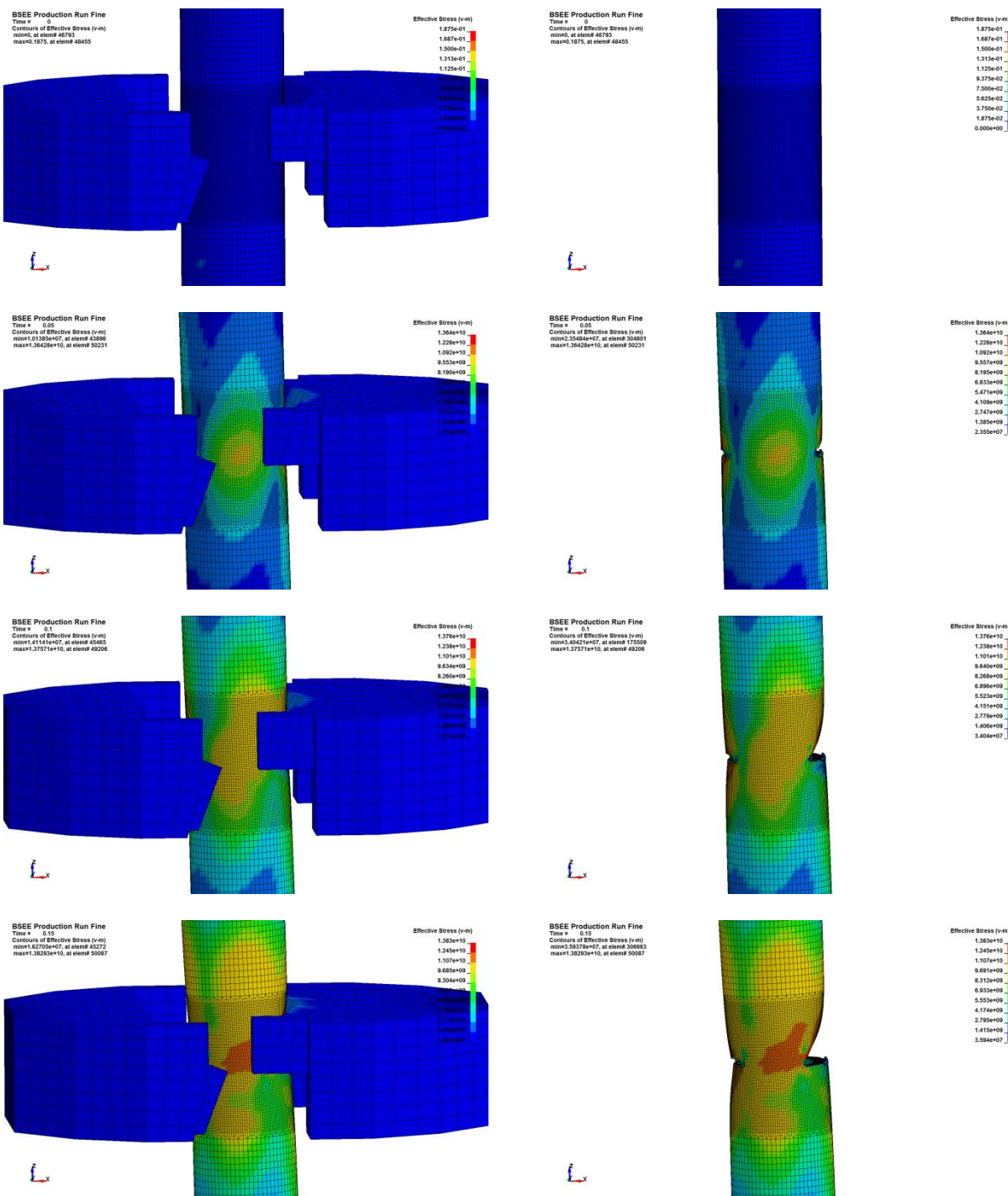
Figure 2-17. Images from the Tier 1 FEA Simulation

The color scale shows local Von Mises stress on the drill pipe surface. The initial tearing of the drill pipe before complete failure and separation is visible in the beginning of the simulation. Images correspond to 29.8%, 25.7%, 21.1%, and 16.8% area open to flow remaining.
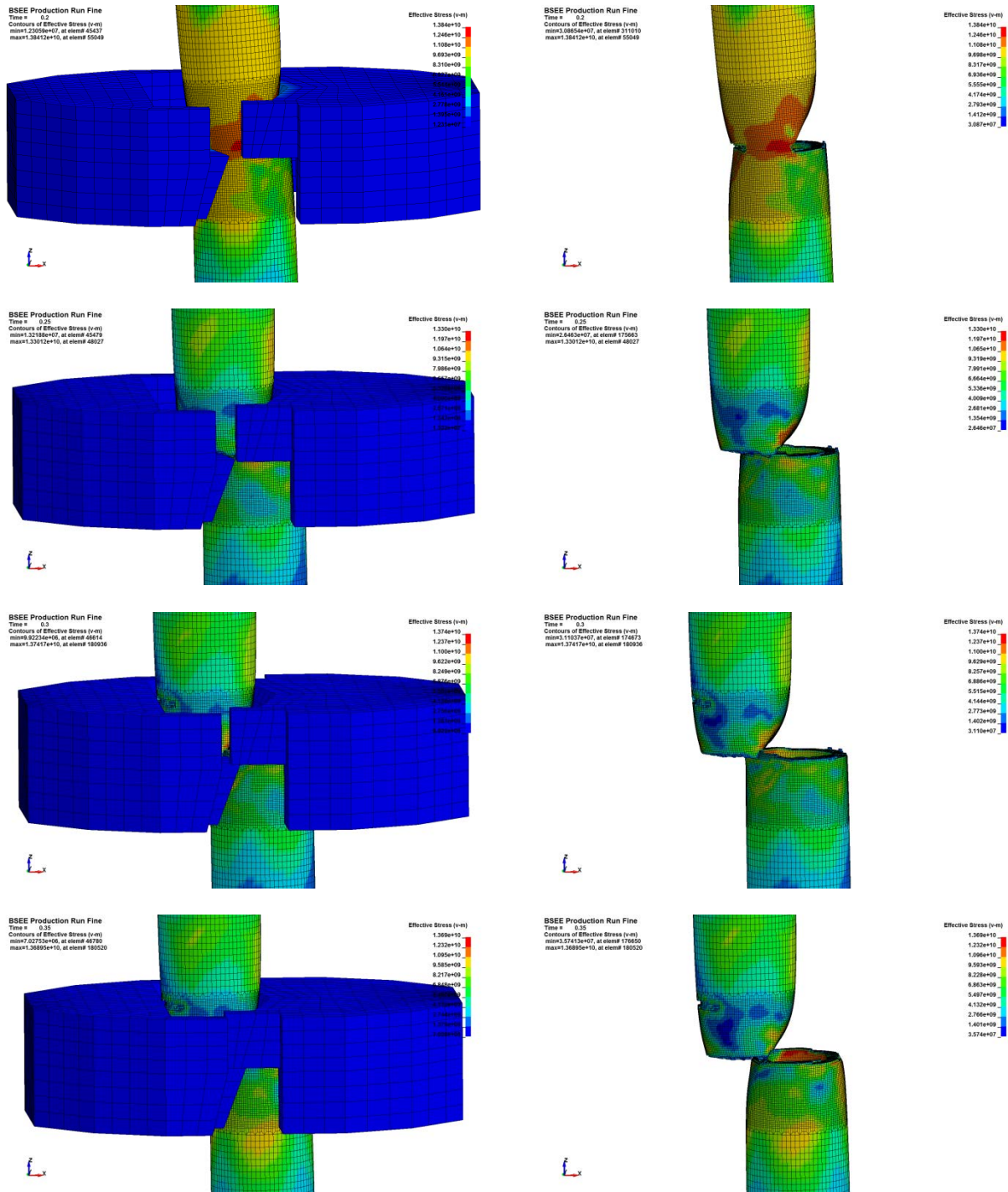
Figure 2-18. Images from the Tier 1 FEA Simulation (continued)
The color scale shows local Von Mises stress on the drill pipe surface. Eventually, the weakened pipe undergoes a rapid failure where the remainder of the connected pipe material fails. Images correspond to 12.9%, 9.4%, 5.6%, and 2.8% area open to flow remaining.
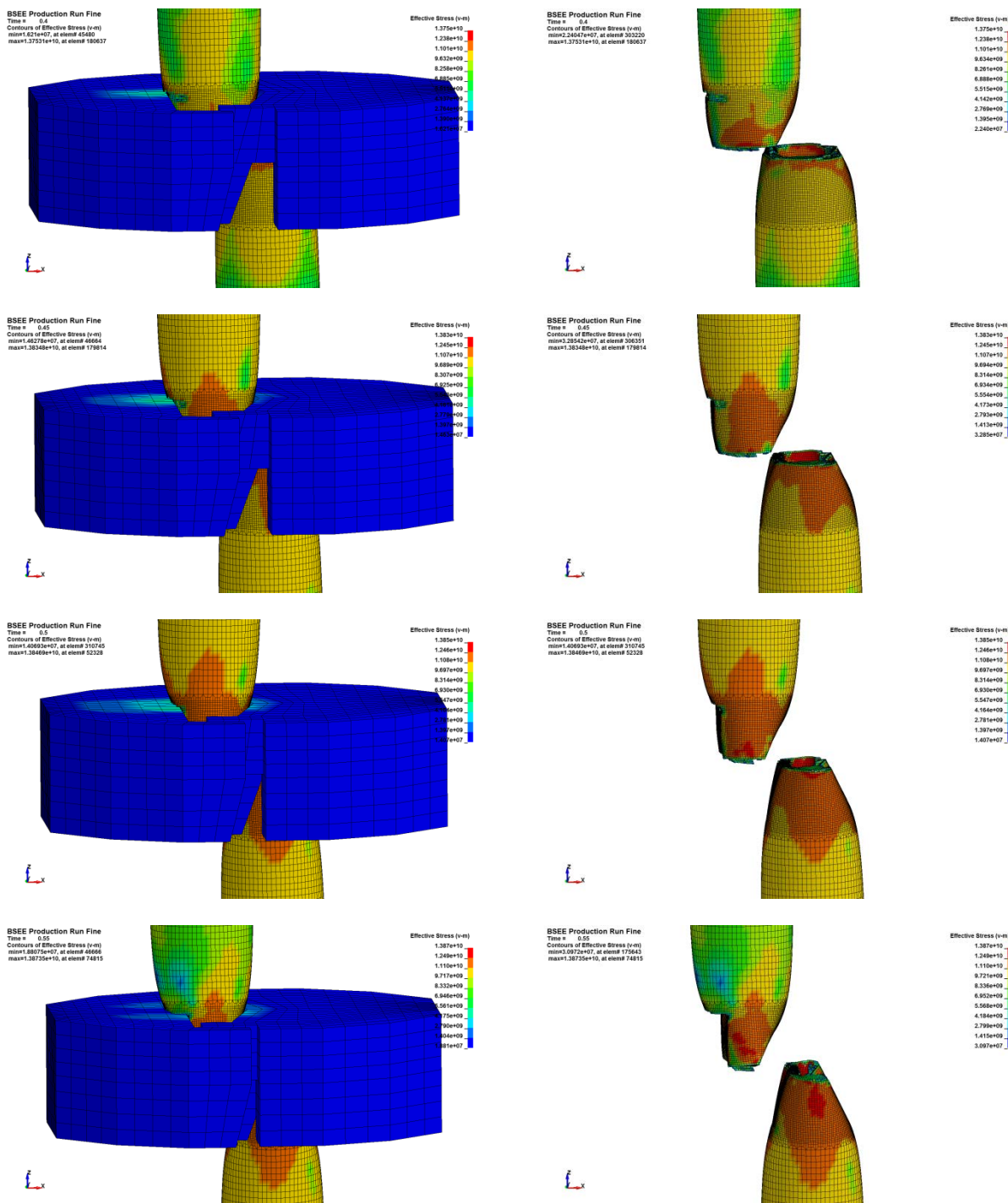
Figure 2-19. Images from the Tier 1 FEA Simulation (continued)

The color scale shows local Von Mises stress on the drill pipe surface. The final crimping of the drill pipe can be seen during the last simulation. Images correspond to 1.2%, 0.9%, 0.5%, and 0.2% area open to flow remaining.

Figure 2-20 shows the collection of shear forces measured in the simulations as a function of FEA grid resolution and ram travel speed. The simulations with only two grid cells across the pipe wall thickness are under-resolved and provide non-converged, erroneous results. The simulations with four grid cells and eight grid cells across the pipe wall thickness provide similar force-time histories and are deemed to be numerically converged. In addition, it can be seen that the numerically converged results are insensitive to the range of ram travel speeds examined. The reason for this is primarily due to the lack of strain-rate dependence in the Johnson-Cook strength and damage model, where material parameters C and D_4 are zero. This will allow for future simulations to be potentially run with faster ram travel speeds (e.g., 4× or 16×) and require less wall clock time to complete.
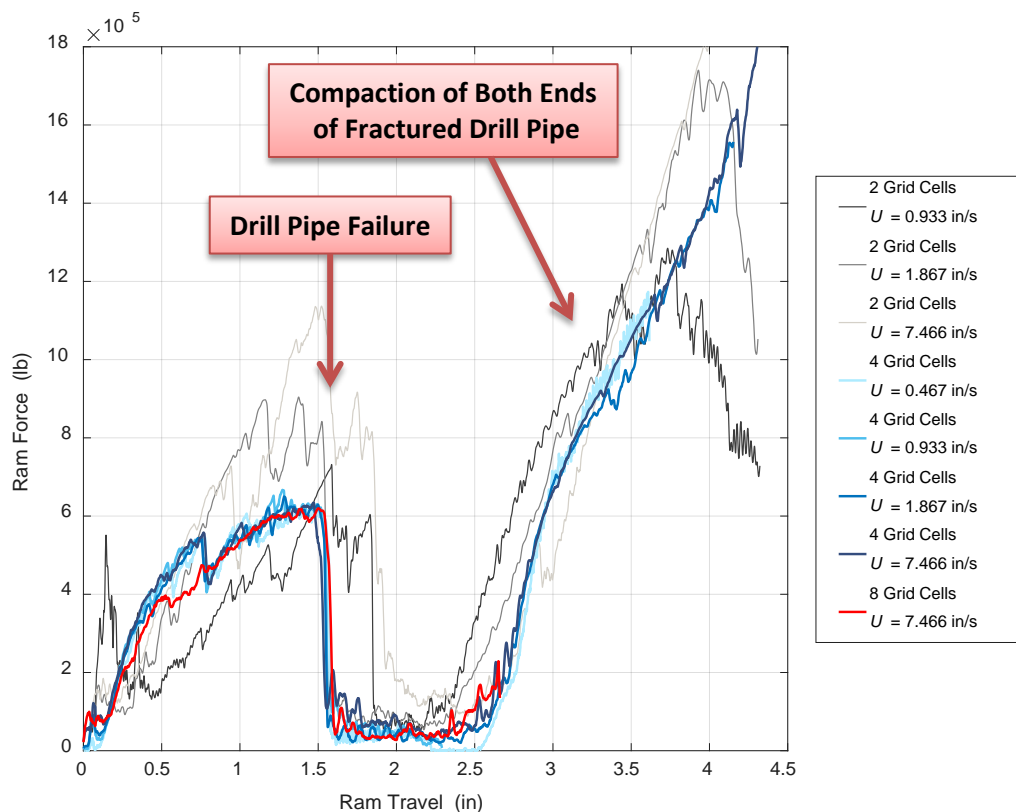
Figure 2-20. Comparison of Shear Ram Forces for the Baseline Simulation Case
The resulting forces on the shear rams are shown for different ram travel speeds and computational grid resolutions. The distance on the x-axis is measured from the initial contact of the shear rams with the drill pipe. Simulations with two grid cells across the pipe wall thickness are under-resolved and not converged. Simulations with four and eight grid cells across the pipe wall thickness are in agreement. The model shows the pipe failing after each ram has travelled 1.6 inches after contacting the centered drill pipe. The spike in forces shown after 2.5 inches of travel is attributed to the crimping of the severed pipes.

Figure 2-21 shows a small region from Figure 2-20, examining the period of time before the drill pipe has failed. Only the numerically converged results are shown in this figure. All results show that the drill pipe is severed after 1.6 inches of shear ram travel, after coming into contact with the centered drill pipe. The lower resolution simulations recorded peak forces of 633,000-666,000 lbs, depending on the ram travel speed. The maximum force recorded in the high-resolution simulation was 626,200 lbs, which occurred right before the failure of the pipe.

This value of 626,200 lbs will be used as the baseline force required to shear the baseline drill pipe in the absence of hydrodynamic forces and downhole conditions.
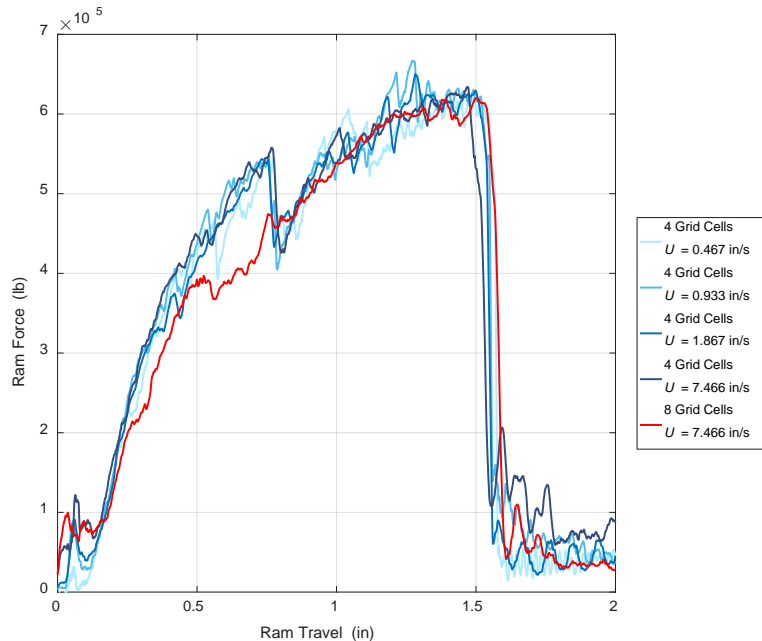
Figure 2-21. Comparison of Shear Ram Forces for the Baseline Simulation Case
The resulting forces on the shear rams are shown for different ram travel speeds and computational grid resolutions. The distance on the x-axis is measured from the initial contact of the shear rams with the drill pipe. Simulations with two grid cells across the pipe wall thickness are under-resolved and not converged. Simulations with four and eight grid cells across the pipe wall thickness are in agreement. The model shows the pipe failing after each ram has travelled 1.6 inches after contacting the centered drill pipe.

In order to provide a quantitative comparison between the Tier 1-4 simulations, the mechanical shearing, hydrostatic, and hydrodynamic forces were tabulated at different points in the shearing and sealing process. The shear ram positions are described on the basis of the nominal annulus area that is not blocked by the shear rams. There are small perturbations to the actual flow area as the drill pipe is squeezed and ruptured and these perturbations will vary from case to case. These perturbations are not included in the calculation of the "Open Area" values listed in Table 2.5 and similar tables throughout this report. Table 2.5 shows the breakdown of force contributions from each force category at the initial (100%) position and five different points in the ram shearing and sealing process. Note that the drill pipe is sheared at the 12.9% open area remaining point and, thus, the forces listed at the 10% and 5% points are small and associated with maneuvering the drill pipe into position for crimping.

Table 2.5. Force Breakdown for Tier 1 Simulations

The individual contributions to the total shear ram closing forces are provided at five different points in the closing process. Hydrostatic and hydrodynamic forces are not included in Tier 1 FEA simulations. The columns for listing the fluid forces are retained here for direct comparison to data tables in later sections.

Open Area %	Ram Piston Rod Force (lbs, per ram)				Total Axial Hydrodynamic Force
	Shearing	Hydrostatic	Lateral Hydrodynamic	Total Rod Force	
5	37,000 (100%)	n/a	n/a	37,000	n/a
10	31,500 (100%)	n/a	n/a	31,500	n/a
12.9 (max shear)	626,200 (100%)	n/a	n/a	626,600	n/a
20	466,100 (100%)	n/a	n/a	466,100	n/a
40	0 (0.0%)	n/a	n/a	0	n/a
100	0 (0.0%)	n/a	n/a	0	n/a

2.6   Tier 2 Analysis, Linear Superposition FEA/CFD Modeling

Recall that the Tier 2 methodology is based on one-way coupling of FEA shearing forces with CFD fluid forces. An overview of the process is as follows. First, the hydrostatic force from the baseline downhole pressure (11,000 psi) was applied to the pipe and rams from the Tier 1 FEA setup, and the FEA simulation re-run. This was done because the confinement pressures generated by the well flowing pressure affect the stress-strain and failure behavior of the drill pipe material when a full Johnson-Cook material strength and damage model is used. Geometries from the FEA simulation were then exported at five discrete time points: 100%, 40%, 20%, 10%, and 5% shear ram fraction area opening. These geometries were then exported to the CFD software ANSYS® Fluent®, where steady-state simulations were carried out to solve for the hydrodynamic forces on the rams. The hydraulic forces from CFD were then linearly added to the FEA mechanical shearing forces to compute a combined total force exerted on the rods driving the rams.

The CFD simulations solved the steady-state, Reynolds-averaged conservation of mass, momentum, turbulent kinetic energy, and dissipation rate transport equations. The flow in the vicinity of the BOP stack was assumed to be incompressible (negligible density changes over the range of pressures within the domain) and single phase. The potential for multiphase flow, such as the presence of solid rock or sand matter within liquid flow or various combined gas/liquid flow regimes, was not included in this study. The fluid domain consisted of the annular region between the inner drill pipe and outer casing and rams. For the simulations where the fluid volume within the drill pipe remained hydraulically isolated from the annulus, i.e., before the failure of the drill pipe, it was assumed that the hydrostatic pressure within the drill pipe and annulus were in equilibrium. For the simulation cases where the rams have sheared, a portion of the volume within the drill pipe was incorporated in the fluid domain. The fluid within the drill pipe was considered to be essentially stagnant, i.e., was not actively being driven or pumped.

2.6.1   CFD Grid Structure

Preliminary simulations were first carried out to evaluate the gridding strategy and test the solution sensitivity, stability, and accuracy with respect to numerical modeling forms and grid resolution. These first simulations examined the flow through the BOP where the blind shear rams have completed 50% of their total linear translation (10.5 inches out of 21.0 inches).

A view of the raw CAD geometry used to construct the CFD model is shown in Figure 2-22. The flow rate was set to 100,000 stb/d, which translates to an annular flow velocity of 6.56 ft/s [2.0 m/s] for the pressure/temperature conditions of 11,000 psia and 300°F at the BOP. The fluid density and viscosity are $\rho = 38.88$ lb/ft^3 [622.8 kg/m^3] and $\mu = 0.344$ cP, respectively. The inlet (bottom of the domain) was set to a constant velocity inlet with $U = 6.56$ ft/s [2.0 m/s]. The outlet (top of the domain) was set to an 11,000-psia constant pressure boundary.
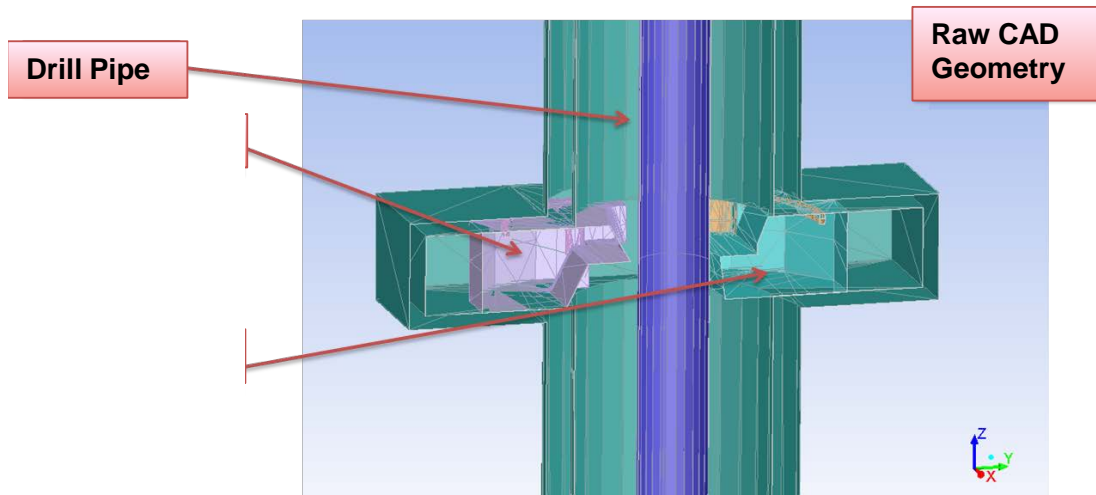
Figure 2-22. Base CAD Model for the CFD Analysis
The CFD model requires that the volume within the wellbore and BOP that is open to fluid flow be defined. To accomplish this, a CAD model was created that uses the shear rams defined in the baseline conditions and is augmented with the associated wellbore casing and drill pipe.

The computational mesh that occupies the annular region open to flow has a significant impact on the quality and accuracy of the resulting solution. The meshes used in this study were constructed by defining a high-quality surface mesh around all CAD geometry components. That refined mesh was then used to seed the generation of an internal, unstructured, volume mesh. An image of one of the generated surface meshes is shown in Figure 2-23. In the regions away from the rams, an unstructured "swept" grid with hexahedral elements was used to provide a more uniform mesh and aid numerical convergence. This gridding approach was not feasible near the rams, and thus, a fully unstructured tetrahedral mesh was used instead. The interface between these meshing regions is fully conformal, i.e., there is a one-to-one relationship between all grid cell faces. It should be noted that after the rams begin to interact with the pipe, the sheared pipe geometry is exported from the FEA solution in an STL file format. This faceted surface must then be "cleaned" prior to importation into the CFD solver. This was accomplished in ANSYS SpaceClaim® using a surface wrapper approach. The FEA and CFD meshes extended approximately five BOP diameters upstream and downstream from the BOP position.
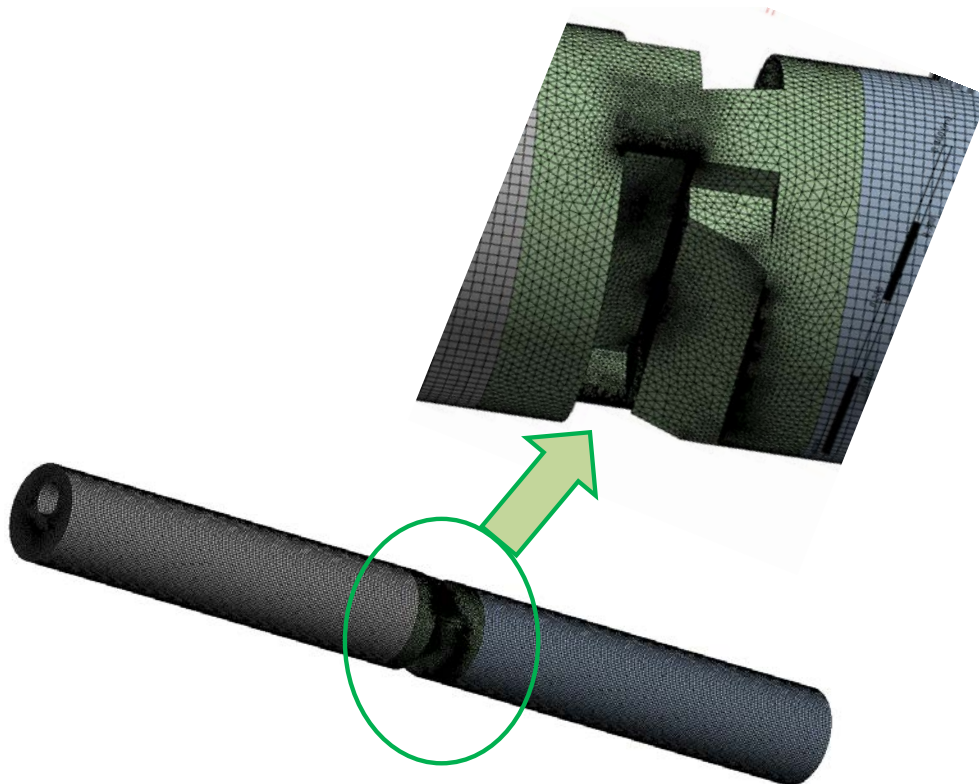
Figure 2-23. Volume Mesh for the CFD Analysis
The computational mesh filling the annular region open to flow shows the domain of interest that is considered in the CFD simulations.

2.6.2   CFD Turbulence Model Selection

As previously noted, the CFD model solved the steady-state, Reynolds-averaged conservation of mass, momentum, turbulent kinetic energy, and dissipation rate equations. The goal of these simulations is to accurately predict the added hydrodynamic forces exerted on the rams as they close on flow. In such an event, the local flow in the annulus will accelerate in order to move through the reduced cross sectional area open to flow. A benchmark validation case with experimental measurements was selected to confirm that the CFD model is accurately accounting for the dynamic pressures that arise from flow being diverted around bluff bodies protruding into an already fully developed turbulent flow in the annulus.

Martinuzzi and Tropea (1993) used flow visualization techniques and surface mounted pressure probes to experimentally measure the flow and local dynamic pressures that develop as a turbulent flow is diverted around a bluff body protruding into a fully turbulent flow. A simulation model of the experiments was constructed to evaluate the ability of the CFD model and selected turbulence model to accurately predict the flow field and dynamic pressures around the flow obstruction. Specifically, the experimentally and computationally measured pressures are compared at different points around the obstacle. Specifically, Martinuzzi and Tropea (1993) reported the dimensionless pressure coefficient for different blockage geometries.   The dimensionless pressure coefficient C_p is defined:

$$C_p = \frac{P - P_{ref}}{\frac{1}{2}\rho U^2}, \qquad [6]$$

where P is the local pressure on any surface, P_{ref} is the free stream pressure, ρ is the density of the fluid, and U is the mean fluid velocity in the channel.

For the validation problem examined here, a square obstacle half the height of a channel was examined. Images of the full computational domain and the region of interest around the obstacle for the validation case simulation are shown in Figure 2-24. Images of the streamlines along the channel floor and symmetry plane as well as the pressure coefficient are shown in Figure 2-25. The effect of the blockage on the incoming flow can be seen by examining the streamlines. Flow is diverted and accelerated around the blockage. In the wake surrounding the blockage, the formation of strong recirculation zones is observed. These results are in agreement with the flow visualization images and schematics reported by Martinuzzi and Tropea (1993). The ability of the simulation to accurately predict these streamlines and recirculation zones is directly related to the prediction of the local hydrodynamic pressures exerted on the obstacle and surrounding surfaces.

Note that the images in Figure 2-25 show the results from a single simulation using one potential choice for a turbulence model. Five different simulations were run so that the different turbulence model options could be evaluated. The five simulations examined the use of (1) no turbulence model, (2) the "standard" form of the k-ε model, (3) the "realizable" form of the k-ε model, (4) the "standard" k-ω model, and (5) the full Reynolds stress transport model. Each turbulence model has application areas where it excels and different areas where it fails. In depth discussions on the nuanced distinctions between the different model forms are available elsewhere (Pope 2000) and are not repeated here.

Martinuzzi and Tropea (1993) reported the value of C_p along the floor of the channel at multiple points around the obstacle. See red lines in Figure 2-24 for locations of streamwise and spanwise pressure profile measurements. Figure 2-26 and Figure 2-27 show the comparison of the experimental measurements and CFD simulations. In general, all turbulence models produced good agreement with the measured pressure data. The simulation that excluded any explicit model accounting for the effects of turbulence on the mean flow field produced dramatically less accurate results. Overall, the full Reynolds stress turbulence model produces the most accurate results for this validation test; however, the added computational expense of this model was not deemed justifiable with respect to the results generated by the two-equation k-ε turbulence models. Thus, the realizable k-ε model was selected for use in all subsequent Tier 2 and Tier 3 CFD simulations for the baseline case and all CFD simulations for the parametric cases that use the Tier 2 approach.
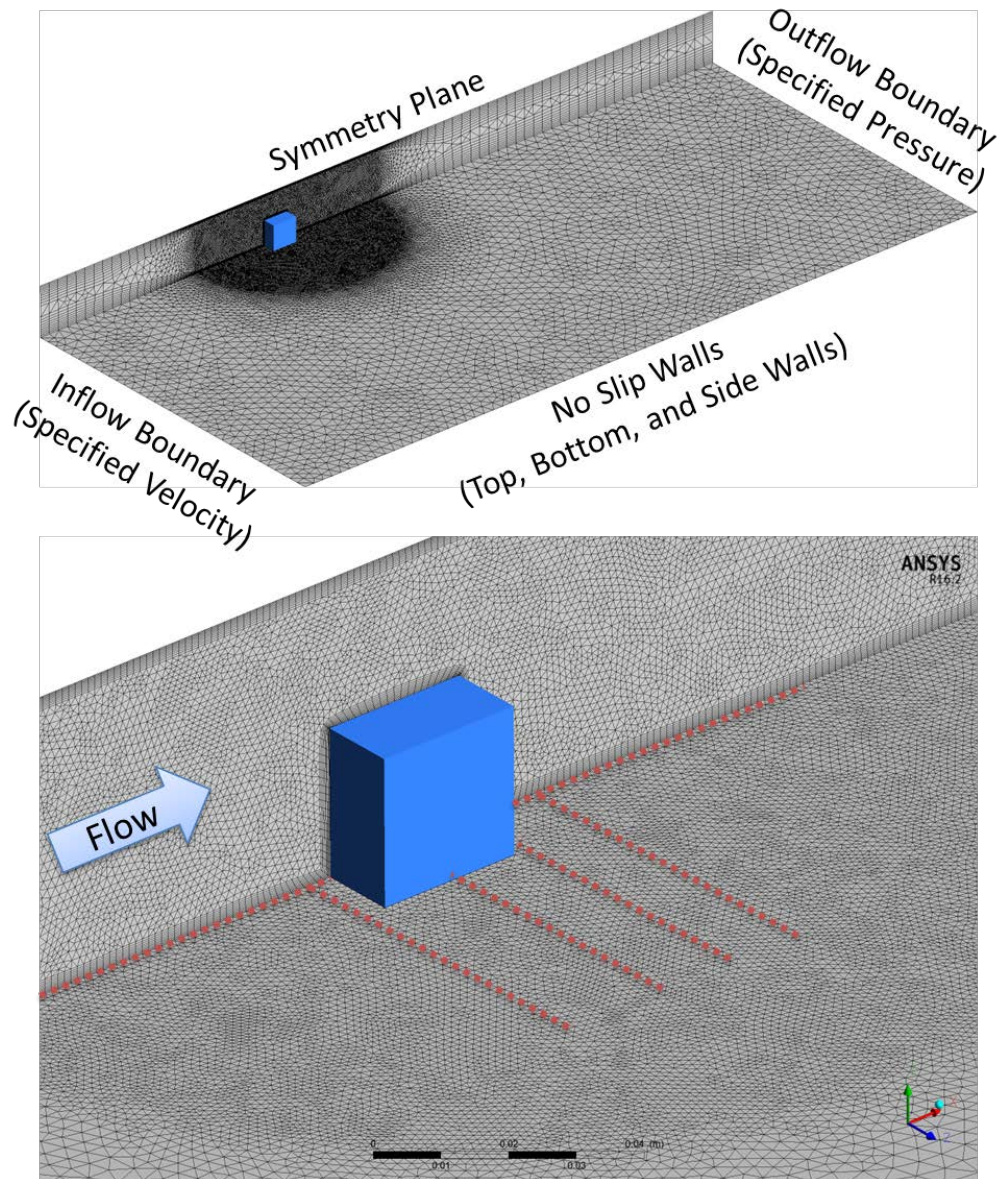
Figure 2-24. Domain, Boundary Conditions, and Computational Mesh for Turbulence Model Validation Case

Fully developed turbulent channel flow provided at inlet boundary. The blockage (blue object) is a cube where the cube dimension H is half the channel height h. Computational mesh is refined around the region of interest. Red lines show streamwise (x-axis) and four spanwise (z-axis) locations of measured dynamic pressures around the blockage.
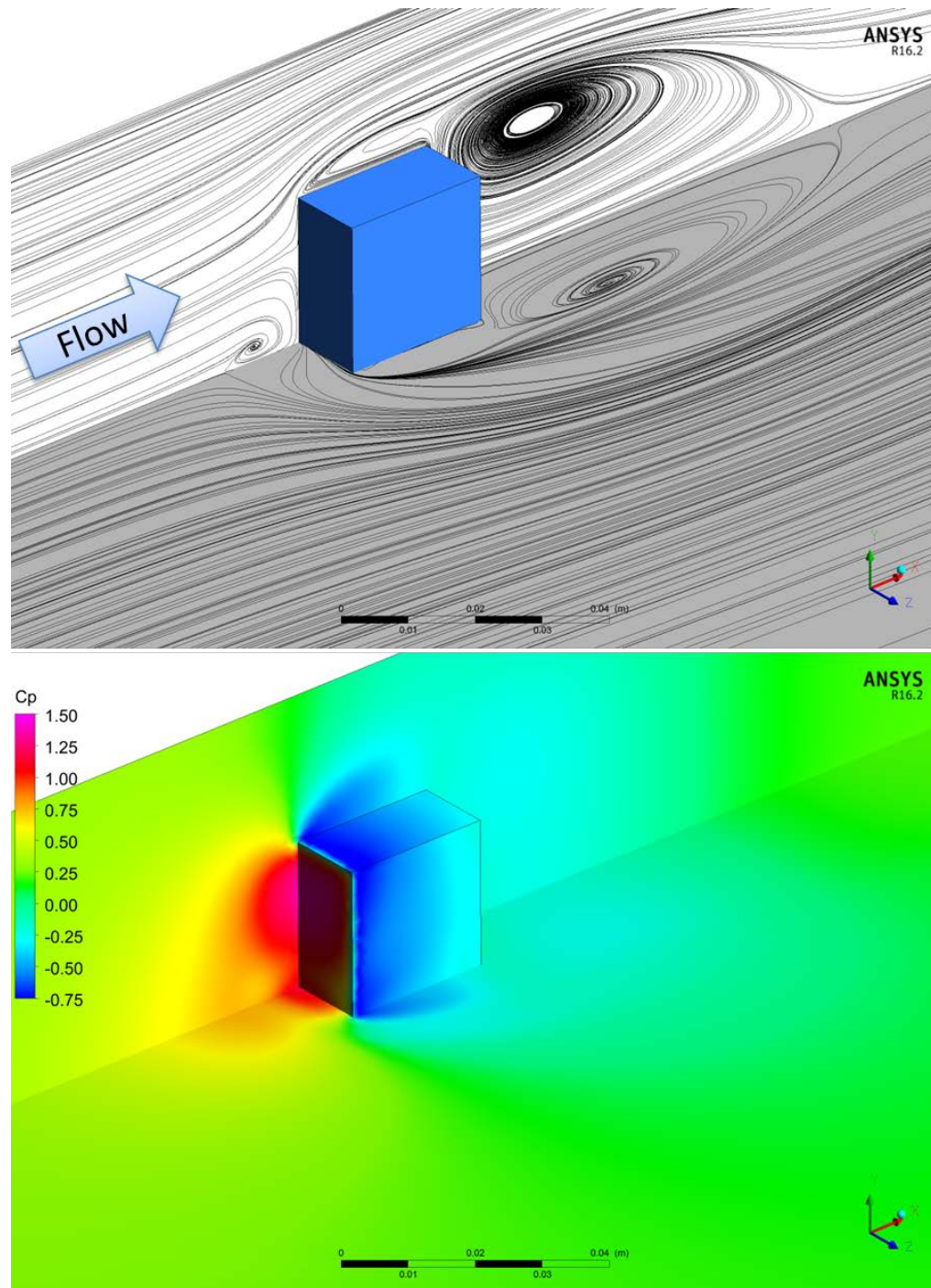
Figure 2-25. Streamlines and Pressure Coefficient for Simulation Using Realizable k-ε Model
Streamlines (top image) show diversion of flow around the obstacle and the formation of a wake region behind the obstacle. The distribution of pressure coefficient (bottom image) shows a very large positive pressure on the face of the blockage (red region). A smaller in magnitude, negative, and varying pressure distribution is observed around the faces that are aligned with the primary flow direction (blue and cyan colored faces).
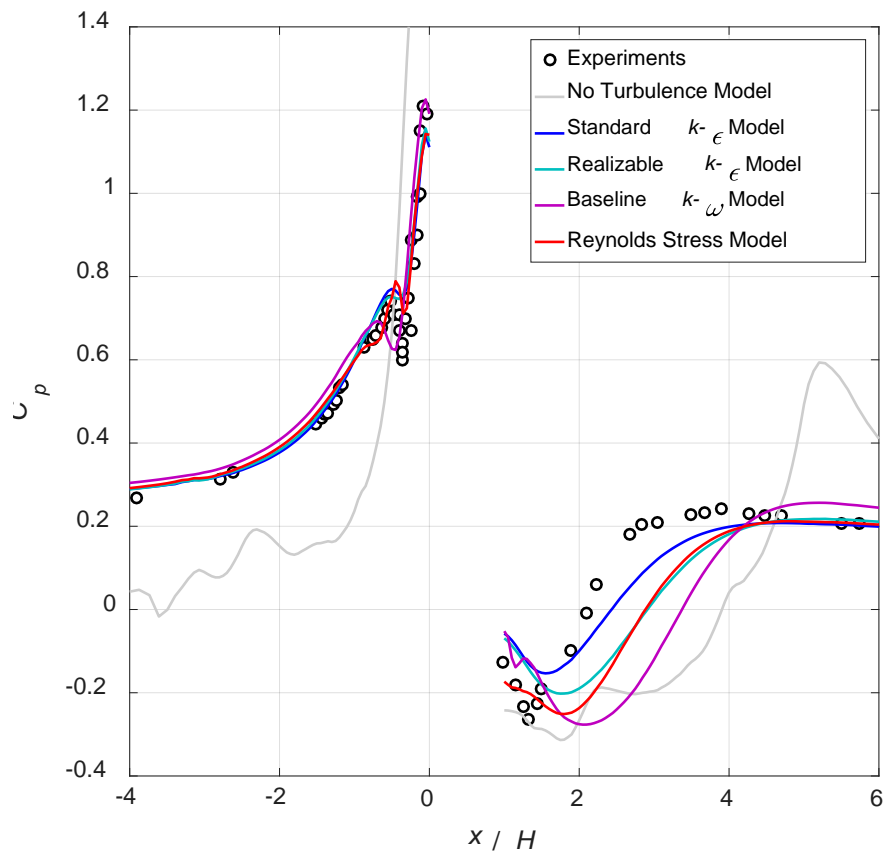
Figure 2-26. Pressure Coefficient Values in Streamwise (*x*) Direction
In general, all of the turbulence models tested reproduce the pressures leading up to the blockage. The pressures downstream of the blockage are captured reasonably well. The realizable k-ε model and full Reynolds stress model performed the best in the region immediately following the blockage.
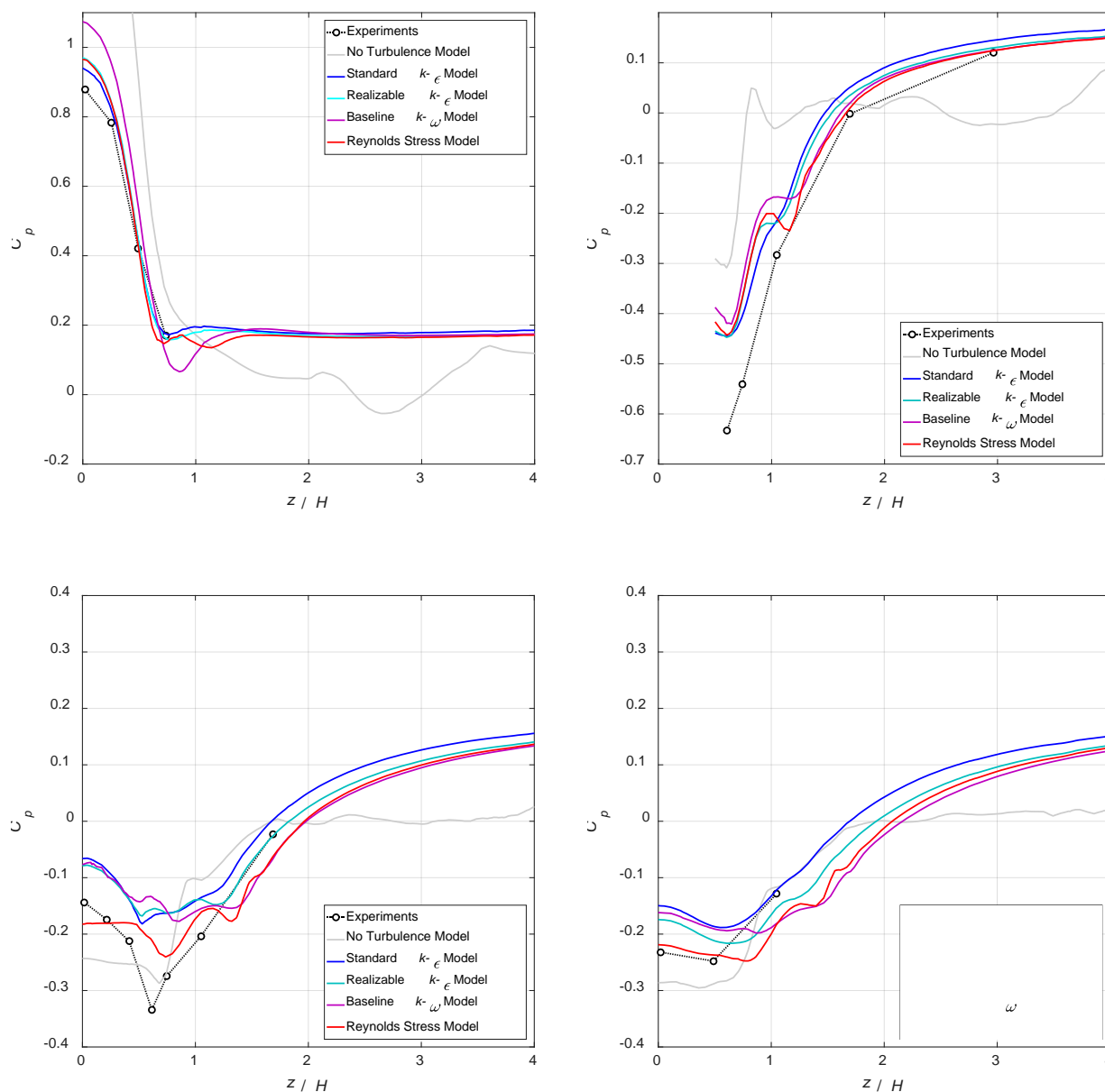
Figure 2-27. Pressure Coefficient Values in Spanwise (*z*) Direction

Measurement locations are at x/H = -0.18 (top-left), x/H = 0.5 (top-right), x/H = 1.06 (bottom-left), and x/H = 1.46 (bottom-right), where H is the height of the square blockage and x = 0 is defined by the leading face of the blockage. Again, all of the turbulence models tested performed reasonably well, with the full Reynolds stress model showing the best agreement.

2.6.3   Transient Pressure-Flow Conditions at BOP

As the rams begin to close on the pipe, flow through the annulus continues to decrease until the point at which it stops entirely as the opening is sealed. The flow rate corresponding to the fractional opening of the rams was simulated using valve models in two separate one-dimensional (1D) well-modeling programs, SINDA/FLUINT (2011) and OLGA®. Sensitivity to

valve coefficients was considered in both software packages. As shown in Figure 2-28, both OLGA and SINDA/FLUINT produced similar curve shapes. Since the actual valve coefficient that would replicate the particular BOP in the baseline case was unknown, it was decided to use the curve that maintained a high flow rate for the longest period during closing. This curve (SINDA/FLUINT, K=1) represents the most conservative estimate that would allow the fluid to generate the highest hydrodynamic forces on the ram faces.

BSEE and SwRI jointly decided that the discrete CFD simulations of Tiers 2 and 3 would be carried out for ram closures equivalent to 100%, 40%, 20%, 10%, and 5% of the full fractional opening. As shown in Figure 2-29, this focuses the CFD simulations around the time when the flow rate becomes meaningfully affected by the decreasing cross-sectional area.
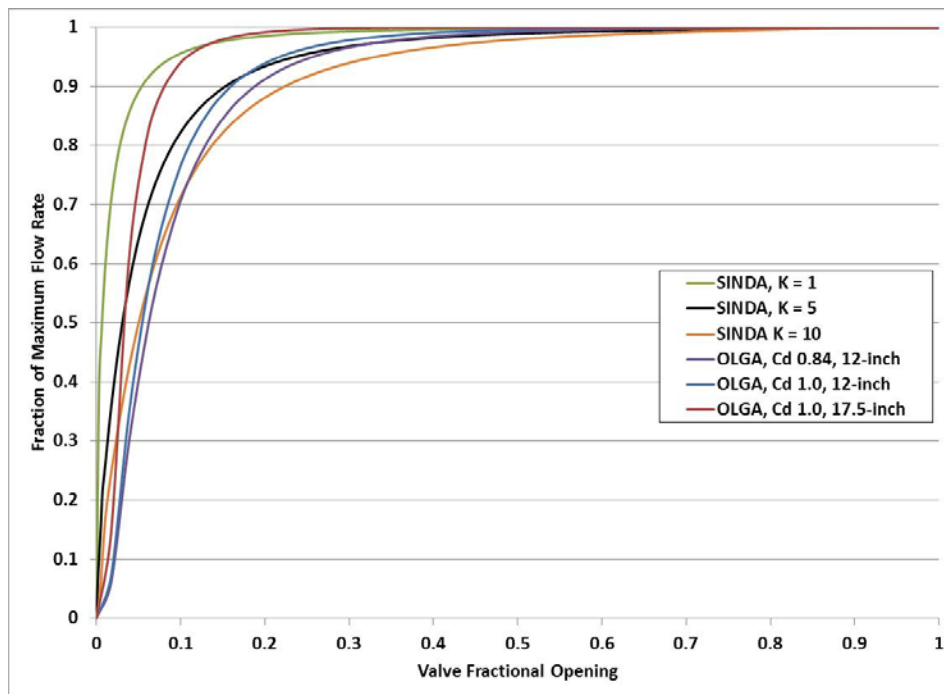
Figure 2-28. One-Dimensional Well Modeling of Valve Closure Percentage versus Fraction of Maximum Flow for the Baseline Case
The trend of decreasing flow with increasing valve closure was modeled using both OLGA and SINDA/FLUINT with various valve coefficients to gauge sensitivity.
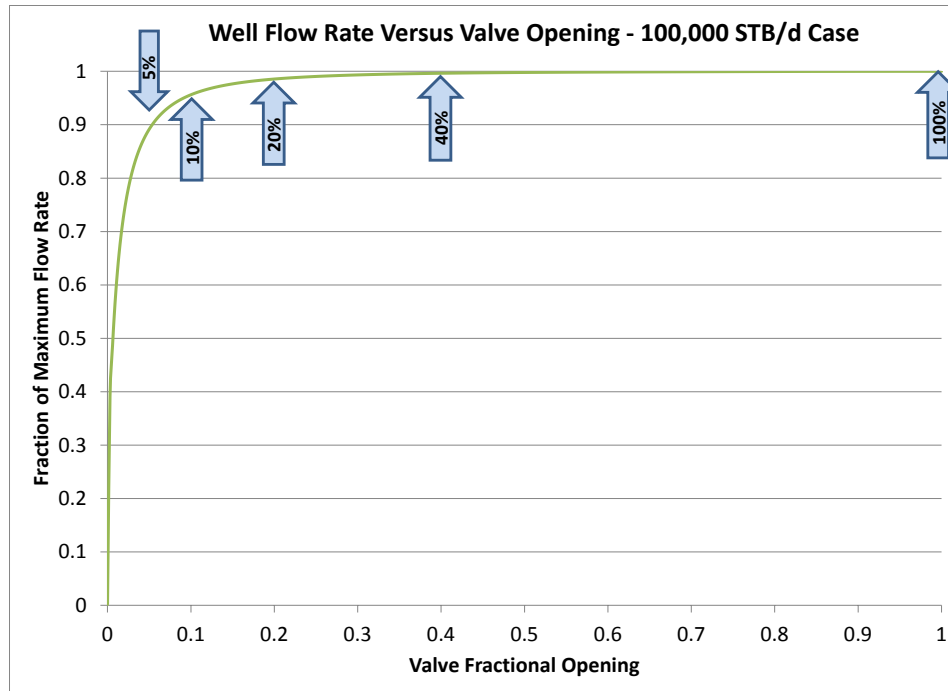
Figure 2-29. Maximum Flow Rate Fraction versus Open Area for the Baseline Case
Five CFD simulations at 100%, 40%, 20%, 10%, and 5% of fractional area open to flow have been carried out for the Tier 2 and Tier 3 work.

The closing of a BOP stops the flow, but as the momentum of the fluid upstream of the valve is stopped, there can be a sudden pressure increase at the valve. This is the familiar waterhammer effect that can lead to large transient forces on a pipeline in which a valve is suddenly closed. The need to consider these rapid pressure and flow transients during BOP closure is addressed here.

Wylie and Streeter (1983) showed that the pressure rise resulting from a nominally incompressible fluid being suddenly stopped can be estimated from basic fluid mechanics considerations as expressed by Eq. 7.

$$\Delta P \approx \rho c \Delta V$$

[7]

where ΔP is the pressure change, ρ is the fluid density, c is the speed of sound in the fluid, and ΔV is the fluid velocity change. Using the baseline flow conditions described in Table 2.1 and the pressure-density correlation in Figure 2-4, values for the density, fluid velocity, and speed of sound at the BOP location are estimated to be as follows.

$\rho = $ 39.3 lb/ft^3
$V = $ 4.3 ft/s
$c = $ 3,940 ft/s

Using these values, the pressure rise due to a sudden BOP closure that can be expected is approximately $\Delta P \approx$ 140 psi. Considering the fact that the flowing pressure for the baseline conditions at the BOP location is 11,000 psi, this estimated pressure rise due to waterhammer is negligible.

It is recognized that the preceding analysis is highly approximate. A more detailed investigation of BOP waterhammer was conducted with a 1D transient numerical analysis using the commercial software package SINDA/FLUINT (2011). The SINDA/FLUINT software is a widely used tool for analyzing pipeline flow and general heat transfer problems. Its usage for waterhammer analysis has been thoroughly validated by its developer. A view of the flow model of the casing from the SINDA/FLUINT graphical user interface is shown in Figure 2-30.
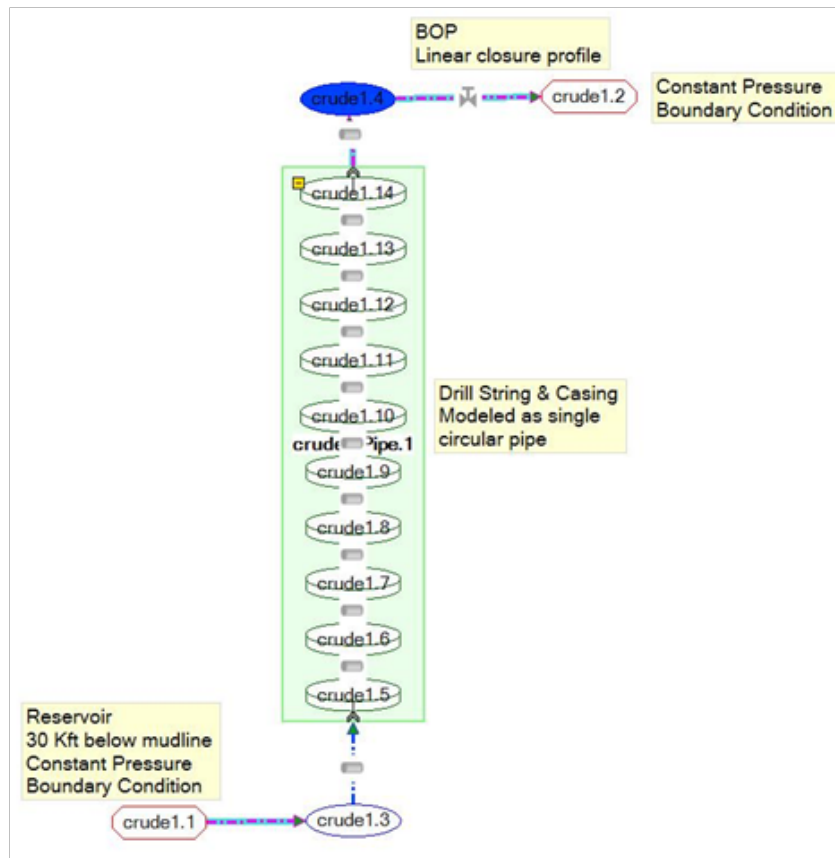
Figure 2-30. SINDA/FLUINT Model of Casing Flow
The hydraulic transients at the BOP location were computed for different BOP closure times.

As indicated in Figure 2-30 the casing was modeled as a straight vertical pipe of a single diameter with a cross section equal to that of the actual annulus geometry. For these example calculations, the pressure at the BOP stack outlet was held constant at 11,000 psi and the reservoir pressure was held constant at 20,000 psi (consistent with the hydrostatic pressure gradient). The grid resolution for the casing was varied between 10 nodes and 100 nodes.

The pressure oscillations at the BOP resulting from BOP closure times between 5 s and 45 s were obtained from the SINDA/FLUINT simulations. The simulation results are compared in Figure 2-31.
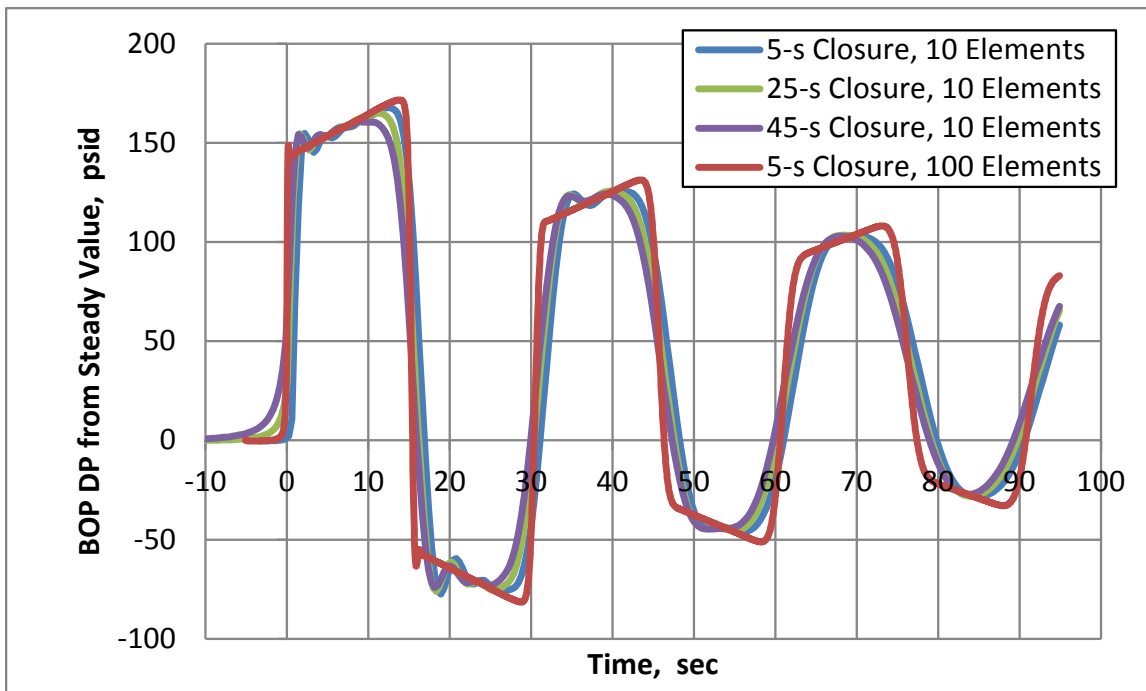
Figure 2-31. Pressure Oscillations at the BOP from SINDA/FLUINT Simulations
The SINDA/FLUINT simulations show that the peak pressure rise at the BOP resulting from waterhammer is estimated to be about 160 psi above the local hydrostatic flowing pressure.

First, these simulations show that results are relatively insensitive to the grid resolution. Second, the peak pressure achieved after the valve closes slightly decreases as the BOP closure time increases. Even for a fast closure time of 5 seconds, the peak pressure is about 165 psi above the steady flowing pressure of about 11,000 psi. This small amplitude of oscillating pressure will have an almost negligible effect on the pressure forces acting on the BOP shear ram because these forces are transverse to the flowing direction.

This pressure increase will, however, produce a significant force in the rams in the flow direction, which will act to force the shear rams against the upper and lower guide surfaces until the oscillations damp out. These axial hydrodynamic forces are discussed in the context of the overall detailed CFD/FEA analyses described in Sections 2.7 to 2.9 and Section 3.

The final factor to address with respect to fluid pressure and flow transients is the effect of multiphase flow. Wellbores can contain a wide range of multiphase flows. Examples are solids such as sand, gravel, and drill cuttings being transported in a drilling mud; sand transported with produced oils and water; and gas in bubbly or slug flow with liquids. The multiphase flow with possibly the most severe pressure effects is a slug flow where a long section of gas-dominant flow mixture is followed by a slug of liquid. This can produce extreme forces in the BOP and any other well control equipment.

As was mentioned previously, only single phase oil flow was considered within the scope of this project. Multiphase flow effects on well control equipment, such as those described in the preceding paragraph, are left to other research projects.

2.6.4   *Fluid Flow Field at BOP*

At the conclusion of each CFD case, the velocity vectors and streamlines were post-processed and examined to ensure fidelity and proper convergence of the solution. Figure 2-32 and Figure 2-33 show flow streamlines through the entire domain for varying amounts of ram closure. As the rams close, the relatively uniform flow field becomes diverted preferentially to one side of the annulus as a large recirculation zone is established on the opposite side. Figure 2-34 shows velocity vectors on the vertical plane cutting through the middle of the BOP stack. With 40% and 20% area open to flow remaining, the local fluid velocity around the rams shows some marginal acceleration, with local fluid velocities on the order of 10 ft/s. As the rams move closer to a fully closed position, the local fluid velocities around the cutting edges of the rams are significantly higher at 20-80 ft/s. Figure 2-35 shows the hydrodynamic pressures exerted on the drill pipe and casing walls. Figure 2-36 shows the hydrodynamic pressures on the ram faces. These pressures are integrated in the direction of the ram travel in order to compute the hydrodynamic force contribution to the overall force required to close the rams. These pressures are also integrated in the vertical or axial direction to compute the vertical force on the rams as they close on flow.
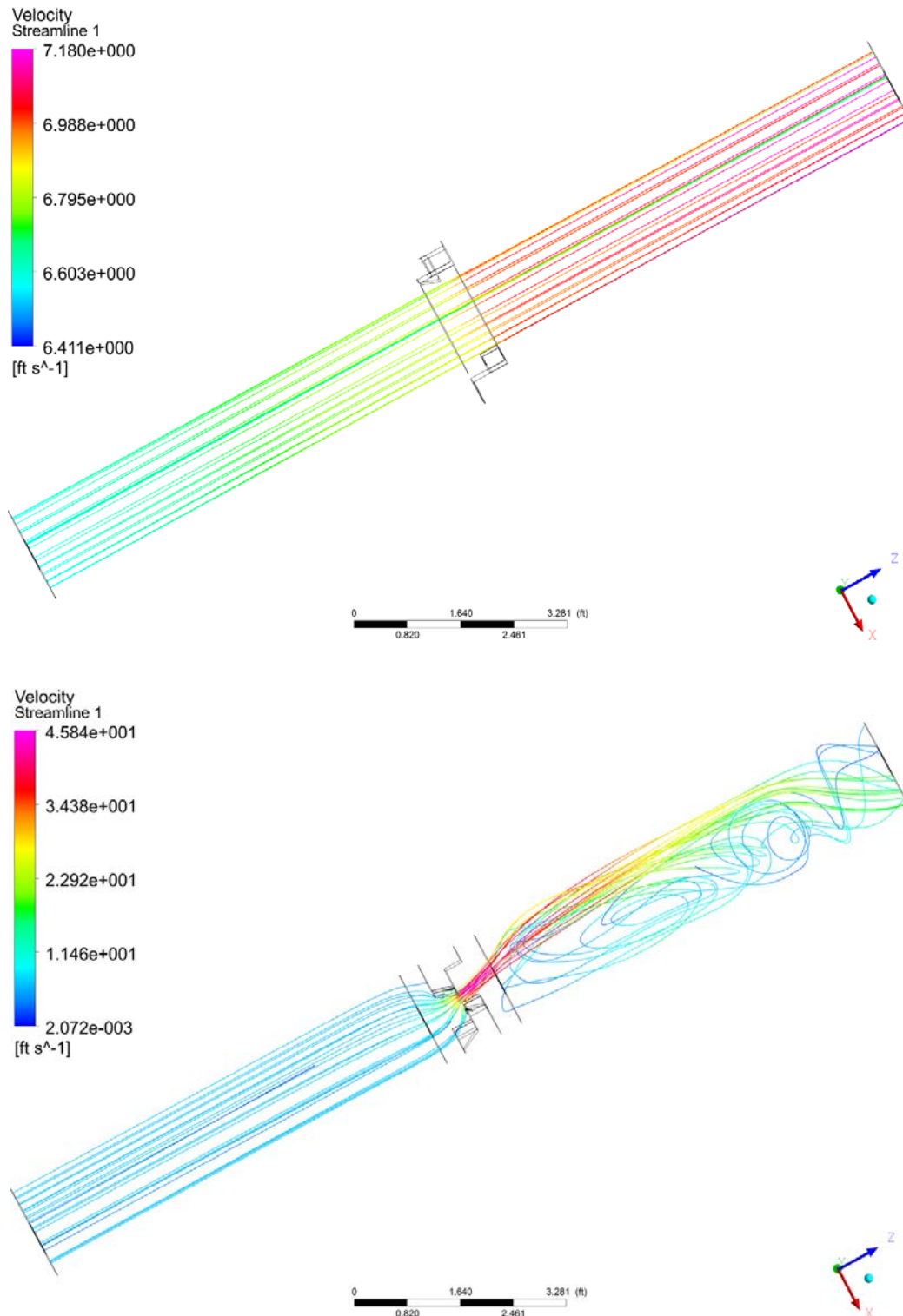
Figure 2-32. Tier 2 Flow Results (Streamlines) from CFD at 40% and 20% Open Area
Flow streamlines are examined following simulations to ensure adequate resolution and domain extents.
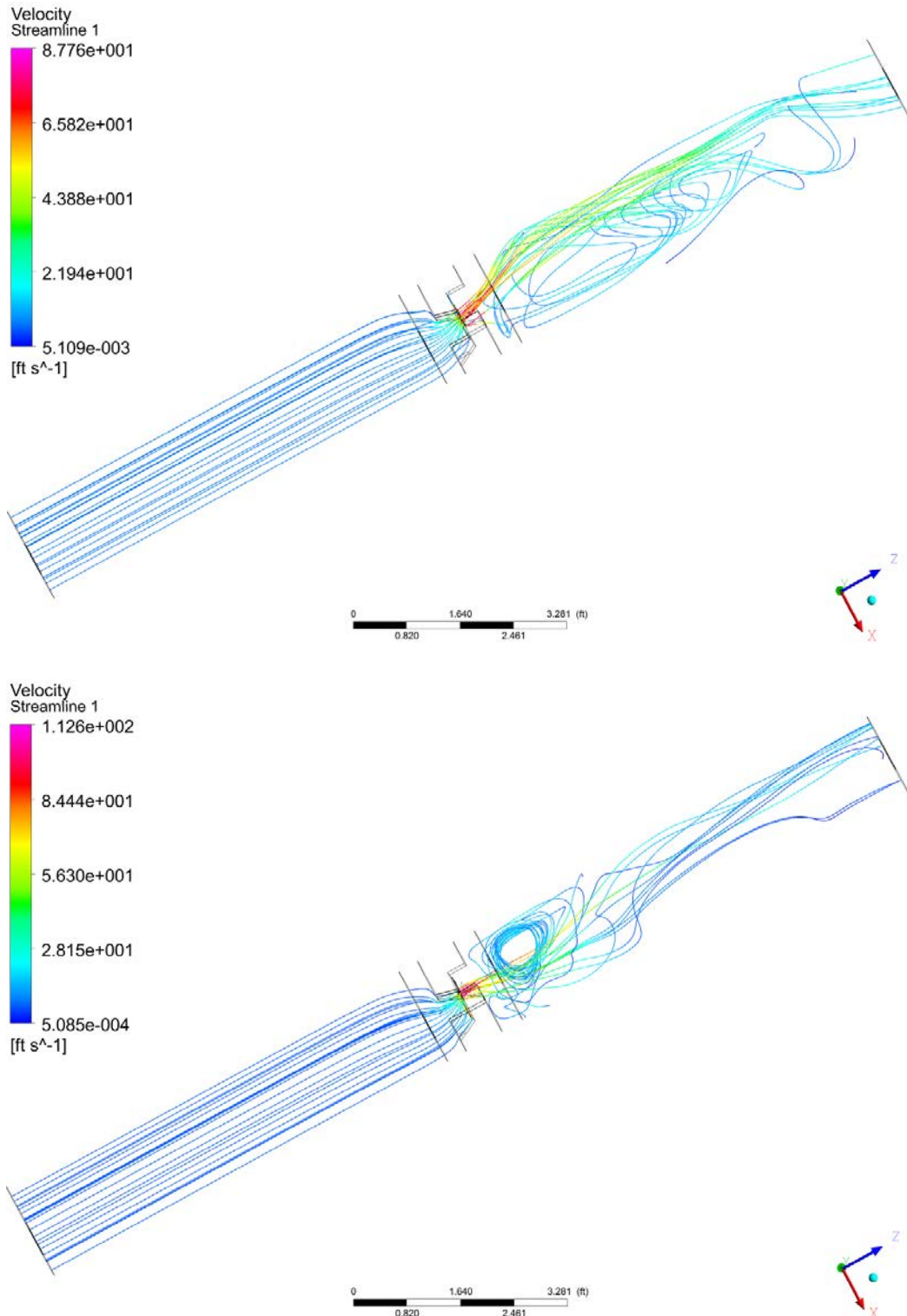
Figure 2-33. Tier 2 Flow Results (Streamlines) from CFD at 10% and 5% Open Area
Flow streamlines are examined following simulations to ensure adequate resolution and domain extents.
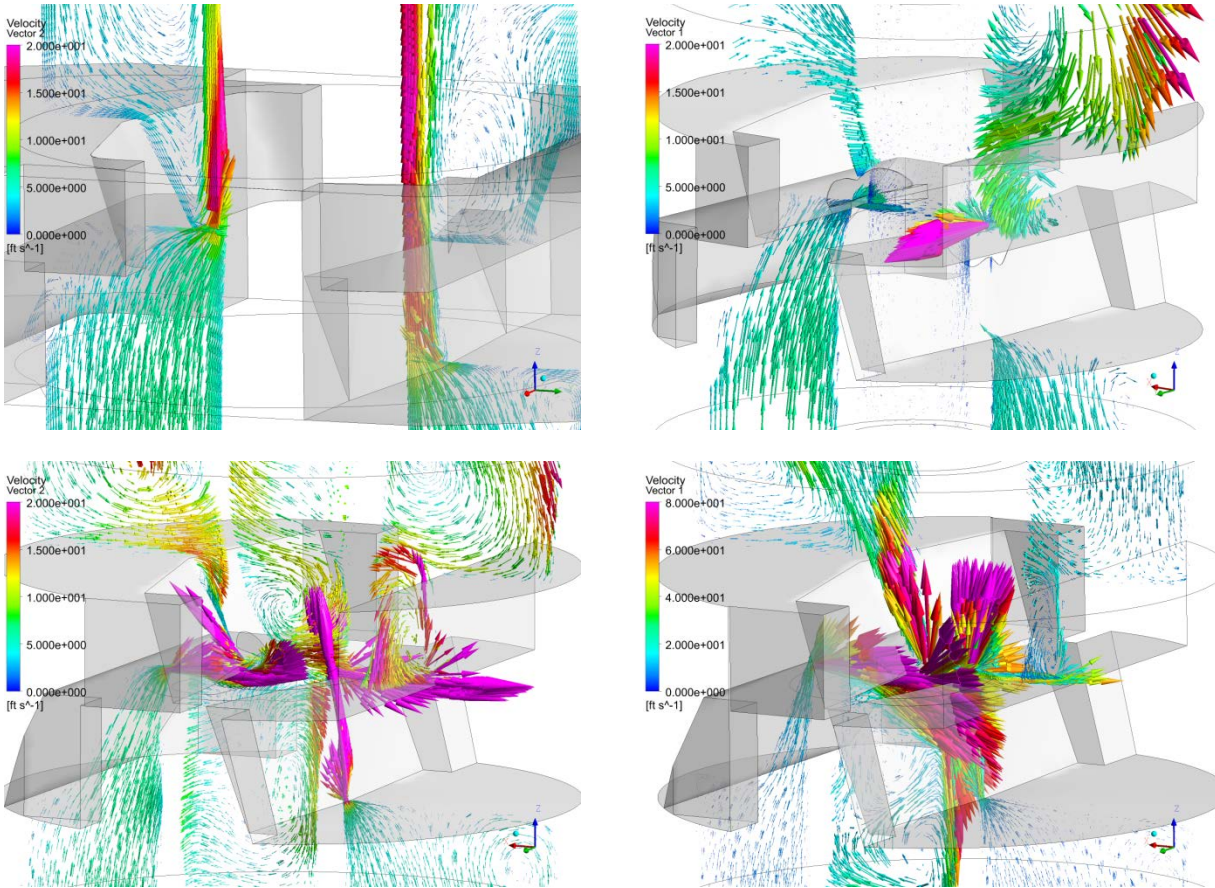
Figure 2-34. Flow Field in Vicinity of Rams
Velocity vectors are shown on the mid-plane in the vicinity of the rams for varying amounts of ram closure. Images show velocity fields with rams 40% (top-left), 20% (top-right), 10% (bottom-left), and 5% (bottom-right) closed. As the rams move to a fully closed position, the local fluid velocity around the rams becomes substantially larger than the nominal annular flow velocity.
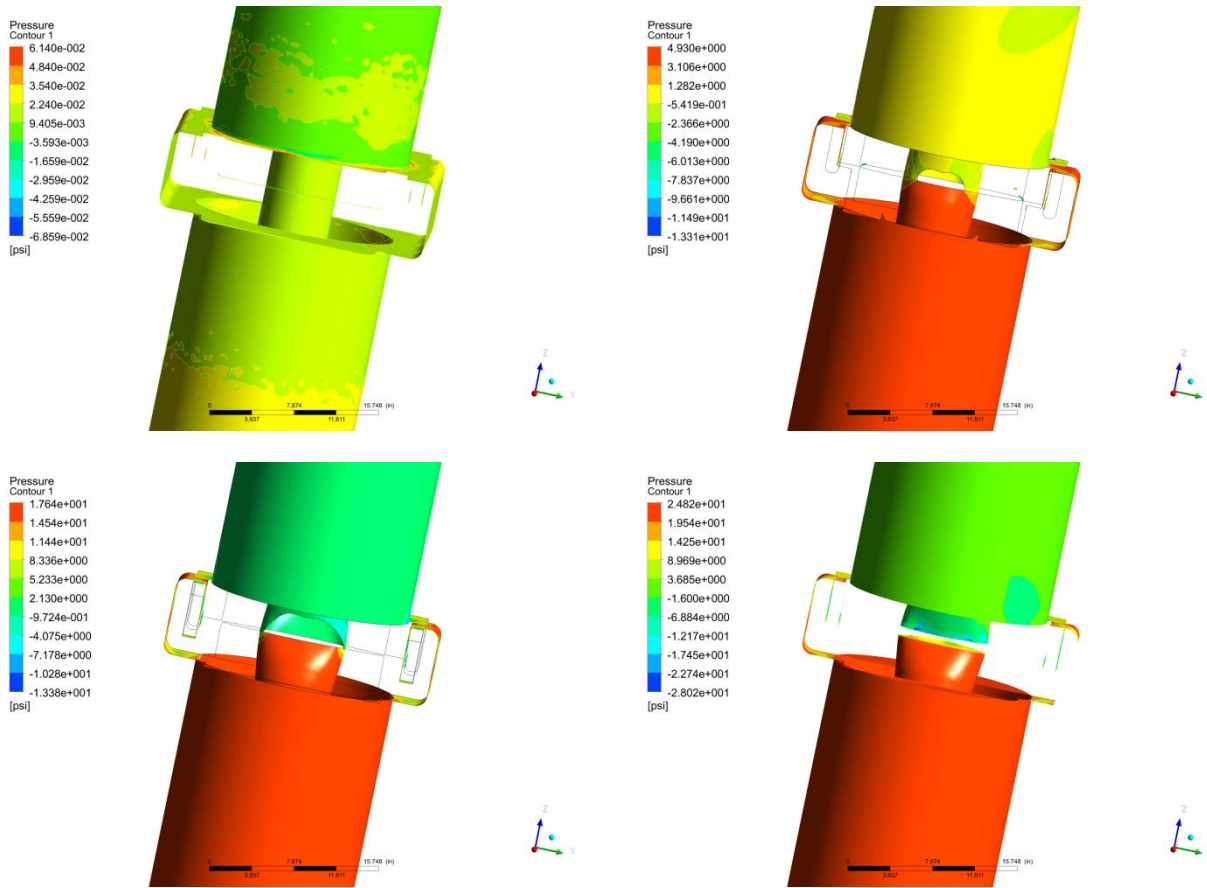
Figure 2-35. Dynamic Pressure on Casing and Drill Pipe
As the rams close, a greater pressure drop across the rams is observed.
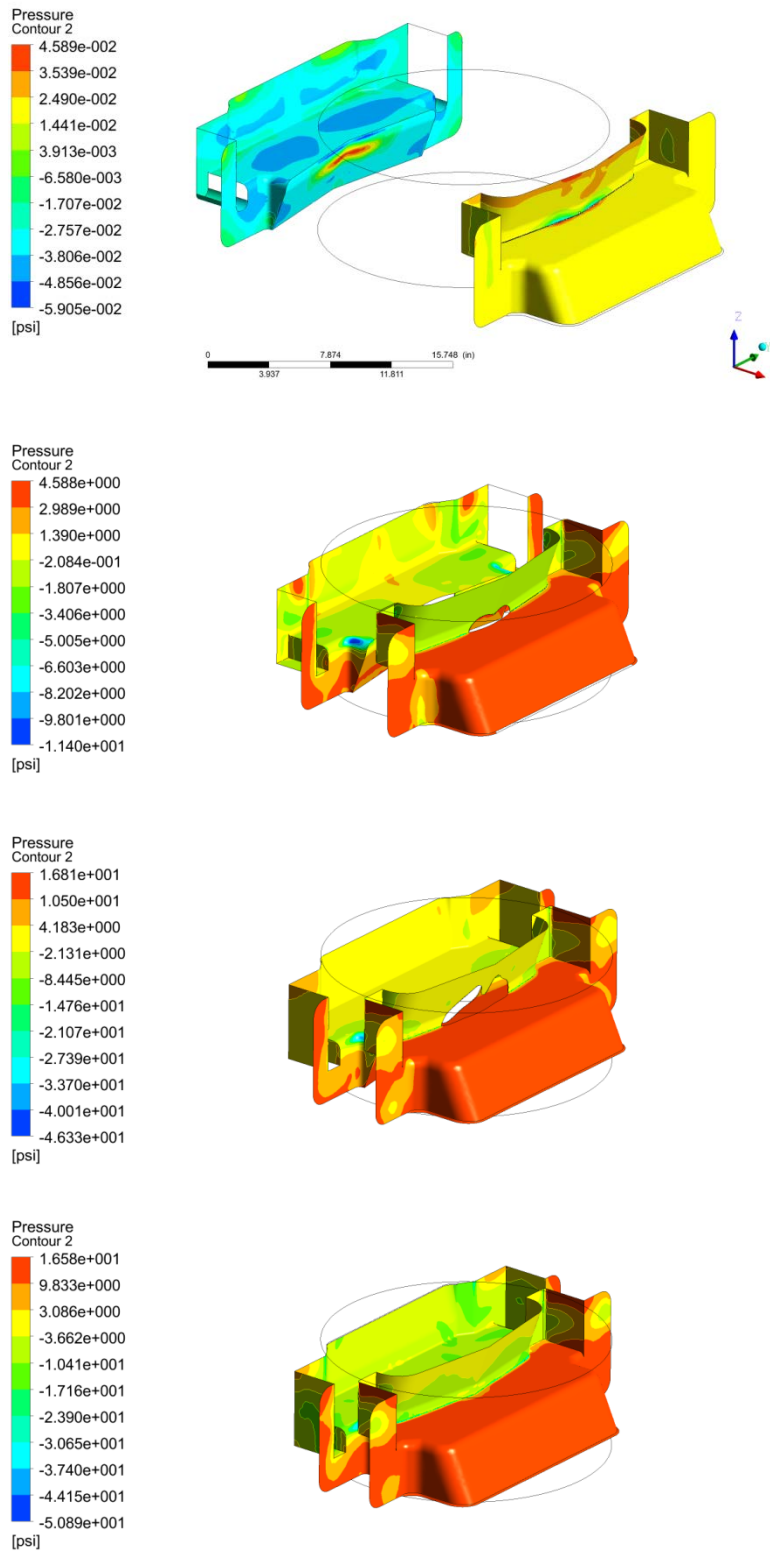
Figure 2-36. Dynamic Pressure on Ram Faces

*The local pressures on the ram faces are integrated in the direction aligned with the axis of motion closing
the rams in order to compute the hydrodynamic forces acting on the BOP rods.*

2.6.5 Tier 2 Analysis Force Summary

A summary of the force breakdown on the ram faces using the Tier 2 solution methodology is shown in Table 2.6 for each of the five discrete points during BOP closure (100%, 40%, 20%, 10%, and 5% fraction area opening). As indicated, the hydrostatic and mechanical shearing forces dominate the hydrodynamic forces generated by the fluid inertia impinging on the rams. The hydrostatic force is directly linked to the pressure magnitude in the annulus region, which was 11,000 psi for the baseline case and remained unchanged throughout the BOP closure. The lateral hydrodynamic forces tended to increase as the rams closed, due to acceleration of the fluid through the remaining cross-sectional area. Similarly, the axial hydrodynamic force increased as the BOP closed and the pressure difference across the BOP increased. Note that the axial hydrodynamics force is given as the total force on the BOP rams in the flow direction, whereas the other forces are given on a per ram basis.

Table 2.6. Ram Force Breakdown for Tier 2 Results
The hydrostatic and mechanical shearing forces are shown to dominate over the hydrodynamic force.

Open Area %	Ram Piston Rod Force (lbs, per ram)				Total Axial Hydrodynamic Force
	Shearing	Hydrostatic	Lateral Hydrodynamic	Total Rod Force	
5	85,550 (21.4%)	311,000 (77.9%)	2,608 (0.7%)	399,200	28,910
10	35,300 (10.2%)	311,000 (89.5%)	1,246 (0.4%)	347,600	13,970
20	494,000 (61.3%)	311,000 (38.6%)	278 (0.0%)	805,300	5,792
40	0 (0.0%)	311,000 (100.0%)	35 (0.0%)	311,100	2,701
100	0 (0.0%)	311,000 (100.0%)	5 (0.0%)	311,000	0

As in Tier 1 (Figure 2-37), the mechanical shearing force increased as the rams gained contact with the pipe, and continued up to a peak when the drill pipe sheared. The shearing force then decreased abruptly, before beginning to increase again as the rams crimped the sheared drill pipe. A comparison of Tier 1 and Tier 2 results indicates little change in the magnitude of the mechanical shearing force as a result of including hydrostatic effects in the FEA of the Tier 2 analysis. However, the pipe was shown to shear slightly faster for the Tier 2 case, as shown in Figure 2-37. This is likely related to the slight increase in the overall triaxiality under the hydrostatic pressure present in the Tier 2 analysis.
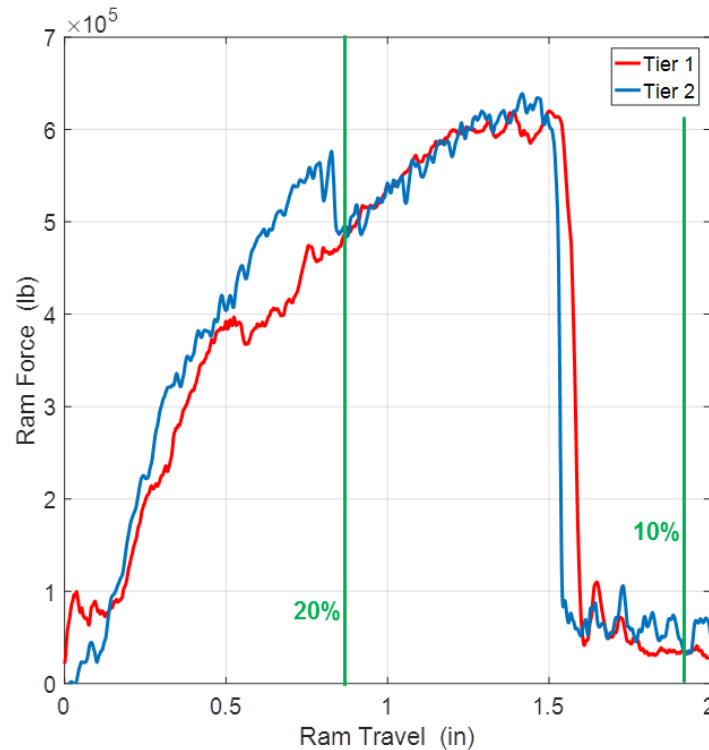
Figure 2-37. Shearing Force per Ram, Tier 1 vs. Tier 2

A comparison of Tier 1 and Tier 2 transient average shearing force per ram is shown. Distance on the x-axis is measured from the initial contact of the shear rams with the drill pipe. Locations of 20% and 10% fractional area opening are noted on graph.

2.7   Tier 3 (Lock-Step Coupled FEA/CFD) Modeling

The Tier 3 analysis is similar to that of Tier 2, with the exception that two-way coupling between the FEA and CFD occurs at the discrete update points of 40%, 20%, 10%, and 5% fractional area opening of the rams. FEA simulations were carried out with hydrostatic force applied from fully open down to 40% open area remaining, after which the simulation was paused. A CFD simulation was then performed, and the resulting spatial pressure distribution from the hydrodynamic forces applied to the FEA model. The FEA simulation then resumed until 20% open area remaining was reached, and the CFD force contribution was again solved and applied. This process was repeated for the 10% and 5% closure points.

Similar to the Tier 2 process, the velocity vectors and streamlines from the CFD were post-processed and examined to ensure fidelity of the solution at each stage. As an example, Figure 2-38 presents images of the velocity vectors and streamlines for the point of 5% fractional open area. Likewise, Figure 2-39 presents the spatial pressure distribution on the boundaries of the rams and pipe at 5% open. Recall that the pressure distributions are interpolated onto the FEA domain to incorporate two-way coupling of the fluid and shearing results. Figure 2-40 shows the distribution of the hydrodynamic forces from CFD at 5% opening. Note that this is the last position examined prior to closing, and has the largest total inertial force on the rams compared to earlier positions.
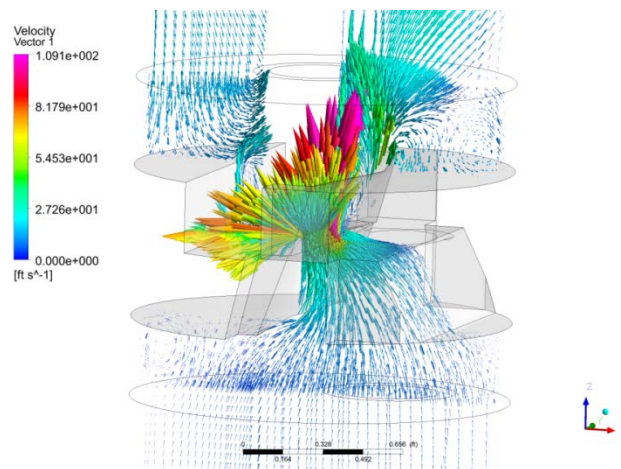
Figure 2-38. Tier 3 Flow Results (Velocity Vectors and Streamlines) from CFD at 5% Open Area
Velocity magnitudes and streamline contours are examined following simulations to ensure adequate resolution and domain extents.
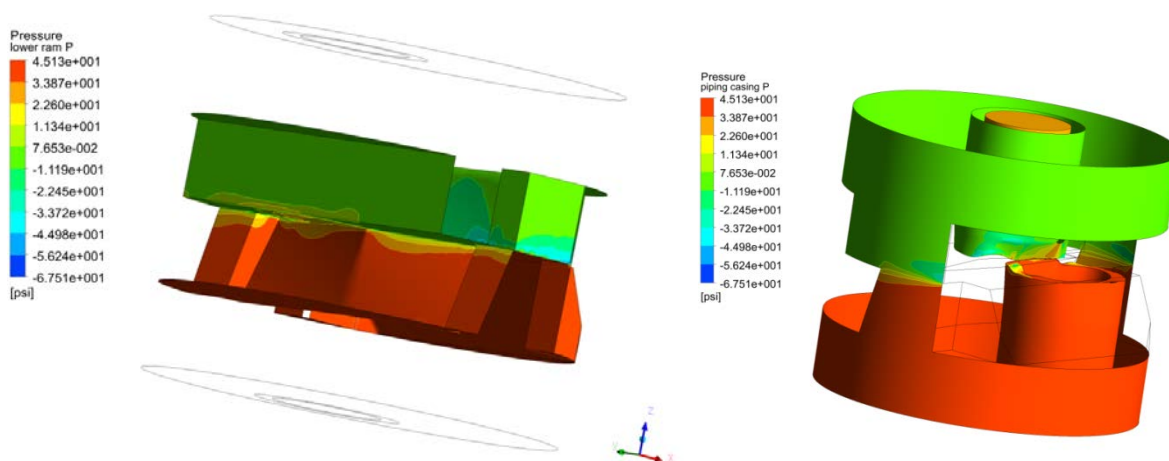
Figure 2-39**. Tier 3 Relative Pressure Results on Boundaries at 5% Open Area**
These figures show the pressure relative to the system absolute pressure (11,000 psia). The spatial pressure profiles are taken from CFD and applied to the FEA solution at each paused time point.
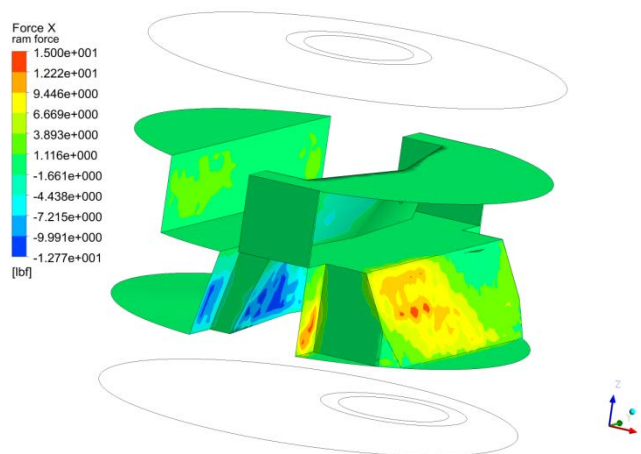
Figure 2-40. Tier 3 Hydrodynamic Force Results on Ram Faces at 5% Open Area
This image shows an example of the distribution of hydrodynamic force on the ram faces in the direction of ram motion.

A summary of the force breakdown on the ram faces using the Tier 3 solution methodology is shown in Table 2.7 for each of the five discrete points during BOP closure (100%, 40%, 20%, 10%, and 5% fractional area opening). Like the Tier 2 case, the hydrostatic and mechanical shearing forces dominate over the hydrodynamic forces generated by the fluid impinging on the rams. A comparison of the total rod force in Table 2.6 and Table 2.7 indicates less than a 2% change in the maximum force between the Tier 2 and Tier 3 results. Figure 2-41 confirms the marginal change in shearing force between the two tiers, 2 and 3, where the difference in maximum mechanical shearing force is less than 1% on average. This suggests one-way coupling (Tier 2) may be sufficient for inclusion of fluid effects to compute the total force the BOP must close against.

Table 2.7. Ram Force Breakdown for Tier 3 Results
The hydrostatic and mechanical shearing forces are shown to dominate over the hydrodynamic force.
Maximum total ram force is shown to be within 2% of the Tier 2 results.

Open Area %	Ram Piston Rod Force (lbs, per ram)				Total Axial Hydrodynamic Force
	Shearing	Hydrostatic	Lateral Hydrodynamic	Total Rod Force	
5	44,686 (12.5%)	311,000 (86.9%)	2,608 (0.7%)	358,000	28,910
10	53,595 (14.7%)	311,000 (85.2%)	1,246 (0.3%)	365,000	13,970
20	506,968 (62.0%)	311,000 (38.0%)	278 (0.0%)	818,000	11,580
40	0 (0.0%)	311,000 (100.0%)	35 (0.0%)	311,000	5,792
100	0 (0.0%)	311,000 (100.0%)	5 (0.0%)	311,000	0

Figure 2-41. Shearing Force per Ram, Tier 2 vs. Tier 3
This figure shows a comparison of the Tier 2 and Tier 3 transient average shearing force per ram. Distance on the x-axis is measured from the initial contact of the shear rams with the drill pipe. Locations of 20% and 10% fractional area opening are noted on the graph.

2.8   Tier 4 (Dynamically Coupled FEA/CFD) Modeling

Tier 4 simulations expand the two-way coupling strategy used in the Tier 3 simulations. Tier 4 simulations use the fully coupled FEA and CFD solvers in the LS-DYNA code to solve the complete fluid-structure interaction (FSI) problem. This allows for hydrodynamic forces on the solid FEA components to be updated on each grid cell dynamically as the simulation advances in time. Similarly, the solid component deformation and displacement will be reflected dynamically in an updated CFD mesh as the simulation progresses. Figure 2-42 shows an image of the FEA and CFD domains used for the Tier 4 simulations.

Due to the disparity in FEA and CFD simulation time step sizes ($\Delta t_{FEA} \approx 1\times10^{-7}$ s vs. $\Delta t_{CFD} \approx 1\times10^{-3}$ s), a loose FSI coupling scheme was used. In this scheme, the hydrodynamic forces are updated on each FEA solid element at each FEA time step. However, the solid component displacements are used to update the CFD mesh at every CFD time step (approximately every 1,000 FEA time steps). This results in approximately one million to 10 million hydrodynamic force updates for each FEA grid cell over the course of the simulation. As a point of reference, hydrodynamic forces are updated only five times over the course of a Tier 3 simulation. As a result, the significant amount of data transfer between the FEA and CFD solver in Tier 4 simulations results in very long simulation run times. Table 2.8 provides the estimated run time for the baseline Tier 4 simulations (assuming parallel computations on a Linux server with dual 8-core AMD Opteron 6100 series CPUs). Even with coarsening the drill pipe mesh resolution to the point where the FEA results may no longer be trusted and increasing the speed of the ram travel, the total simulation time remains prohibitively long.

Figure 2-42. Tier 4 FEA and CFD Simulation Discretized Domains
The left column shows FEA mesh components. The middle column shows the exterior surface of CFD mesh. The right column shows an internal slice of CFD/FEA mesh.

Table 2.8. Tier 4 Simulation Run Time

The fully dynamically coupled CFD/FEA model requires significant run times due to the large amount of data transfer between CFD and FEA solvers at each computational time step.

Nominal FEA Resolution (grid cells across drill pipe wall)	Ram Travel Speed	Number of FEA Elements	Number of CFD Elements	Anticipated Run Time (years)
2	1x	39,525	575,403	**7.25**
2	16x	39,525	575,403	**0.46**
8	1x	140,613	575,403	**18.42**
8	16x	140,613	575,403	**1.28**

In order to produce a functioning Tier 4 simulation that is capable of running to completion in a realistic amount of time, the three-dimensional (3D) solid elements of the drill pipe were replaced with two-dimensional (2D) shell elements, i.e., 2D quadrilateral elements with the appropriate material thickness. The switch to shell elements, the reduction in total element count, and the reduction in drill pipe resolution resulted in a simulation model that could be run in approximately one day. However, due to the changes in element type and reduction in numerical resolution, the reduced Tier 4 CFD/FEA model is no longer connected with the validated Tier 1 FEA model. Results are presented here for comparison with Tier 1-3 simulations, but the final force measurements and drill pipe failure predictions are considered to be not physically accurate.

Figure 2-43 through Figure 2-45 show the fluid flow in the annulus, hydrodynamic forces on the shear rams and drill pipe, and local Von Mises stress on the surface of the shear ram and drill pipe. Figure 2-46 shows the comparison of the force history on the shear rams from the validated Tier 1 FEA model and the Tier 4 CFD/FEA model. Phenomenologically, the flow in the annulus, hydrodynamic forces, and solid stresses appear to be similar to those shown in the Tier 1-3 simulations. However, the coarsened shell element mesh used to represent the drill pipe is incapable of accurately predicting when the drill pipe will fail. This leads to a significant overestimate of the force required to fail the drill pipe. For comparison purposes, Table 2.9 lists the breakdown of mechanical shearing, hydrostatic, and hydrodynamic forces for the Tier 4 simulation.
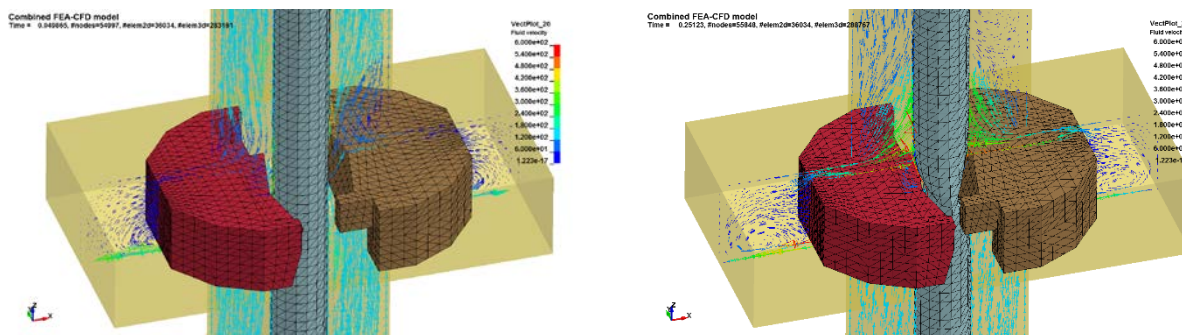
Figure 2-43. Tier 4 Flow Results
Fluid velocity vectors are shown at two different times, 26.9% open area to flow (left) and 10.3% open area to flow (right).
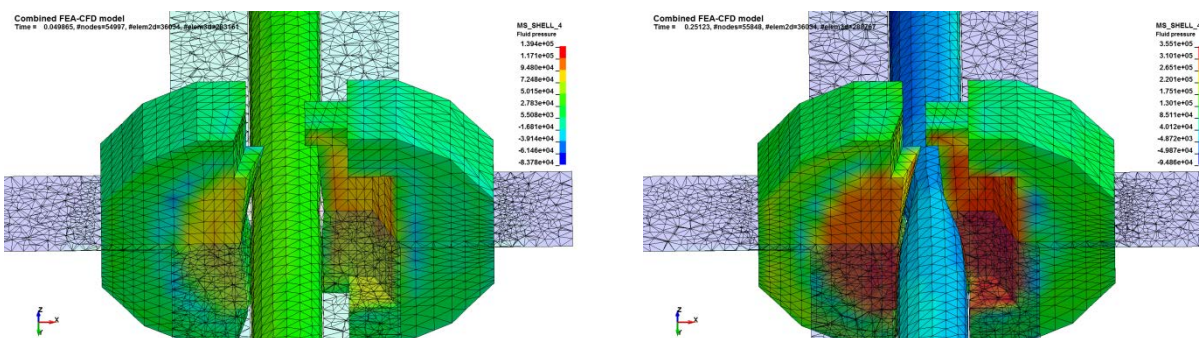
Figure 2-44. Tier 4 Relative Hydrodynamic Pressure Results on Rams and Drill Pipe

Local hydrodynamic pressures due to impinging annular flow on shear rams are shown at two different times, 26.9% open area to flow (left) and 10.3% open area to flow (right). Hydrostatic pressure was removed so that smaller hydrodynamic pressures are visible.
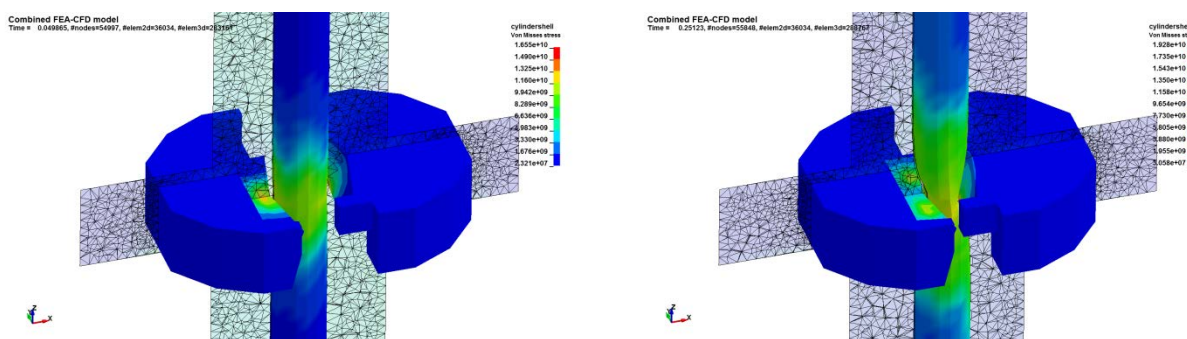
Figure 2-45. Tier 4 Shear Ram and Drill Pipe Stress Results

Von Mises stresses on the surfaces of the shear rams and drill pipes are shown at two different times, 26.9% open area to flow (left) and 10.3% open area to flow (right).
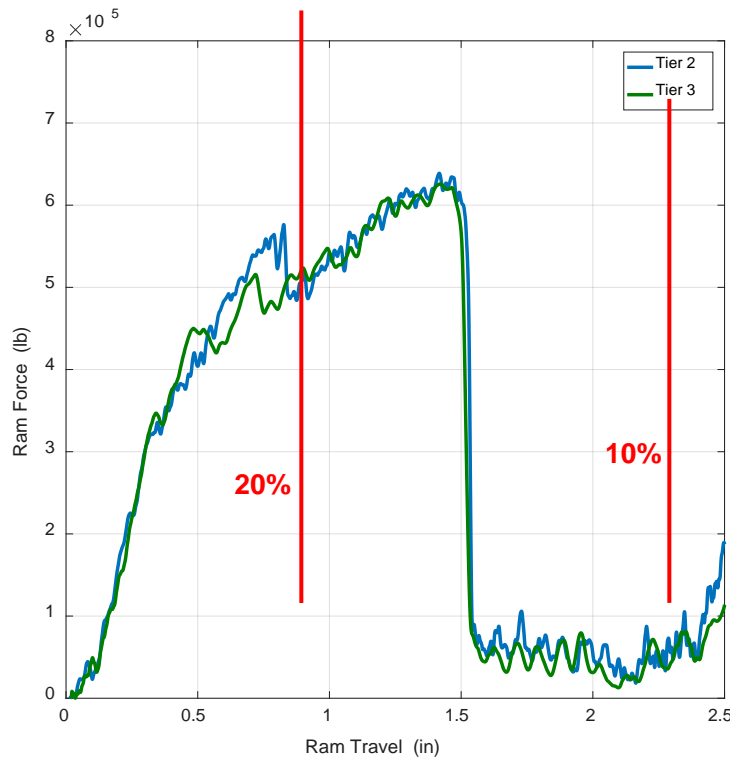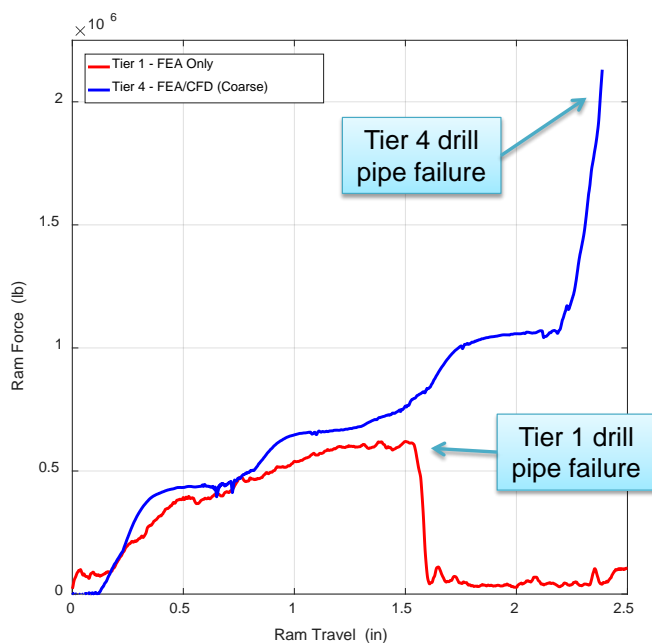

Figure 2-46. Shearing Force per Ram, Tier 1 vs. Tier 4

A comparison of the Tier 1 and Tier 4 transient average shearing force per ram. The distance on the x-axis is measured from the initial contact of the shear rams with the drill pipe.

Table 2.9. Ram Force Breakdown for Tier 4 Results

The coarsened resolution of the Tier 4 simulation results in an overprediction of the mechanical shearing force required to fail the drill pipe is shown. The shearing force for this case is unrealistically high, so the axial hydrodynamic force was not computed for this case. This simulation was initiated at an annulus open position of 30%; forces for greater annulus open areas are not available.

Open Area %	Ram Piston Rod Force (lbs, per ram)				Total Axial Hydrodynamic Force
	Shearing	Hydrostatic	Lateral Hydrodynamic	Total Rod Force	
5	2,133,280 (87.3%)	311,000 (12.7%)	157 (0.0%)	2,444,000	1,254
10	1,047,480 (77.1%)	311,000 (22.9%)	128 (0.0%)	1,358,000	856
20	636,140 (67.2%)	311,000 (32.8%)	70 (0.0%)	947,000	402
30	0 (0.0%)	311,000 (100.0%)	32 (0.0%)	311,000	~0

2.9 Summary

Section 2 describes the work that was performed to develop a recommended methodology for simulating the combined processes of structural deformations, structural failure, and fluid pressure changes that occur during the closure of BOP shear rams. Specifically, the following conclusions and recommendation can be stated.

- The Johnson-Cook material and failure model is recommended for use in the FEA simulations. This model provides the appropriate fidelity for modeling drill pipe as it undergoes the large deformations and fracture processes when sheared by the BOP shear rams.

- Methodologies for utilizing widely used commercial FEA and CFD software packages were developed for analysis approaches ranging from FEA-only to fully dynamically coupled structural and fluid dynamic simulations.

- Pressure waves are created as a result of the closing of the BOP, but the amplitude of theses waves is small compared to the overall hydrostatic pressure for the conditions considered here. These relatively small hydraulic transients, or "waterhammer," can be neglected with respect to BOP closure forces. The pressure differential across the BOP, however, can create considerable forces on the BOP rams in the flow direction that must be reacted by the BOP housing.

- The mechanical shearing forces calculated by Tiers 1, 2, and 3 are essentially equivalent and provide the largest contribution to the overall force required to close the rams on the flowing conditions analyzed.

- The Tier 2 methodology in which the FEA and CFD simulations are joined in a one-way coupling is shown to be the appropriate analysis approach to BOP shear ram simulations. The shear ram forces computed with the Tier 2 approach are in close agreement with those of the more complicated Tier 3 approach, but the Tier 2 solutions are obtained much faster than those of Tier 3.

3. PARAMETRIC ANALYSIS

The initial efforts of this project focused on developing an optimized and validated approach to simulating forces imparted on blind shear rams closing on a flowing well. Given the down-selected Tier 2 simulation methodology (see Section 2.4 for details on the tiered simulation approaches), the next goal of the project was to perform a parametric study. Six different physical parameters were selected to be varied. For each parameter variation, the remaining conditions defined in the baseline case were held fixed. A summary of the parameter variations examined is provided in Table 3.1. In this section, the mechanical, net hydrostatic, hydrodynamic, and total force on the rams are reported using the Tier 2 simulation methodology.

Table 3.1. Parameter Variation Matrix
For each parameter variation considered, the remaining parameters were held fixed at the baseline case conditions.

PARAMETRIC CASE	DESCRIPTION
Baseline	Baseline conditions (see Table 2.1)
1	Ram geometry, OEM #1
2	Ram geometry, OEM #2
3	Ram geometry, OEM #3
4	Closing time = 30 s
5	Closing time = 8 s
6	Flow rate = 60,000 stb/d
7	Flow rate = 30,000 stb/d
8	Flowing pressure = 7,000 psi
9	Flowing pressure = 5,000 psi
10	Flowing pressure = 3,000 psi
11	Fluid property (API 26, GOR 800 scf/stb)
12	Tubing geometry (Drill pipe 5.5 inch)
13	Tubing geometry (Drill pipe 5.875 inch)

3.1   OEM Variations – Parametric Cases 1 to 3

The first three parametric runs conducted examined the effects of different ram geometries. All conditions from the baseline case were held fixed, i.e., drill pipe, flow rate, fluid properties, etc., and only the ram geometry was replaced with one of three different ram geometries provided by the OEMs. Figure 3-1 shows a comparison of the three different OEM geometries used in the respective parametric runs. Note that the detailed shear ram geometry is proprietary information to each OEM and is covered by a nondisclosure agreement between BSEE, SwRI, and the OEMs. In general, the OEM #1 and OEM #2 ram geometries have similar overlapping V-style blade designs. The OEM #3 rams use V-style blades as well, but are designed as such that there are more points of contact on the drill pipe than the other two OEMs. Additional details on the differences in the cutting edge of the OEM ram geometries with respect to the baseline conditions, where an approximated OEM #1 ram geometry was used, are discussed later.

Image Redacted

Image Redacted

Image Redacted

Figure 3-1. Comparison of OEM Shear Ram Geometries
Shear ram geometries are shown for OEM #1 (top), OEM #2 (middle), and OEM #3 (bottom).

The nominal closing time of an actual installed BOP was taken as 45 seconds for the baseline case, which corresponds to the rams having a travel speed of 0.23 in/s. Recall that for the approximate ram geometry and drill pipe material modeled in the baseline investigations described in Section 2, it was shown that the total ram force was virtually the same for shear ram closing times ranging from 45 s to 2.8 s (ram speeds of 0.23 in/s to 3.7 in/s). The choice of ram speed, however, strongly affects the computational time required for a simulation. So, a ram speed of 1.87 in/s (closing time of 5.6 s), which is a factor of eight greater than the actual baseline speed, was selected as an appropriate compromise between simulation fidelity and computational turn-around time for the remainder of the parametric runs (except for those cases with a specified closing time).

Figure 3-2 through Figure 3-4 show images from the FEA simulations at four different times during the shearing process. These correspond to 20%, 10%, and 5% of the annulus flow open area and at the point of maximum mechanical shearing force. In general, the shear rams come into contact with the drill pipe when the annulus cross section is reduced to approximately 25% of its fully open area for all of the cases.
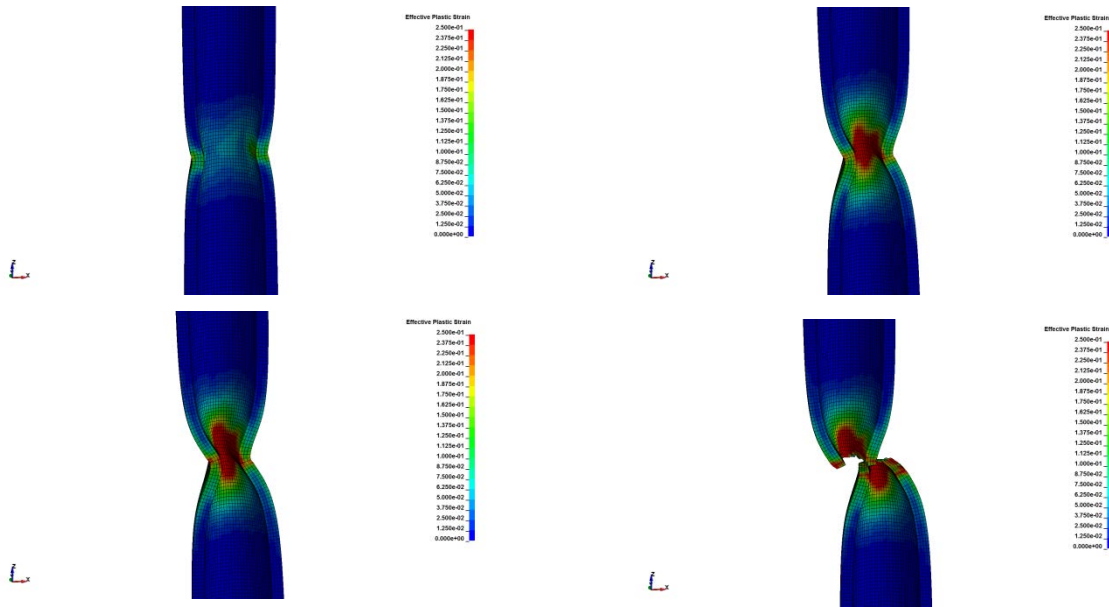
Figure 3-2. Images from the FEA Simulation of the OEM #1 Shear Ram Geometry
Proprietary ram designs have been redacted from all images.
Images show the effective plastic (permanent) deformation to the drill pipe at four different times during the ram closure corresponding to the following annulus open area ratios: 20% (top-left), 10% (top-right), 7% (bottom-left), and 5% (bottom-right). The maximum shear force occurs at 7.0% annulus open area for the OEM #1 geometry. The color scale indicates effective plastic deformation, and has a range of 0.0 (blue) to 0.25 (red).
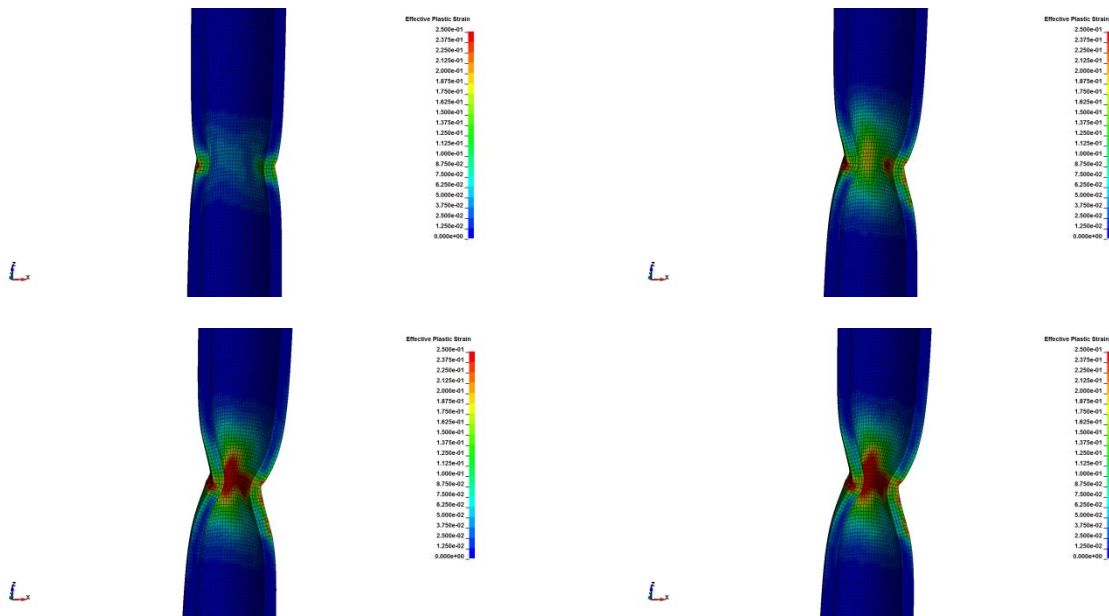
Figure 3-3. Images from the FEA Simulation of the OEM #2 Shear Ram Geometry
Proprietary ram designs have been redacted from all images.
Images show the effective plastic (permanent) deformation to the drill pipe at four different times during the ram closure corresponding to the following annulus open area ratios: 20% (top-left), 10% (top-right), 5% (bottom-left), and 3.7% (bottom-right). The maximum shear force occurs at 3.7% annulus open area for the OEM #2 geometry. The color scale indicates effective plastic deformation, and has a range of 0.0 (blue) to 0.25 (red).
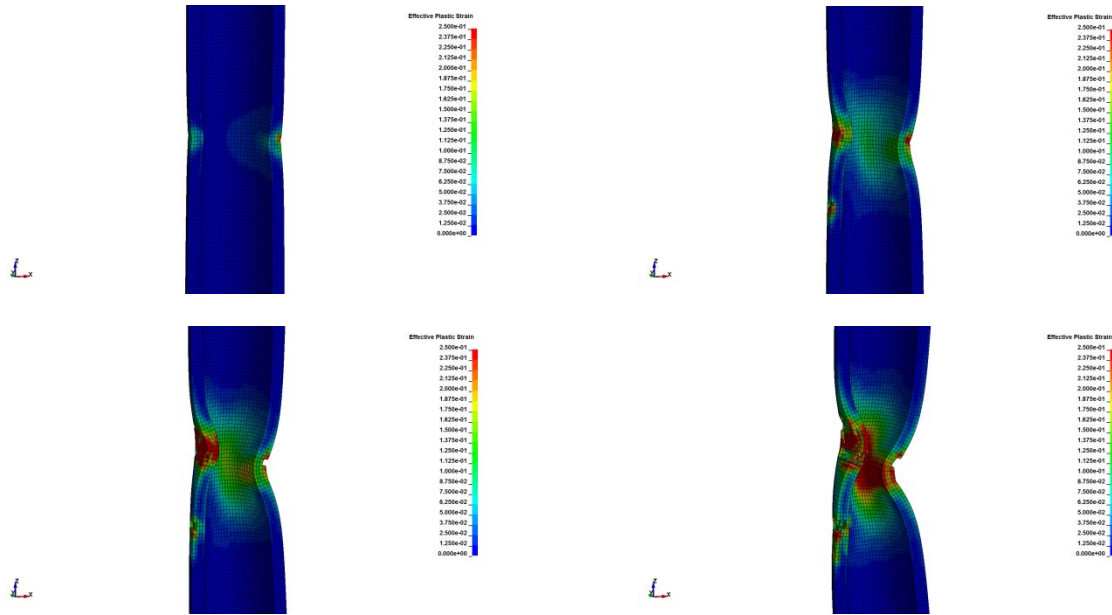
Figure 3-4. Images from the FEA Simulation of the OEM #3 Shear Ram Geometry
Proprietary ram designs have been redacted from all images.
Images show the effective plastic (permanent) deformation to the drill pipe at four different times during the ram closure corresponding to the following annulus open area ratios: 20% (top-left), 10% (top-right), 5% (bottom-left), and 1% (bottom-right). The maximum shear force occurs at 1.0% annulus open area for the OEM #3 geometry. The color scale indicates effective plastic deformation, and has a range of 0.0 (blue) to 0.25 (red).

Figure 3-5 shows a comparison of the mechanical shearing force (per ram) as a function of distance traveled. The origin of the *x*-axis for each simulation starts when the shear rams are just beginning to touch the drill pipe. All three OEM shear ram geometries tested required about 1.2-1.3 million pounds of mechanical force (per ram) to shear the drill pipe. The OEM #1 and OEM #2 shear rams produced a failure after approximately 2.1 inches of travel (per ram) once contact was made, while the OEM #3 rams traveled almost 2.5 inches (per ram) before the drill pipe failed. With the exception of the total ram travel required to shear the drill pipe, the simulation results for the total mechanical force required to shear the pipe are considered to be similar for each of the geometries examined here.
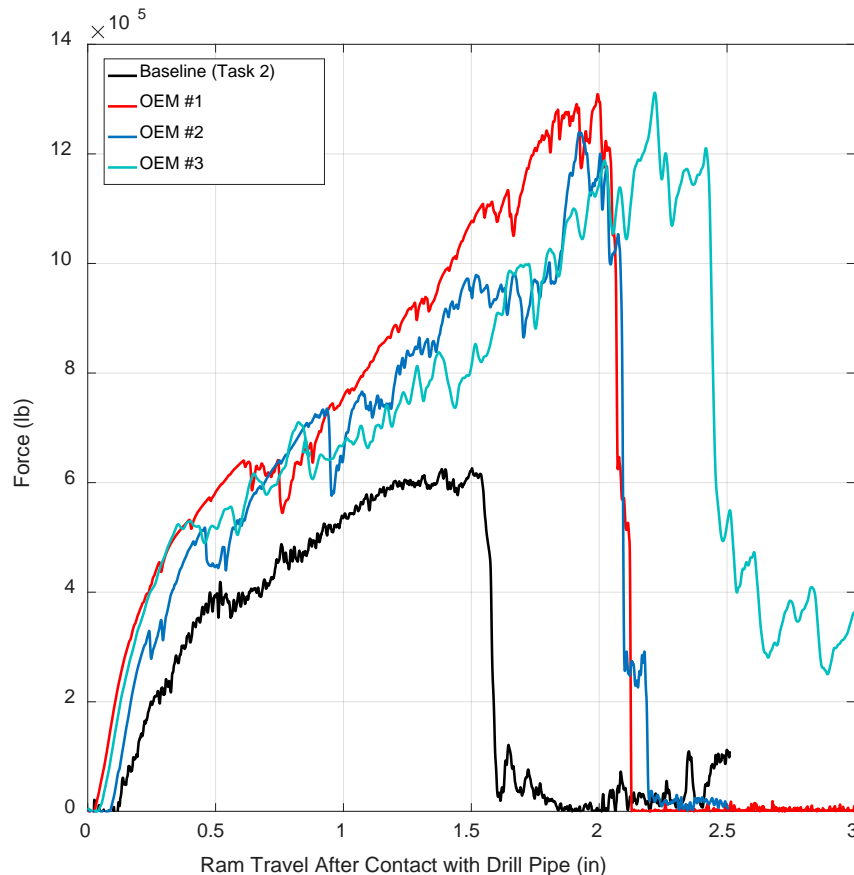
Figure 3-5. Comparison of Mechanical Shearing Force as a Function of Shear Ram Travel
All three OEM shear ram geometries show maximum mechanical shearing forces of 1.2-1.3 million pounds (per ram). The speed of the rams was specified as 1.87 in/s for these four simulations. The differences between the approximated baseline geometry and the OEM #1 geometry are described in Figure 3-6 and Figure 3-7.

The primary differences between the approximate ram geometry used in the baseline simulations and the OEM #1 ram geometry are the blade profile and the angles of the cutting edges that contact the drill pipe. Figure 3-6 shows enhanced views of the bottom shear ram blade for the approximate ram geometry used in the baseline simulations. Figure 3-7 shows similar views of the OEM #1 geometry. It can be seen that the OEM #1 ram geometry has a blunter cutting edge than the baseline geometry. This difference in the cutting surface profile from the baseline approximated geometry angle is echoed for all of the OEM-provided geometries.
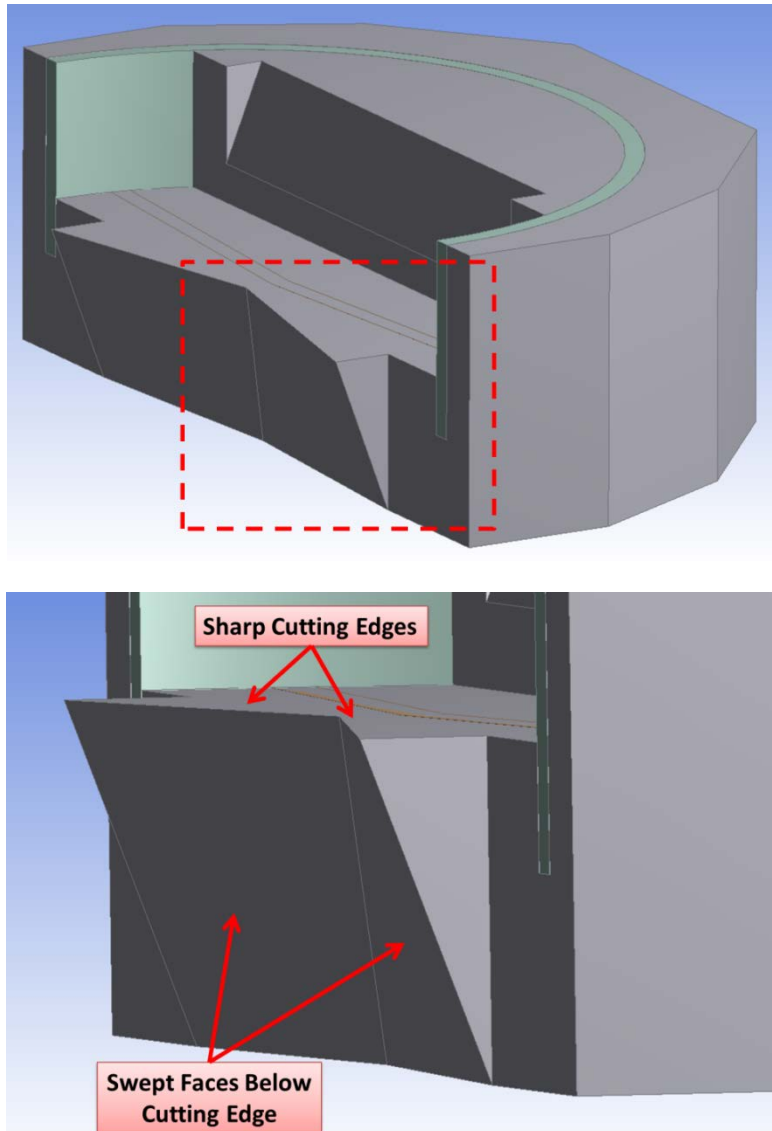
Figure 3-6. Approximated Shear Ram Geometry Used for the Baseline Investigations
This figure shows an enhanced view of the bottom shear ram cutting edge surface for the baseline geometry. This geometry, used in the baseline simulations, was originally intended to approximate the OEM #1 ram geometry. However, the sharp edge of the approximated ram geometry differs from all of the OEM-provided geometries.
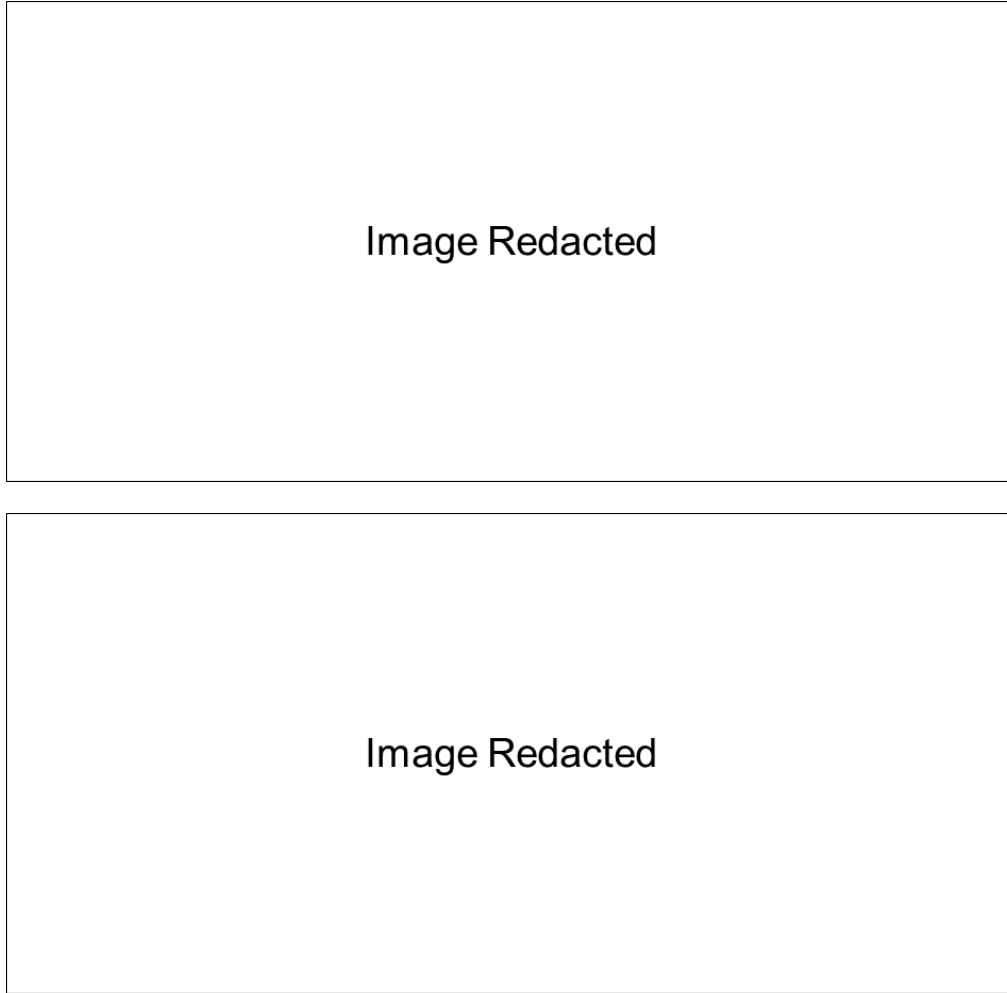
Figure 3-7. OEM #1 Shear Ram Geometry

This figure shows an enhanced view of the bottom shear ram cutting edge surface for the OEM #1 ram geometry. In contrast to the baseline approximated geometry, the cutting edge has a more flattened angle.

Figure 3-8 and Figure 3-9 show comparisons of the FEA simulations using the approximate and OEM #1 ram geometries at 20% and 10% annulus open area. In Figure 3-8, it can be seen that the sharper cutting edge (top image) begins to cut into and separate the drill pipe at a very early stage by imparting a fracture on the outside of the pipe. The blunter geometry (bottom image) is still only compressing the pipe at that stage. Figure 3-9 shows that the sharp cutting edge (top image) of the approximated geometry has almost entirely cut through the drill pipe. Conversely, the blunter cutting edge (bottom image) continues to pinch the drill pipe at this stage.
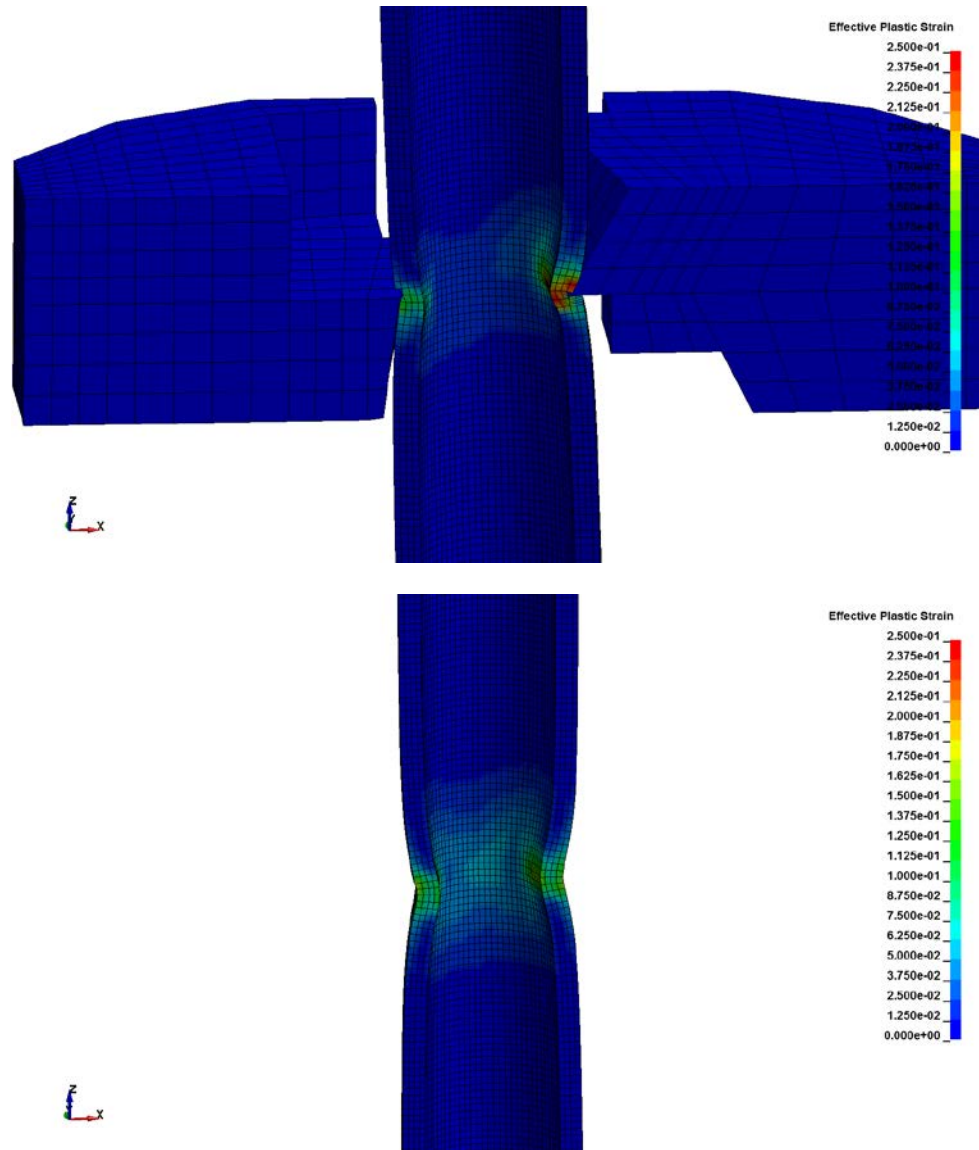
Figure 3-8. Comparison of Sharp (approximated OEM #1 ram geometry) and Chamfered (OEM #1 geometry) Cutting Edge Shearing at 20% Open to Flow Area Remaining
<u>**Proprietary ram designs have been redacted from all images.**</u>
The sharp cutting edge of the approximated geometry (top) can be seen cutting into the drill pipe at an early stage in the shearing process, while the chamfered cutting edges (bottom) are compressing the pipe instead of cutting it.
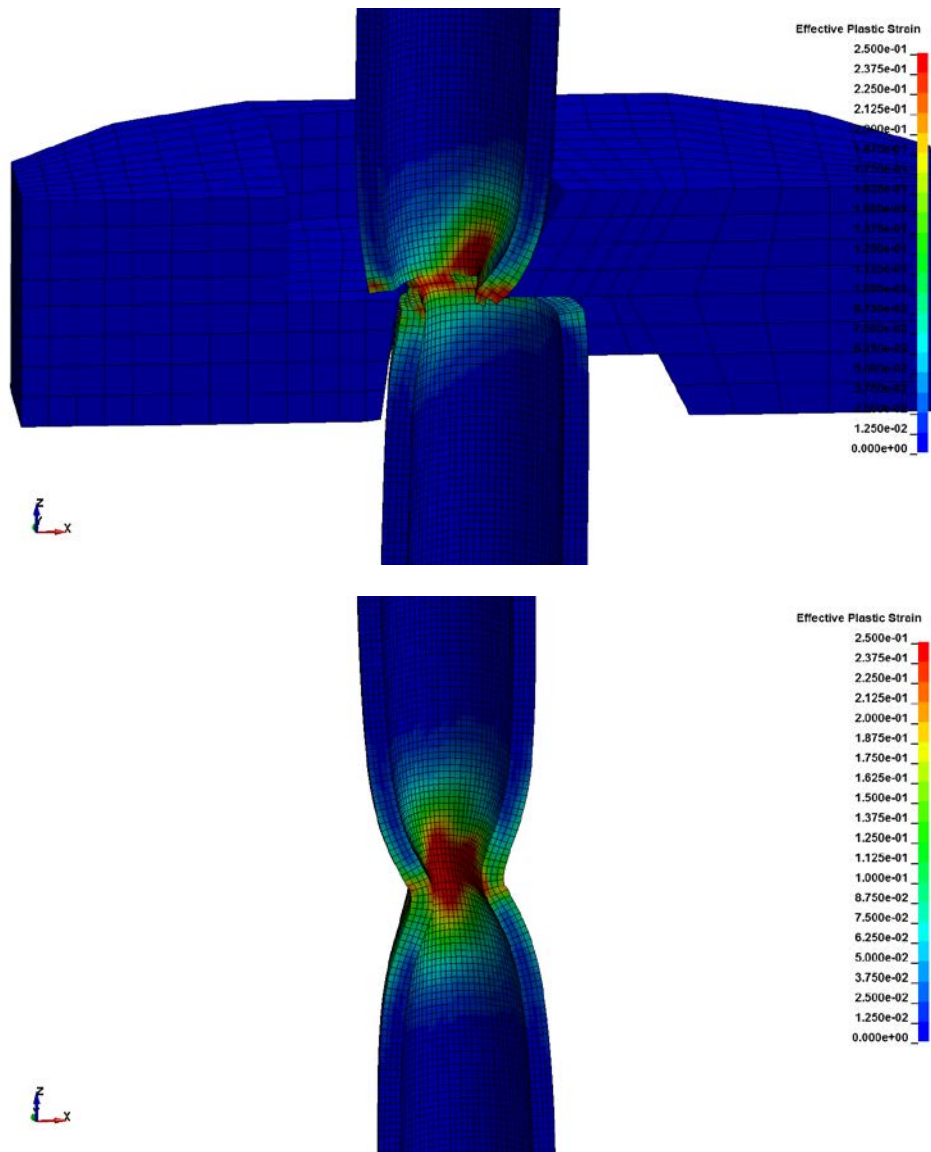
**Figure 3-9. Comparison of Sharp (approximated OEM #1 ram geometry) and Chamfered (OEM #1
geometry) Cutting Edge Shearing at 10% Open to Flow Area Remaining**
<u>**Proprietary ram designs have been redacted from all images.**</u>
*Similar to the 20% area open to flow remaining results, it can be seen that the sharper cutting edge (top)
results in a different shearing mechanism than the chamfered cutting edges (bottom) of the
OEM-provided geometry.*

Due to the differences in how the drill pipe is sheared and the mechanical forces required
between the baseline approximate shear ram geometry and the OEM-provided shear ram
geometries, it was recommended to BSEE that all subsequent parametric runs (Cases 4-13) use
the OEM #1 ram geometry instead of the approximated geometry used in the baseline case. This
modification was approved by BSEE on November 22, 2016.

In addition to the mechanical shearing forces, net hydrostatic and hydrodynamic forces
for each of the different geometry cases have also been computed. Following the Tier 2 solution
methodology outlined in Section 2, CFD calculations were carried out at five discrete stages of

valve closure (100%, 40%, 20%, and 5% annulus open area and at the position of maximum shear force) using one-way fluid-structure-interaction coupling analyses. The complete results, including the total required force at each position, are shown in Table 3.2 through Table 3.4.

Table 3.2. Force on Rams (lbf) – OEM #1 Geometry
The hydrostatic and mechanical shearing forces are shown to dominate over the hydrodynamic force. The maximum total required ram force is computed to be 1.59 million lbf.

Open Area %	Ram Piston Rod Force (lbs, per ram)				Total Axial Hydrodynamic Force
	Shearing	Hydrostatic	Lateral Hydrodynamic	Total Rod Force	
5	0 (0.0%)	311,000 (99.4%)	1,814 (0.6%)	312,800	14,840
7.0 (max shear)	1,281,000 (80.4%)	311,000 (19.5%)	2,211 (0.1%)	1,594,000	30,290
10	1,101,000 (77.9%)	311,000 (22.0%)	1,247 (0.1%)	1,413,000	22,600
20	613,600 (66.4%)	311,000 (33.6%)	167 (0.0%)	924,900	7,352
40	0 (0.0%)	311,000 (100.0%)	15 (0.0%)	311,000	1,691
100	0 (0.0%)	311,000 (100.0%)	3 (0.0%)	311,000	0

Table 3.3. Force on Rams (lbf) – OEM #2 Geometry
The hydrostatic and mechanical shearing forces are shown to dominate over the hydrodynamic force. The maximum total required ram force is computed to be 1.53 million lbf.

Open Area %	Ram Piston Rod Force (lbs, per ram)				Total Axial Hydrodynamic Force
	Shearing	Hydrostatic	Lateral Hydrodynamic	Total Rod Force	
3.7 (max shear)	1,239,000 (81.1%)	285,600 (18.7%)	2,874 (0.2%)	1,528,000	19,710
5	965,700 (77.1%)	285,600 (22.8%)	1,788 (0.1%)	1,253,000	9,795
10	923,400 (76.3%)	285,600 (23.6%)	1,451 (0.1%)	1,211,000	7,032
20	639,300 (69.1%)	285,600 (30.9%)	766 (0.1%)	925,700	1,248
40	0 (0.0%)	285,600 (100.0%)	78 (0.0%)	285,700	619
100	0 (0.0%)	285,600 (100.0%)	8 (0.0%)	285,600	0

Table 3.4. Force on Rams (lbf) – OEM #3 Geometry
The hydrostatic and mechanical shearing forces are shown to dominate over the hydrodynamic force. The maximum total required ram force is computed to be 1.55 million lbf.

Open Area %	Ram Piston Rod Force (lbs, per ram)				Total Axial Hydrodynamic Force
	Shearing	Hydrostatic	Lateral Hydrodynamic	Total Rod Force	
1.0 (max shear)	1,336,000 (86.2%)	212,500 (13.7%)	850 (0.1%)	1,550,000	52,130
5	791,900 (78.8%)	212,500 (21.1%)	619 (0.1%)	1,005,000	27,490
10	664,300 (75.7%)	212,500 (24.2%)	314 (0.0%)	877,200	14,920
20	505,900 (70.4%)	212,500 (29.6%)	100 (0.0%)	718,500	7,481
40	0 (0.0%)	212500 (100.0%)	24 (0.0%)	212,600	1,554
100	0 (0.0%)	212500 (100.0%)	1 (0.0%)	212,500	0

For all OEMs, the total force required was dominated by the mechanical shearing force, ranging from 66.4 to 86.2% of the total force contribution for the given drill pipe and flowing

pressure. Next, the net hydrostatic forces (related to the baseline case flowing pressure of 11,000 psi) contributed 18.7-33.6% of the total force required. The hydrodynamic contribution to the overall force remained very small. For all points simulated, it remained less than 1%, often in the range of 0.0-0.2% of the total force contribution. Finally, the total axial hydrodynamic force in each case increased as the flow area decreased. In each case the maximum axial hydrodynamic force occurred at the same ram position where the maximum shear force occurred.

For the OEM #2 and OEM #3 geometries, the hydrodynamic force increased as the valve continued to close past the 5% open area position. This is expected, as the pressure rises with increasing valve restriction. In the OEM #1 case, the hydrodynamic force increased up to the point of maximum shear (7%), whereupon a decrease was observed. This response was unexpected and these simulation results were analyzed to reveal the underlying causes.

Images of the rams, pipe, and annulus fluid pressure contours for the OEM #1 ram positions just before and just after the pipe fracture event are shown in Figure 3-10. It was found that at the 7% annulus open area ram position, large portions of the ram and pipe surfaces are in intimate contact and fluid pressure cannot directly act on these areas. At the 5% annulus open area ram position (after the pipe fractures), the pipe and rams are separated and the entire outer surface area of the pipe can be acted on by the fluid. However, the overall pressure acting on the pipe upstream of the rams is greater when the rams are at the 7% annulus open area position than at the 5% annulus open area position. The net effect of the combination of the available surface area and the local pressure results in a greater contribution from the hydrodynamic pressure at the 7% position than at the 5% position.

To summarize this set of parametric cases, the following are observations based on the simulations of the three different OEM geometries.

- The sharp edge defined for the baseline simulations resulted in a maximum total required force of about 626,200 lbf to close the rams. The simulations with the OEM-provided ram geometries with chamfered cutting edges resulted in a predicted maximum total force range of 1,240,000-1,340,000 lbf required to close the rams. Clearly, using a sharp cutting edge in BOP closure analyses results in simulations that underpredict the mechanical forces required to shear the drill pipe in consideration.

- The mechanical force required to shear the drill pipe is the dominant contributor to the total required ram force. The net hydrostatic contribution is smaller, but non-negligible and is dependent upon the magnitude of the well flowing pressure. Finally, the hydrodynamic component is very small compared with the mechanical and hydrostatic force components.

- The details of the force profile with respect to the ram position for the three OEM ram geometries are slightly different. The simulations show that the drill pipe fracture event is relatively sudden and occurs when the rams are 93 to 99% closed, depending on the OEM ram shape.

- In spite of the slight differences in the ram position at the time the drill pipe is sheared, the peak forces required to actuate the rams for all three OEMS are roughly equivalent.
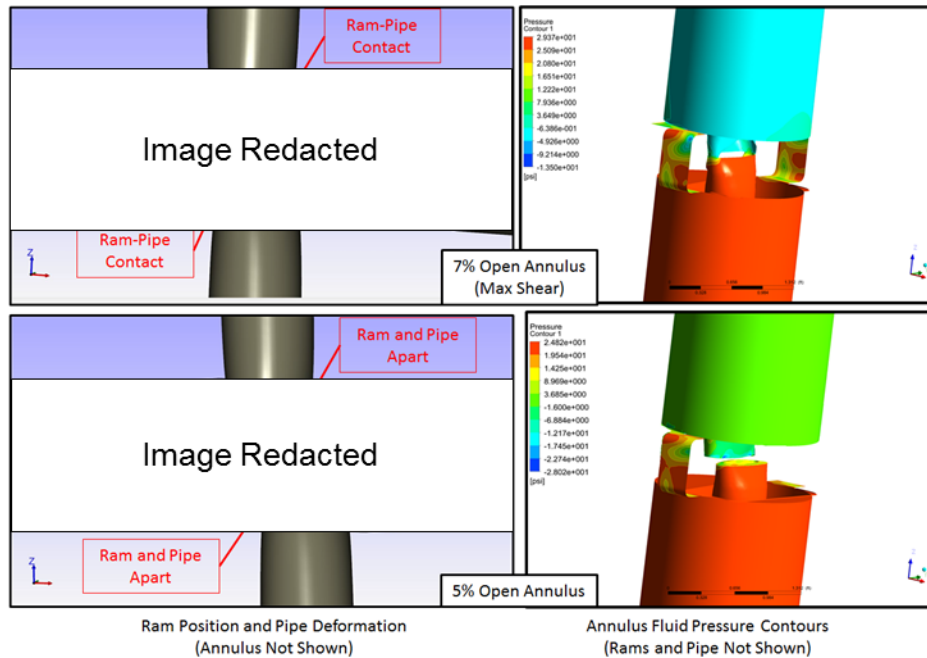
Figure 3-10. Ram and Pipe Interaction at 7% Open Area Versus 5% Open Area for OEM #1 Ram Geometry
Proprietary ram designs have been redacted from all images.
At the point of maximum shear force (7% annulus open area), the ram faces and the pipe are in direct contact. At 5% annulus open area (soon after the pipe ruptures), the pipe and ram faces are separated. The CFD simulations show that the overall fluid pressure near the ram and pipe is greater at the 7% open position than at the 5% open position.

3.2   Closing Speed Sensitivity Study – Parametric Cases 4 and 5

The simulations of the baseline investigations described in Section 2 showed that the shear force profiles for the approximated ram geometry were similar for closure times of 45 s to 2.8 s (ram speeds of 0.23 in/s to 3.7 in/s, respectively). The first three parametric cases reported showed that the shearing forces for the OEM-supplied ram geometries were significantly greater than for the approximated ram geometry. This observation led to the decision to execute all of the remaining simulations with the OEM #1 ram geometry. So, in addition to the ram closure times of 30 s and 8 s required by parametric cases 4 and 5, ram closure times of 45 s and 5.6 s were simulated with the OEM #1 ram geometry. This set of runs allows for the sensitivity of the ram closure forces to closure speed to be thoroughly assessed with consistent ram geometry.

Selected images from the FEA simulations of these four closing speeds are shown in Figure 3-11 through Figure 3-15. The responses of the pipe to shearing, as seen in these images, all look very similar from a qualitative standpoint. The same mode of failure is observed in each of these simulations; namely, as the drill pipe is compressed, a final rapid failure occurs slightly after two inches of ram travel from the ram's initial contact with the pipe. Figure 3-15 shows the mechanical force exerted by the shear rams as a function of distance travelled (per ram) for these four ram speeds. The shearing forces for the 5.6-s and 8-s closure times tend to be slightly greater than the forces for the 30 s and 45 s closure times; however, it is seen that the closing speed for this set of parameters (i.e., drill pipe material, cutting edge geometry, etc.) does not strongly influence mechanical shearing requirements. This is similar to the observations made for the baseline simulations.
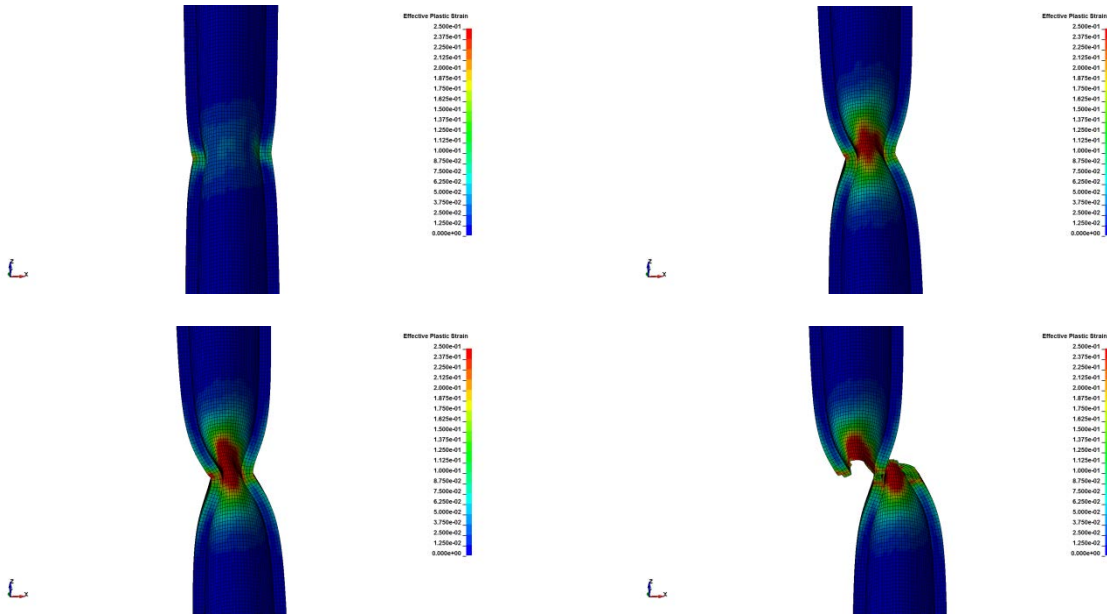
Figure 3-11. Images from the FEA Simulation of the 45-s Closing Time Simulation
Proprietary ram designs have been redacted from all images.

Images show the effective plastic (permanent) deformation to the drill pipe at four different times during the ram closure corresponding to the following annulus open area ratios: 20% (top-left), 10% (top-right), 7.7% (bottom-left), and 5% (bottom-right). The maximum shear force occurs at 7.7% annulus open area for the OEM #1 geometry. The color scale indicates effective plastic deformation, and has a range of 0.0 (blue) to 0.25 (red).
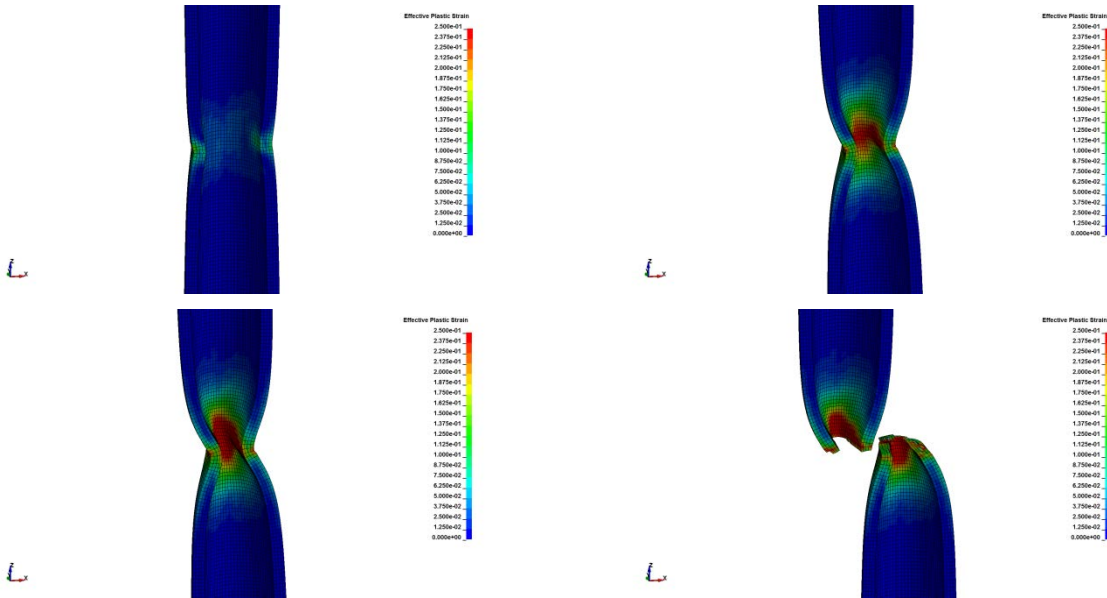
Figure 3-12. Images from the FEA Simulation of the 30-s Closing Time Simulation
Proprietary ram designs have been redacted from all images.

Images show the effective plastic (permanent) deformation to the drill pipe at four different times during the ram closure corresponding to the following annulus open area ratios: 20% (top-left), 10% (top-right), 7.5% (bottom-left), and 5% (bottom-right). The maximum shear force occurs at 7.5% annulus open area for the OEM #1 geometry. The color scale indicates effective plastic deformation, and has a range of 0.0 (blue) to 0.25 (red).
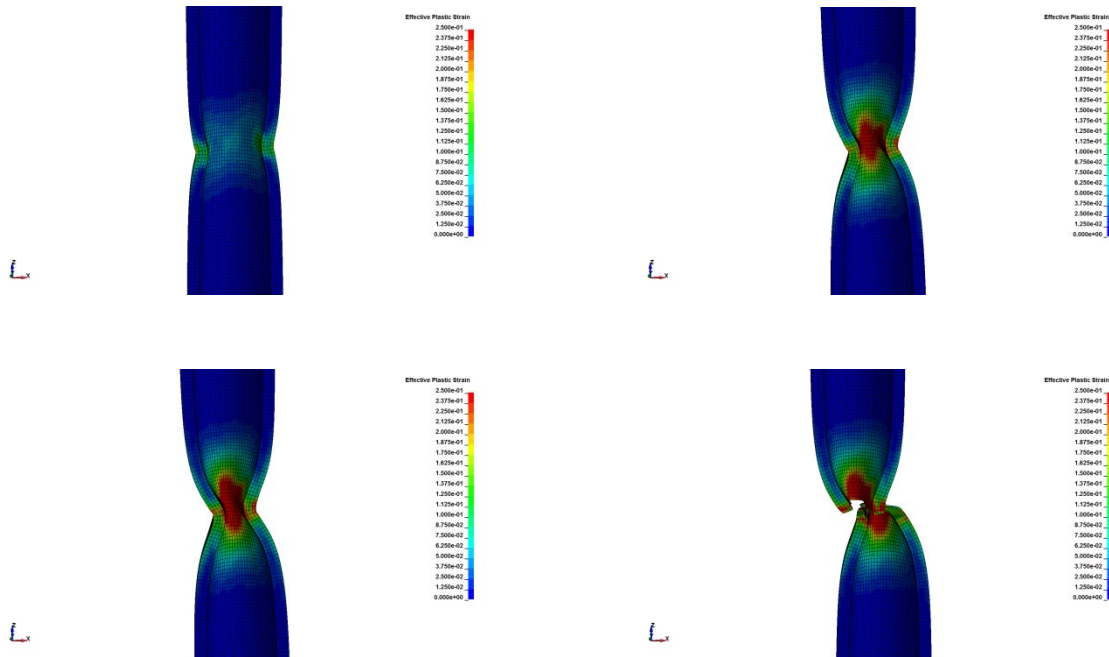
Figure 3-13. Images from the FEA Simulation of the 8-s Closing Time Simulation
Proprietary ram designs have been redacted from all images.
Images show the effective plastic (permanent) deformation to the drill pipe at four different times during the ram closure corresponding to the following annulus open area ratios: 20% (top-left), 10% (top-right), 7.4% (bottom-left), and 5% (bottom-right). The maximum shear force occurs at 7.4% annulus open area for the OEM #1 geometry. The color scale indicates effective plastic deformation, and has a range of 0.0 (blue) to 0.25 (red).
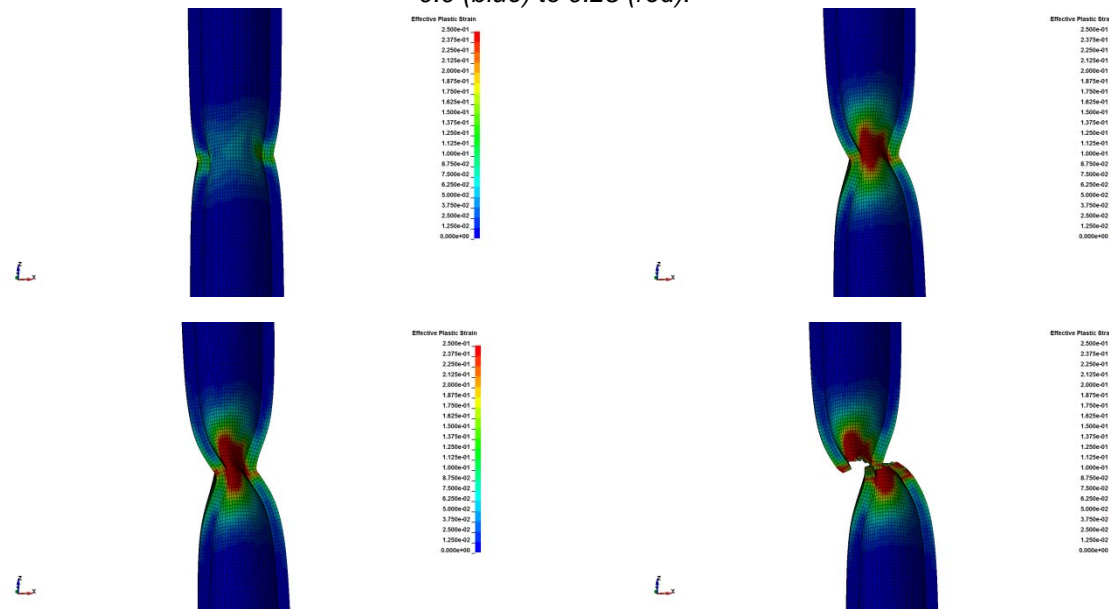
Figure 3-14. Images from the FEA Simulation of the 5.6-s Closing Time Simulation
Proprietary ram designs have been redacted from all images.
Images show the effective plastic (permanent) deformation to the drill pipe at four different times during the ram closure corresponding to the following annulus open area ratios: 20% (top-left), 10% (top-right), 7% (bottom-left), and 5% (bottom-right). The maximum shear force occurs at 7.0% annulus open area for the OEM #1 geometry. The color scale indicates effective plastic deformation, and has a range of 0.0 (blue) to 0.25 (red).
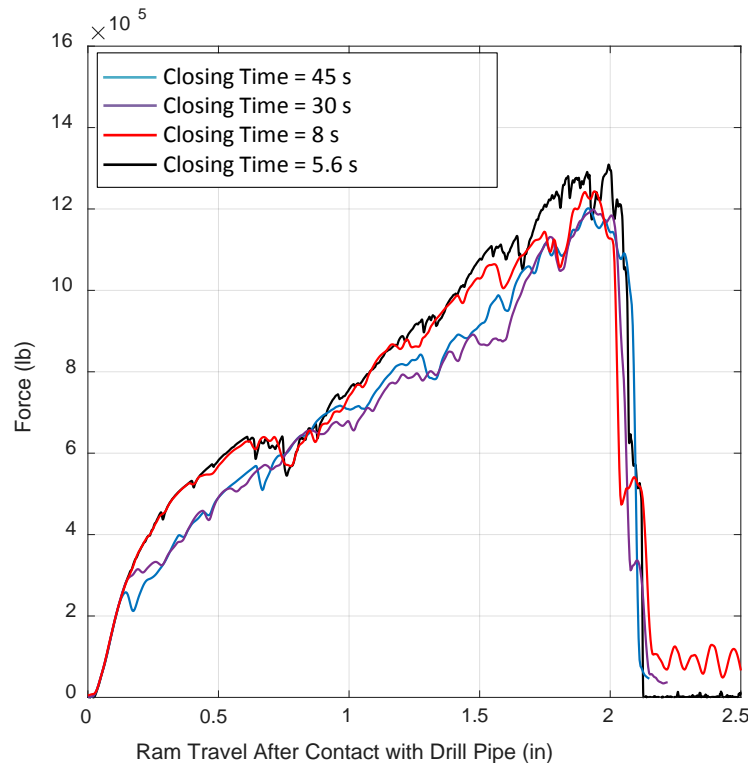
Figure 3-15. Comparison of Mechanical Shearing Force as a Function of Shear Ram Travel
This graph shows the shearing force required by one of the rams. As observed with the baseline approximated geometry, the mechanical shearing force requirements are relatively insensitive to the range of closing times investigated.

In addition to the mechanical shearing forces, hydrostatic and hydrodynamic forces for each of the different geometry cases were also computed. Following the Tier 2 solution methodology outlined in Section 1, CFD calculations were carried out at four discrete stages of valve closure (20%, 10%, and 5% annulus open area, and at the position of maximum shear force) using one-way fluid-structure-interaction coupling analyses. The complete results for each of the four selected closure speeds are shown in Table 3.5 to Table 3.8.

The lateral and axial hydrodynamic forces increase up to the point of maximum shear, whereupon a decrease is observed. In the case of the lateral hydrodynamic force, this decrease is due to the net effect of the combination of the available surface area and the local pressure results being larger from the hydrodynamic pressure at the maximum shearing position than at the 5% position. This is similar to what was observed in the simulations examining the approximated OEM #1 ram geometry described in Section 2. When comparing the different closing time simulations, the lateral hydrodynamic forces are on the same order of magnitude and relatively close in value.

The axial hydrodynamic force is over an order of magnitude greater than the lateral hydrodynamic force. The axial hydrodynamic force decreases after the drill pipe is sheared. This decrease is caused by the fact that there is small increase in the flow area when the pipe is sheared. Recall that the open areas listed in Table 3.5 and similar tables throughout this report indicate the nominal shear ram position in closing off the annulus flow area. Small changes in

actual flow area due to drill pipe deformations and shearing are not included in the nominal open area calculation.

The mechanical shearing force for all closing time simulations is the most dominant force compared to the hydrostatic forces and hydrodynamic forces. The effect of closing time on the mechanical force requirements will be directly linked to the mechanical properties of the pipe being sheared. As the closure rate increases, the local strain rates within the pipe material being sheared will increase. As the strain rate increases, two competing physical properties of the steel being sheared are important to consider. First, for higher strain rates, the stress-strain curve of the pipe material will follow the adiabatic response curve (see Figure 2-8), which is weaker than the unheated material. Secondly, depending upon the exact metallurgy of the steel, it may strain harden. This means that the strength of the steel will increase with increased strain rate. For the S-135 pipe studied in this work, there are no strain hardening effects (see Section 2.3 for more details), but that is not a generalized statement for all S-135 drill pipe material.

Table 3.5. Force on Rams (lbf) – OEM #1 Geometry at 45-s Closing Time
The hydrostatic and mechanical shearing forces are shown to dominate over the hydrodynamic force.
The maximum total required ram force is computed to be 1.51 million lbf.

Open Area %	Ram Piston Rod Force (lbs, per ram)				Total Axial Hydrodynamic Force
	Shearing	Hydrostatic	Lateral Hydrodynamic	Total Rod Force	
5	46,040 (12.9%)	311,000 (86.8%)	1,114 (0.3%)	358,200	27,820
7.7 (max shear)	1,202,000 (79.4%)	311,000 (20.5%)	1,762 (0.1%)	1,514,000	29,780
10	1,058,000 (77.2%)	311,000 (22.7%)	1,115 (0.1%)	1,370,000	19,630
20	580,700 (65.1%)	311,000 (34.9%)	293 (0.0%)	892,000	8,398
40	0 (0.0%)	311,000 100.0%)	≈ 0 (0.0%)	311,000	1,932[1]
100	0 (0.0%)	311,000 (100.0%)	≈ 0 (0.0%)	311,000	0

Note 1. This value is interpolated based on the baseline case described in Table 3.2

Table 3.6. Force on Rams (lbf) – OEM #1 Geometry at 30-s Closing Time
The hydrostatic and mechanical shearing forces are shown to dominate over the hydrodynamic force.
The maximum total required ram force is computed to be 1.51 million lbf.

Open Area %	Ram Piston Rod Force (lbs, per ram)				Total Axial Hydrodynamic Force
	Shearing	Hydrostatic	Lateral Hydrodynamic	Total Rod Force	
5	48,570 (13.5%)	311,000 (86.2%)	1,143 (0.3%)	360,700	13,864
7.5 (max shear)	1,199,000 (79.3%)	311,000 (20.6%)	1,735 (0.1%)	1,512,000	29,645
10	1,029,000 (76.7%)	311,000 (23.2%)	1,001 (0.1%)	1,341,000	18,861
20	564,100 (64.4%)	311,000 (35.5%)	304 (0.0%)	875,500	7,983
40	0 (0.0%)	311,000 (100.0%)	≈ 0 (0.0%)	311,000	2,261[1]
100	0 (0.0%)	311,000 (100.0%)	≈ 0 (0.0%)	311,000	0

Note 1. This value is interpolated based on the baseline case described in Table 3.2

Table 3.7. Force on Rams (lbf) – OEM #1 Geometry at 8-s Closing Time
The hydrostatic and mechanical shearing forces are shown to dominate over the hydrodynamic force.
The maximum total required ram force is computed to be 1.56 million lbf.

Open Area %	Ram Piston Rod Force (lbs, per ram)				Total Axial Hydrodynamic Force
	Shearing	Hydrostatic	Lateral Hydrodynamic	Total Rod Force	
5	106,500 (25.4%)	311,000 (74.3%)	1,228 (0.3%)	418,700	21,170
7.4 (max shear)	1,243,000 (79.9%)	311,000 (20.0%)	1,796 (0.1%)	1,556,000	30,360
10	1,099,000 (77.9%)	311,000 (22.0%)	1,187 (0.1%)	1,411,000	20,560
20	639,700 (67.3%)	311,000 (32.7%)	272 (0.0%)	951,000	5,850
40	0 (0.0%)	311,000 (100.0%)	≈ 0 (0.0%)	311,000	1,346[1]
100	0 (0.0%)	311,000 (100.0%)	≈ 0 (0.0%)	311,000	0

Note 1. This value is interpolated based on the baseline case described in Table 3.2

Table 3.8. Force on Rams (lbf) – OEM #1 Geometry at 5.6-s Closing Time
The hydrostatic and mechanical shearing forces are shown to dominate over the hydrodynamic force.
The maximum total required ram force is computed to be 1.59 million lbf.

Open Area %	Ram Piston Rod Force (lbs, per ram)				Total Axial Hydrodynamic Force
	Shearing	Hydrostatic	Lateral Hydrodynamic	Total Rod Force	
5	0 (0.0%)	311,000 (99.4%)	1,814 (0.6%)	312,800	14,840
7.0 (max shear)	1,281,000 (80.4%)	311,000 (19.5%)	2,211 (0.1%)	1,594,000	30,290
10	1,101,000 (77.9%)	311,000 (22.0%)	1,247 (0.1%)	1,413,000	22,600
20	613,600 (66.4%)	311,000 (33.6%)	167 (0.0%)	924,900	7,352
40	0 (0.0%)	311,000 (100.0%)	15 (0.0%)	311,000	1,691
100	0 (0.0%)	311,000 (100.0%)	3 (0.0%)	311,000	0

3.3   Flow Rate Sensitivity Study – Parametric Cases 6 and 7

For parametric cases 6 and 7, the mass flow rates for the CFD analyses were adjusted to correspond to the full-open flow rates of 30,000 and 60,000 stb/d. As the rams begin to close on the pipe, flow through the annulus decreases until the flow is stopped when the annulus is sealed. The flow rate corresponding to the fractional opening of the rams was simulated with a 1D SINDA/FLUINT flow model using the same methodology described previously in Quarterly Report 3. The fractional opening of the annulus in terms of the maximum flow rate fraction for parametric cases 6 and 7 is shown in Figure 3-16. The complete results, including the total force for each discrete fractional opening, are shown in Table 3.9 and Table 3.10.
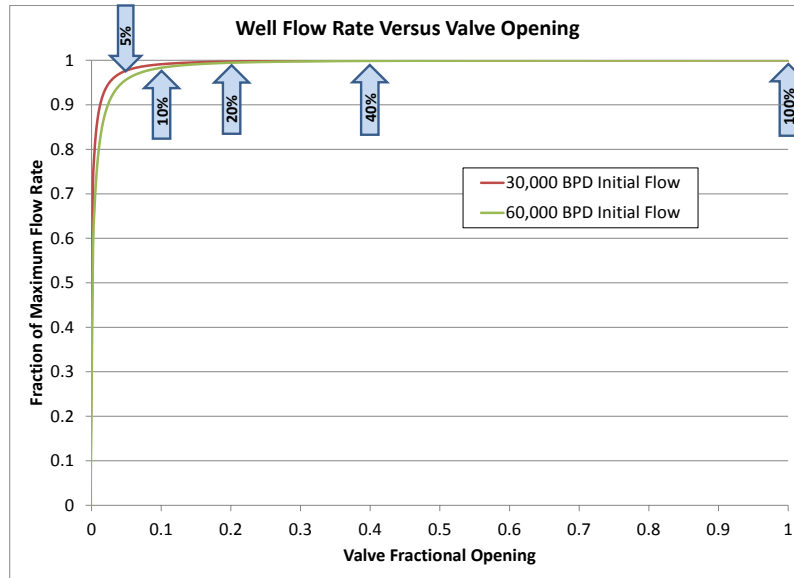
Figure 3-16. One-Dimensional Well Modeling of BOP Closure Percentage versus Fraction of Maximum Flow for Cases 6 and 7

The trend of decreasing flow with increasing valve closure was modeled in SINDA/FLUINT with a valve model for the closing BOP rams to obtain the mass flow rates for the discrete closing stages of the pipe.

Table 3.9. Force on Rams (lbf) – OEM #1 Geometry at 60,000 BPD

The hydrostatic and mechanical shearing forces are shown to dominate over the hydrodynamic force. The maximum total required ram force is computed to be 1.59 million lbf.

Open Area %	Ram Piston Rod Force (lbs, per ram)				Total Axial Hydrodynamic Force
	Shearing	Hydrostatic	Lateral Hydrodynamic	Total Rod Force	
5	0 (0.0%)	311,000 (99.9%)	270 (0.1%)	311,300	0
7.0 (max shear)	1,281,000 (80.4%)	311,000 (19.5%)	307 (0.0%)	1,592,000	10,190
10	1,101,000 (78.0%)	311,000 (22.0%)	169 (0.0%)	1,412,000	8,750
20	613,600 (66.4%)	311,000 (33.6%)	34 (0.0%)	924,700	3,522
40	0 (0.0%)	311,000 (100.0%)	≈ 0 (0.0%)	311,000	615
100	0 (0.0%)	311,000 (100.0%)	≈ 0 (0.0%)	311,000	0

Table 3.10. Force on Rams (lbf) – OEM #1 Geometry at 30,000 BPD

The hydrostatic and mechanical shearing forces are shown to dominate over the hydrodynamic force. The maximum total required ram force is computed to be 1.59 million lbf.

Open Area %	Ram Piston Rod Force (lbs, per ram)				Total Axial Hydrodynamic Force
	Shearing	Hydrostatic	Lateral Hydrodynamic	Total Rod Force	
5	0 (0.0%)	311,000 (100.0%)	76 (0.0%)	311,100	1,189
7.0 (max shear)	1,281,000 (80.5%)	311,000 (19.5%)	83 (0.0%)	1,592,000	2,299
10	1,101,000 (78.0%)	311,000 (22.0%)	46 (0.0%)	1,412,000	1,627
20	613,600 (66.4%)	311,000 (33.6%)	9 (0.0%)	924,600	826
40	0 (0.0%)	311,000 (100.0%)	≈ 0 (0.0%)	311,000	138
100	0 (0.0%)	311,000 (100.0%)	≈ 0 (0.0%)	311,000	0

The hydrodynamic forces increase up to the point of maximum shear at 7% for both flow rate cases. The hydrodynamic forces are also shown to decrease as the initial flow rate decreases. However, since the lateral hydrodynamic force accounts for a small portion of the total force when compared to both the mechanical shearing and hydrostatic forces, the maximum total force remains relatively unaffected at 1.59 million lbf, despite the change in flow rate. Overall, the lateral and axial hydrodynamic forces decrease as the flow rate decreases because the inertial effects of the flow through and across the BOP decrease with decreasing flow velocity.

3.4   Pressure Sensitivity - Parametric Cases 8, 9, and 10

For parametric cases 8, 9, and 10, the flowing pressures seen at the BOP stack were adjusted. The operating flow rate of 100,000 bpd and temperature of 300°F remained constant, while the crude oil density and viscosity were calculated by performing a steady-state nodal analysis, similar to what was accomplished to obtain the baseline conditions in Section 2.1, for flowing pressures of 3 ksi, 5 ksi, and 7 ksi. The result of the nodal analysis based on conditions of API of 35 and GOR of 1,397 scf/stb is shown in Figure 3-17. The resulting fluid properties at the BOP stack for the different flowing pressures are provided in Table 3.11.
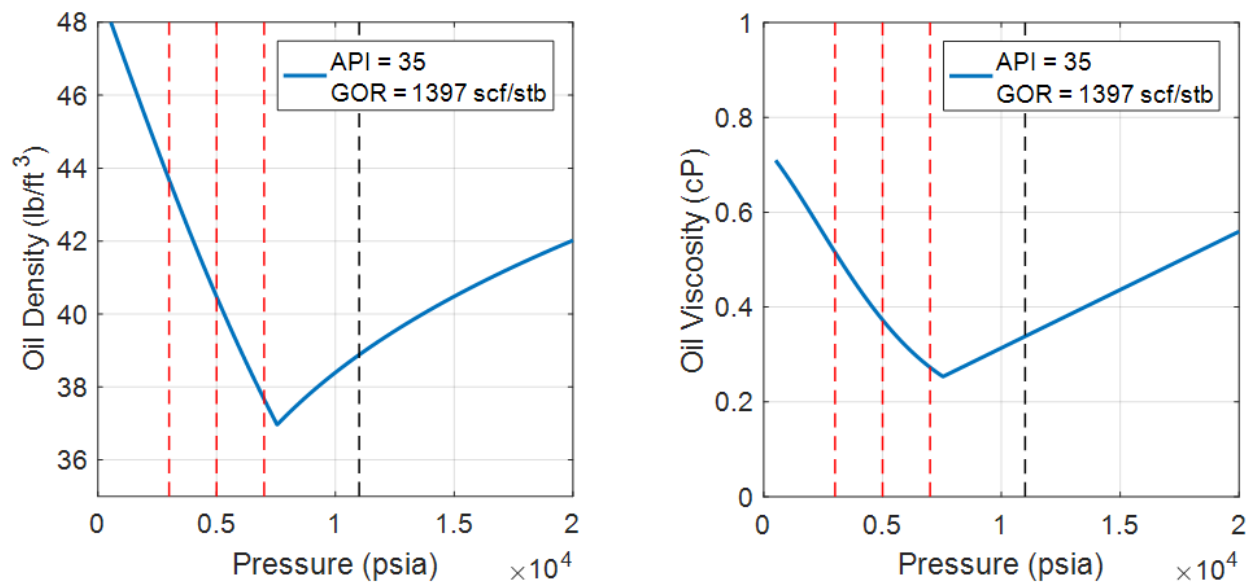
Figure 3-17. Fluid Density and Viscosity for Change in Flowing Pressure
The fluid density and viscosity at the different flowing pressures are based upon a representative Gulf of Mexico crude oil (API 35, 1,397 scf/sbbl GOR).

Table 3.11. Density and Viscosity Values for Different Flowing Pressures

The fluid properties, such as density and viscosity, required by the different simulations, will be calculated by analytical black oil model forms as a function of the various flowing pressures and temperature. The flowing pressure of 11 ksi is the baseline condition.

Flowing Pressure (ksi)	Density (in/ft³)	Viscosity (cP)
3	43.68	0.516
5	40.47	0.373
7	37.66	0.273
11	38.88	0.344

Selected images from the FEA simulations of these four closing speeds are shown in Figure 3-18 through Figure 3-20. The responses of the pipe to shearing, as seen in these images, all look very similar from a qualitative standpoint. The same mode of failure is observed in each of these simulations, namely, as the drill pipe is compressed a final rapid failure occurs slightly after two inches of ram travel from the ram's initial contact with the pipe.
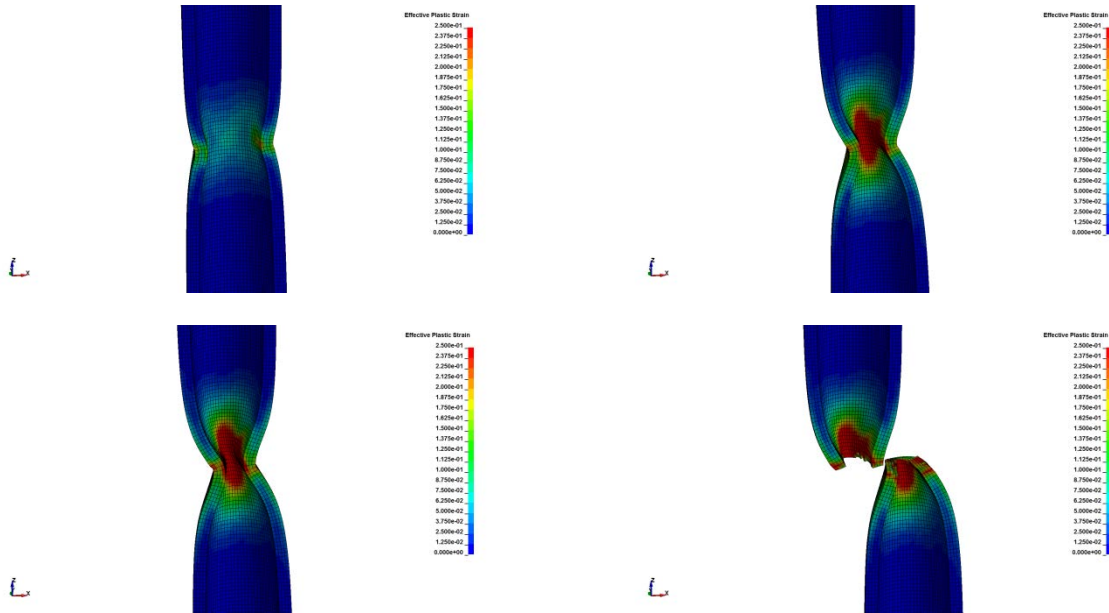
Figure 3-18. Images from the FEA Simulation of the 3-ksi Pressure Simulation
Proprietary ram designs have been redacted from all images.
Images show the effective plastic (permanent) deformation to the drill pipe at four different times during the ram closure corresponding to the following annulus open area ratios: 20% (top-left), 10% (top-right), 6.7% (bottom-left), and 5% (bottom-right). The maximum shear force occurs at 7.0% annulus open area for the OEM #1 geometry. The color scale indicates effective plastic deformation, and has a range of 0.0 (blue) to 0.25 (red).
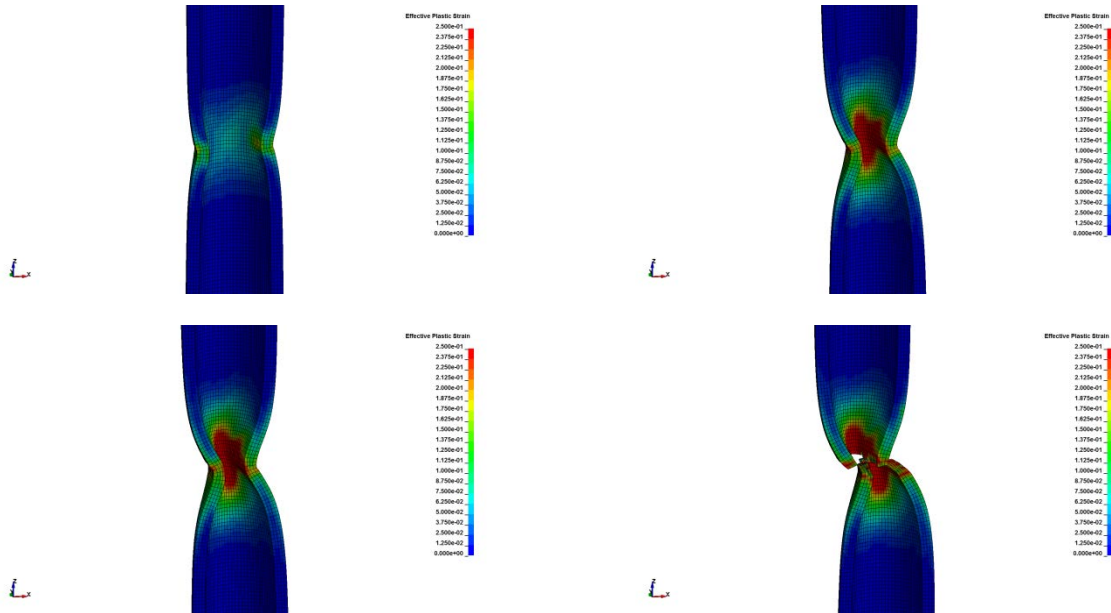
Figure 3-19. Images from the FEA Simulation of the 5-ksi Pressure Simulation
Proprietary ram designs have been redacted from all images.
Images show the effective plastic (permanent) deformation to the drill pipe at four different times during the ram closure corresponding to the following annulus open area ratios: 20% (top-left), 10% (top-right), 7% (bottom-left), and 5% (bottom-right). The maximum shear force occurs at 7.5% annulus open area for the OEM #1 geometry. The color scale indicates effective plastic deformation, and has a range of 0.0 (blue) to 0.25 (red).
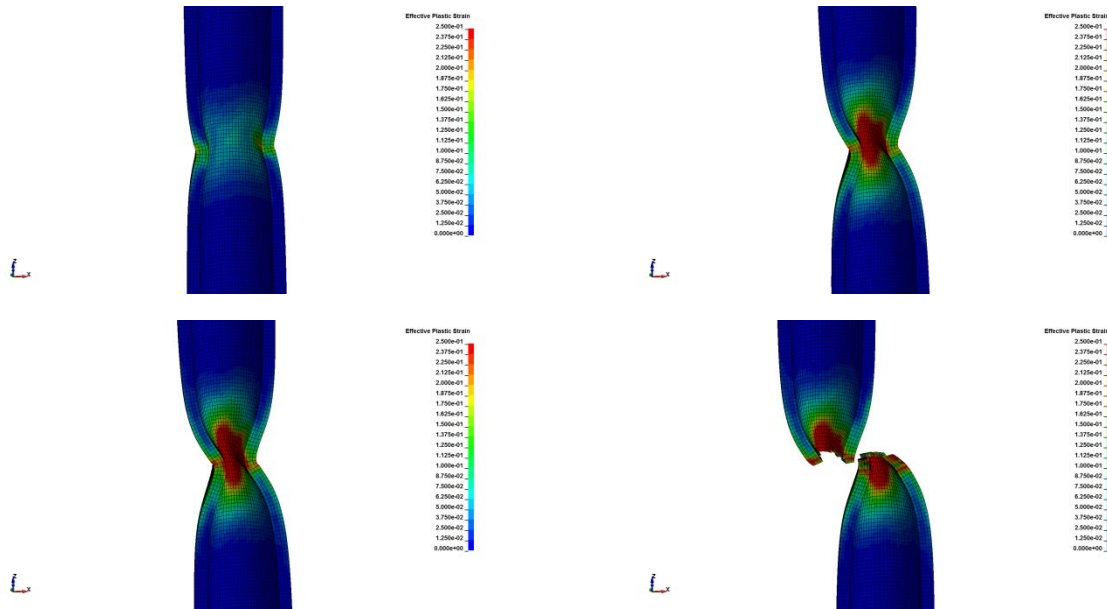
Figure 3-20. Images from the FEA Simulation of the 7-ksi Pressure Simulation
Proprietary ram designs have been redacted from all images.
Images show the effective plastic (permanent) deformation to the drill pipe at four different times during the ram closure corresponding to the following annulus open area ratios: 20% (top-left), 10% (top-right), 6.9% (bottom-left), and 5% (bottom-right). The maximum shear force occurs at 7.0% annulus open area for the OEM #1 geometry. The color scale indicates effective plastic deformation, and has a range of 0.0 (blue) to 0.25 (red).

The mechanical shearing forces from each FEA simulation as a function of ram travel are provided in Figure 3-21. Note that pressure differences between the annulus and inside the drill pipe were not considered in this work. The pressure inside the drill pipe was considered to be in equilibrium with the annular flowing pressure. Still, the change in flowing pressure does have an effect on the mechanical shearing process. As the confinement pressure increases, the triaxiality state of the material decreases (see Figure 2-11). As the triaxiality decreases, the amount of strain required to fail the drill pipe material increases. However, the magnitude of pressures in consideration (3-11 ksi) have a negligible effect on the local triaxiality state of the material and very little difference in the mechanical shearing force is observed. The results from CFD analysis for the various flowing pressures are shown in Table 3.12 through Table 3.14.
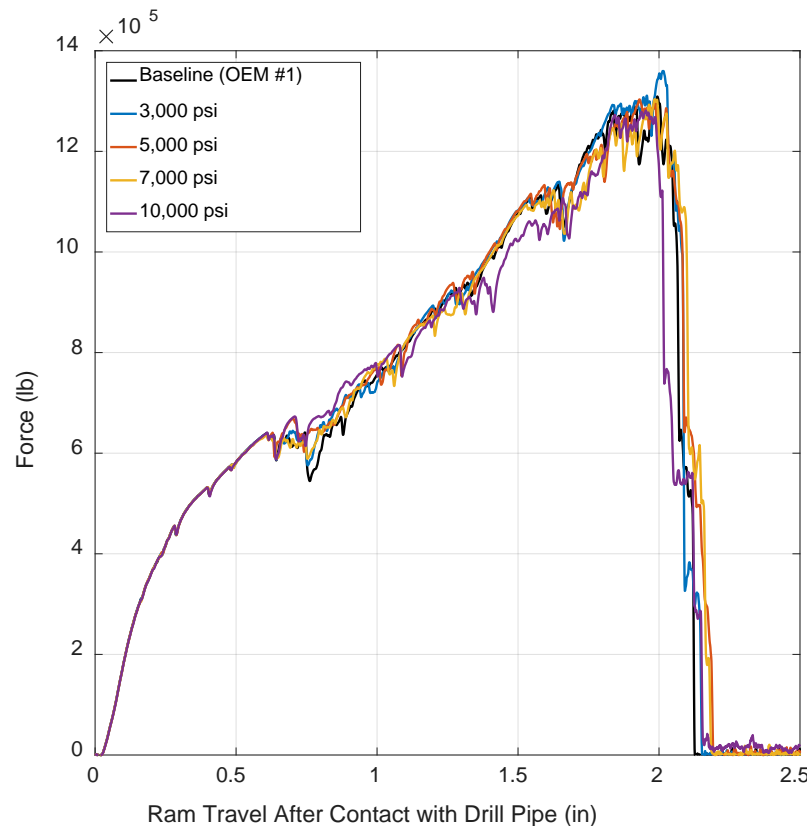
Figure 3-21. Comparison of Mechanical Shearing Force as a Function of Shear Ram Travel
This graph shows the shearing force required by one of the rams. As observed with the baseline approximated geometry, the mechanical shearing force requirements are relatively insensitive to the range of flowing pressures investigated.

Table 3.12. Force on Rams (lbf) – OEM #1 Geometry at 3-ksi Flowing Pressure
The hydrostatic and mechanical shearing forces are shown to dominate over the hydrodynamic force. The maximum total required ram force is computed to be 1.45 million lbf. The percent contribution to the total force from each component is indicated in parentheses next to its value.

Open Area %	Ram Piston Rod Force (lbs, per ram)				Total Axial Hydrodynamic Force
	Shearing	**Hydrostatic**	**Lateral Hydrodynamic**	**Total Rod Force**	
5	0 (0.0%)	84,820 (98.4%)	1,397 (1.6%)	86,220	20,380
6.7 (max shear)	1,360,000 (94.0%)	84,820 (5.9%)	1,709 (0.1%)	1,446,000	29,000
10	1,106,000 (92.8%)	84,820 (7.1%)	1,045 (0.1%)	1,192,000	16,250
20	631,200 (88.1%)	84,820 (11.8%)	245 (0.0%)	716,300	6,129
40	0 (0.0%)	84,820 (100.0%)	≈ 0 (0.0%)	84,820	1410[1]
100	0 (0.0%)	84,820 (100.0%)	≈ 0 (0.0%)	84,820	0

Note: 1. This value is interpolated based on the baseline case described in Table 3.2

Table 3.13. Force on Rams (lbf) – OEM #1 Geometry at 5-ksi Flowing Pressure

The hydrostatic and mechanical shearing forces are shown to dominate over the hydrodynamic force. The maximum total required ram force is computed to be 1.45 million lbf. The percent contribution to the total force from each component is indicated in parentheses next to its value.

Open Area %	Ram Piston Rod Force (lbs, per ram)				Total Axial Hydrodynamic Force
	Shearing	Hydrostatic	Lateral Hydrodynamic	Total Rod Force	
5	279,300 (66.2%)	141,400 (33.5%)	1,333 (0.3%)	422,000	24,470
7.5 (max shear)	1,303,000 (90.1%)	141,400 (9.8%)	2,031 (0.1%)	1,446,000	29,650
10	1,134,000 (88.8%)	141,400 (11.1%)	1,073 (0.1%)	1,276,000	19,340
20	656,500 (82.2%)	141,400 (17.7%)	295 (0.0%)	798,200	5,981
40	0 (0.0%)	141,400 (100.0%)	≈ 0 (0.0%)	141,400	1376[1]
100	0 (0.0%)	141,400 (100.0%)	≈ 0 (0.0%)	141,400	0

Note: 1. This value is interpolated based on the baseline case described in Table 3.2

Table 3.14. Force on Rams (lbf) – OEM #1 Geometry at 7-ksi Flowing Pressure

The hydrostatic and mechanical shearing forces are shown to dominate over the hydrodynamic force. The maximum total required ram force is computed to be 1.50 million lbf. The percent contribution to the total force from each component is indicated in parentheses next to its value.

Open Area %	Ram Piston Rod Force (lbs, per ram)				Total Axial Hydrodynamic Force
	Shearing	Hydrostatic	Lateral Hydrodynamic	Total Rod Force	
5	198,600 (49.9%)	197,900 (49.7%)	1,376 (0.3%)	388,900	19,850
6.9 (max shear)	1,302,000 (86.7%)	197,900 (13.2%)	2,082 (0.1%)	1,502,000	31,470
10	1,105,000 (84.7%)	197,900 (15.2%)	1,141 (0.1%)	1,304,000	22,150
20	611,800 (75.5%)	197,900 (24.4%)	301 (0.0%)	810,000	7,458
40	0 (0.0%)	197,900 (100.0%)	≈ 0 (0.0%)	197,900	1,715[1]
100	0 (0.0%)	197,900 (100.0%)	≈ 0 (0.0%)	197,900	0

Note: 1. This value is interpolated based on the baseline case described in Table 3.2

The lateral hydrodynamic force changes slightly as the flowing pressure at the BOP changes. However, these values are on the same order of magnitude and only account for a small portion of the overall total force (0 to 1%). Similarly, the axial hydrodynamic force changes only slightly with changes in the BOP flowing pressure. The hydrodynamic force increases up to the point of maximum shear for all flowing pressure simulations. The hydrostatic force also increases as the flowing pressure increases, and accounts for a significant portion of the total fluid force (10 to 51%). The shearing force is shown to be the main contributor to the overall total force (50 to 90%). However, the maximum total force remains relatively unaffected being between 1.45 and 1.50 million lbf, despite the change in flowing pressures.

3.5 Fluid Sensitivity - Parametric Case 11

For parametric case 11, the fluid properties were adjusted in the CFD simulation. The operating flow rate of 100,000 bpd, flowing pressure of 11,000 psia, and temperature of 300°F remained constant, while the crude oil density and viscosity were calculated by performing a steady-state nodal analysis calculation based upon an assumed set of reservoir and lower

completion conditions. This approach is similar to what was accomplished to obtain the baseline conditions. The result of the nodal analysis based on conditions of API of 26 and GOR of 800 scf/stb is shown in Figure 3-22. The resulting fluid properties at the BOP stack will have a density of 45.29 lb/ft^3 [725.5 kg/m^3] and have a viscosity of 0.9945 cP. The results from the CFD analysis with the new fluid properties in comparison to the baseline fluid properties are shown in Table 3.15. The deformation and rupture of the drill pipe are not affected by this change in the fluid properties; therefore, the mechanical shearing force for this case is identical to the mechanical shearing force computed for case 1.
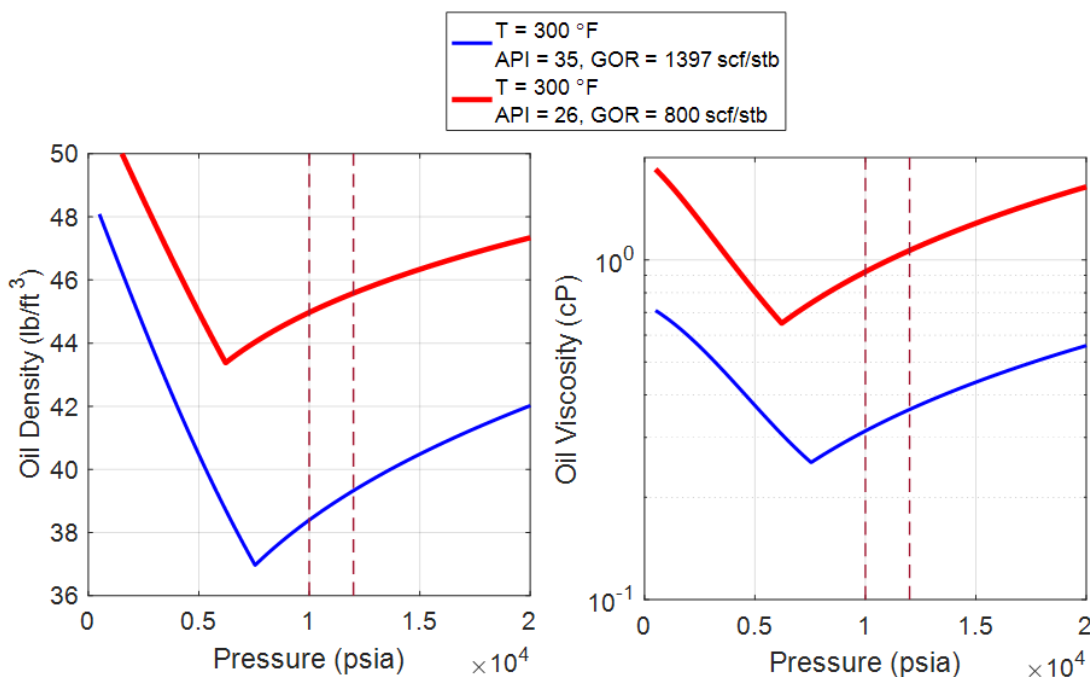
Figure 3-22. Fluid Density and Viscosity for Parametric Case 11
The density and viscosity of the fluid used in Case 11 (red lines) are based upon a representative Gulf of Mexico crude oil (API 26, 800 scf/sbbl GOR). These properties are calculated by the same analytical black oil model described in Section 2.1. The baseline fluid properties (API 35, 1,397 scf/sbbl GOR) are shown in blue for comparison.

Table 3.15. Force on Rams (lbf) – OEM #1 Geometry with the New Fluid Properties (API = 26, GOR = 800 scf/stb)
The hydrostatic and mechanical shearing forces are shown to dominate over the hydrodynamic force. The maximum total required ram force is computed to be 1.59 million lbf. The percent contribution to the total force from each component is indicated in parentheses next to its value.

Open Area %	Ram Piston Rod Force (lbs, per ram)				Total Axial Hydrodynamic Force
	Shearing	Hydrostatic	Lateral Hydrodynamic	Total Rod Force	
5	0 (0.0%)	311,000 (99.7%)	781 (0.3%)	311,800	10,370
7.0 (max shear)	1,281,000 (80.4%)	311,000 (19.5%)	1,780 (0.1%)	1,594,000	25,290
10	1,101,000 (77.9%)	311,000 (22.0%)	1,040 (0.1%)	1,413,000	11,400
20	613,600 (66.3%)	311,000 (33.6%)	221 (0.0%)	924,900	7,617
40	0 (0.0%)	311,000 100.0%)	3 (0.0%)	311,000	735
100	0 (0.0%)	311000 (100.0%)	3 (0.0%)	311,000	0

Overall, the lateral hydrodynamic forces for the new fluid properties are less than those for the case with the baseline fluid properties. The hydrodynamic force increases up to the point of maximum shear at 7% for both sets of fluid properties. However, since the lateral hydrodynamic force accounts for a small portion of the total force (0 to 1%) when compared to both the shearing and hydrostatic forces, the maximum total rod force remains relatively unaffected at 1.59 million lbf, despite the increase in density and viscosity. Similarly, the axial hydrodynamic forces are slightly less than those for the baseline fluid properties.

3.6   Tube Geometry Sensitivity – Parametric Cases 12 and 13

The final parameters investigated were the drill pipe dimensions. The baseline case examined a 6.625-inch diameter OD drill pipe with a wall thickness of 0.813 inches (nominally 50 ppf). Two additional drill pipe sizes were considered. The first pipe was 5.5-inch OD pipe with a 1.125-inch wall thickness (nominally 61.63 ppf). The second pipe was 5.875-inch OD with a 0.938-inch wall thickness (nominally 57.4 ppf). Images from the FEA simulations are shown in Figure 3-23 and Figure 3-24.
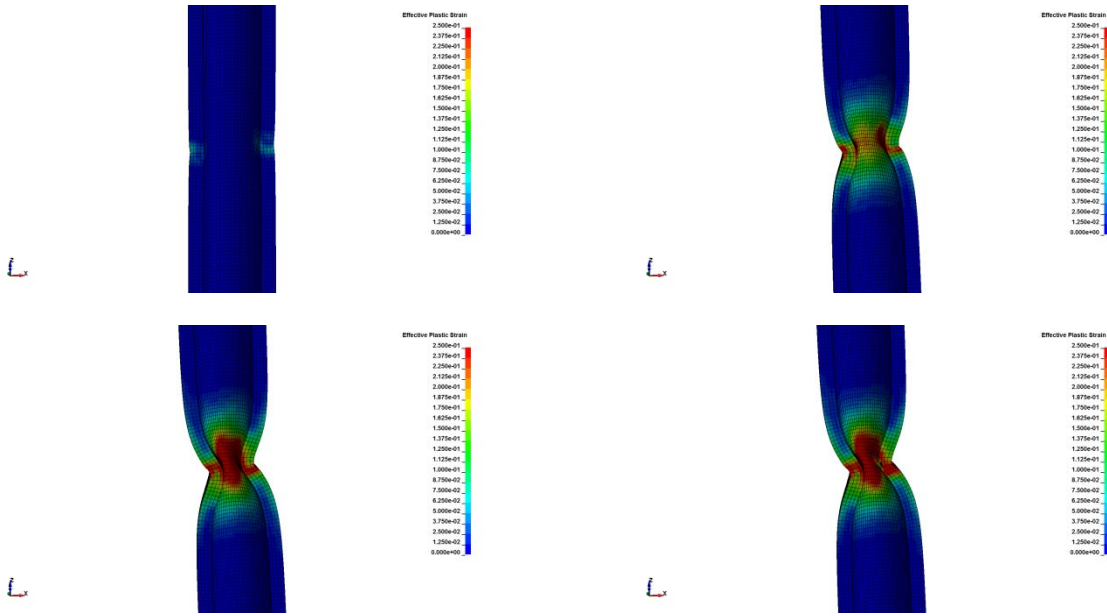
Figure 3-23. Images from the FEA Simulation of the 5.875-inch Drill Pipe Simulation
Proprietary ram designs have been redacted from all images.
Images show the effective plastic (permanent) deformation to the drill pipe at four different times during the ram closure corresponding to the following annulus open area ratios: 20% (top-left), 10% (top-right), 5.8% (bottom-left), and 5% (bottom-right). The maximum shear force occurs at 5.8% annulus open area for the OEM #1 geometry. The color scale indicates effective plastic deformation, and has a range of 0.0 (blue) to 0.25 (red).
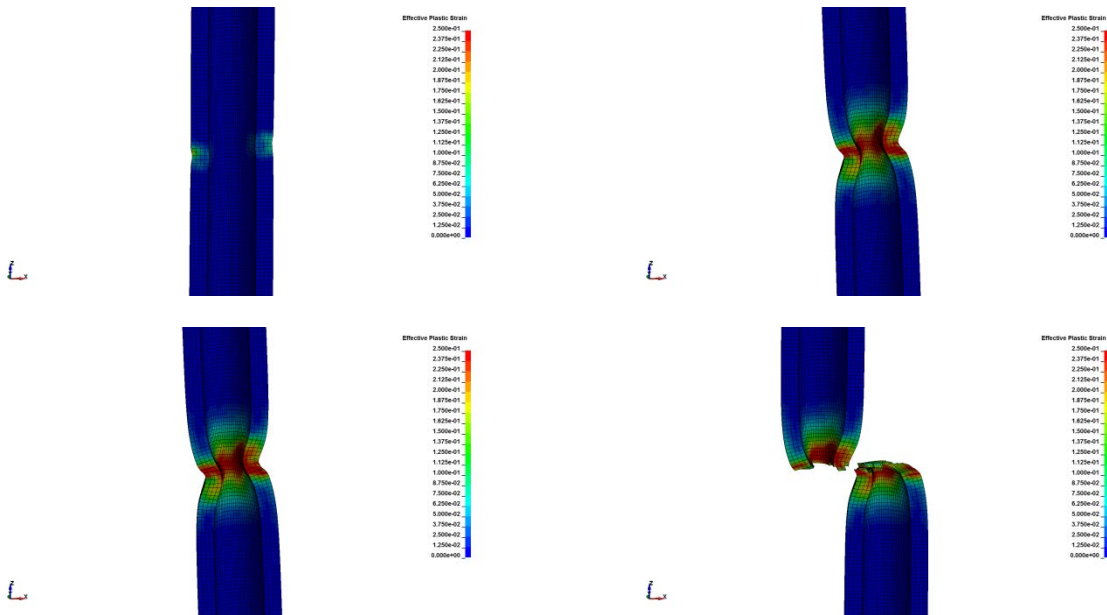
Figure 3-24. Images from the FEA Simulation of the 5.5-inch Drill Pipe Simulation
Proprietary ram designs have been redacted from all images.
Images show the effective plastic (permanent) deformation to the drill pipe at four different times during the ram closure corresponding to the following annulus open area ratios: 20% (top-left), 10% (top-right), 9.7% (bottom-left), and 5% (bottom-right). The maximum shear force occurs at 9.7% annulus open area for the OEM #1 geometry. The color scale indicates effective plastic deformation, and has a range of 0.0 (blue) to 0.25 (red).

The mechanical shearing forces from each FEA simulation as a function of ram travel are provided in Figure 3-25. Both of these pipes represent higher weight pipes than the nominal 6.625-inch diameter pipe. As a result, the maximum shearing force required and the point at which the drill pipe ultimately fails change.
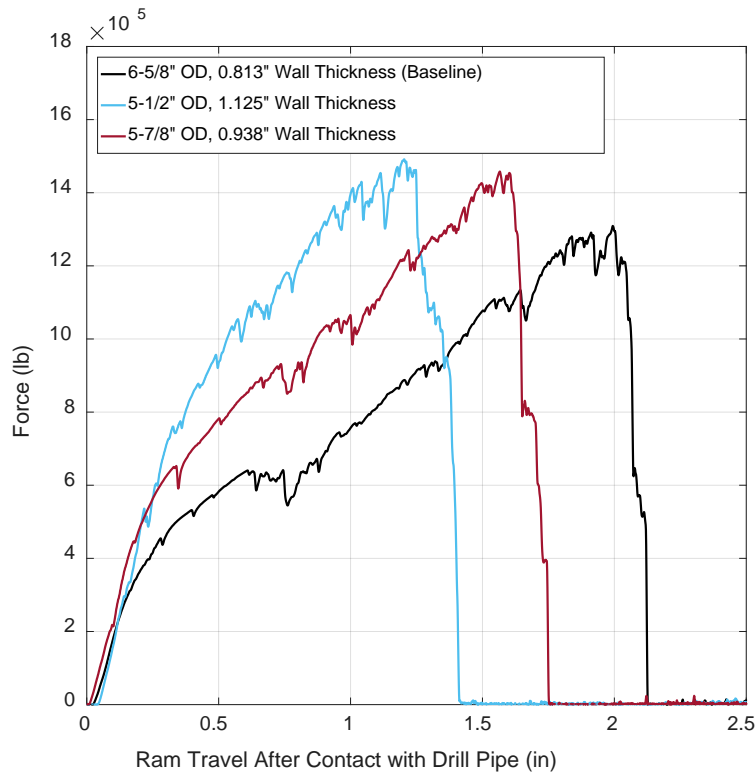
Figure 3-25. Comparison of Mechanical Shearing Force as a Function of Shear Ram Travel
This graph shows the shearing force required by one of the rams. As observed with the baseline approximated geometry, the mechanical shearing force requirements are moderately sensitive to the range of tubing sizes investigated.

In addition to the mechanical shearing forces, hydrostatic and hydrodynamic forces for each new drill pipe geometry were computed for the five discrete stages of ram closure (40%, 20%, 10%, 5% and annulus open area, and at the position of maximum shear force). The flow rate corresponding to the fractional opening of the rams, simulated with the 1D SINDA/FLUINT flow model, were the same as that used for the baseline case, namely 100,000 bpd. As the rams begin to close on the pipe, flow through the annulus decreases until the point at which it stops entirely when the annulus is sealed. The flow rate corresponding to the fractional opening of the annulus in terms of the maximum flow rate fraction for parametric cases 12 and 13 are shown below in Figure 3-26. The complete results of the BOP loads for the two drill pipe sizes of cases 12 and 13 are listed in Table 3.16 and Table 3.17, respectively.
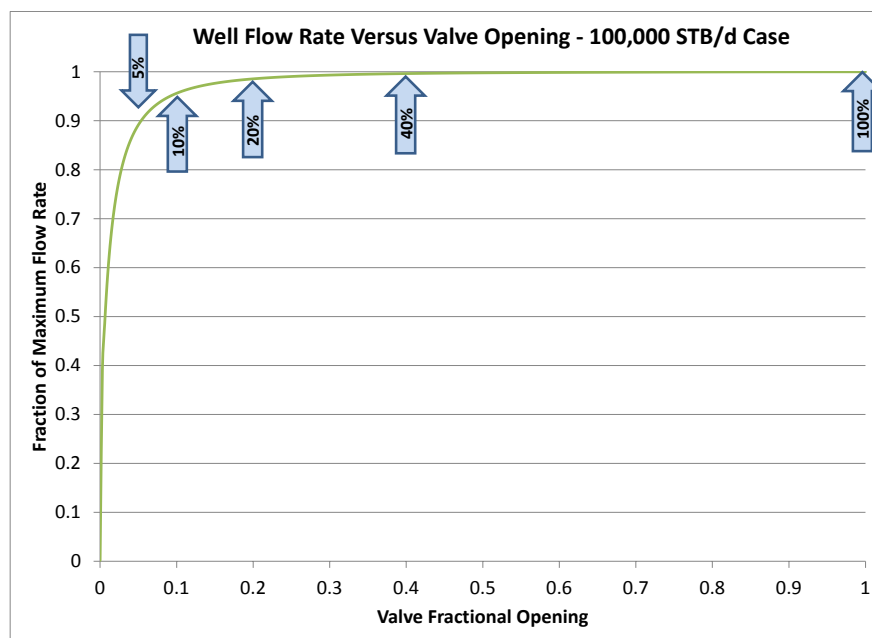
Figure 3-26. One-Dimensional Well Modeling of BOP Closure Percentage versus Fraction of Maximum Flow for Cases 12 and 13

The trend of decreasing flow with increasing valve closure was modeled in SINDA/FLUINT with a valve model for the closing BOP rams to obtain the mass flow rates for the discrete closing stages of the pipe. The flow area of the annulus regions of cases 12 and 13 are both larger than that for the baseline case, but there is only a small difference in the flow profile when compared to the flow profile at the baseline conditions.

Table 3.16. Force on Rams (lbf) – OEM #1 Geometry with 5.875-inch Diameter Tube Geometry

The hydrostatic and mechanical shearing forces are shown to dominate over the hydrodynamic force. The maximum total required ram force is computed to be 1.77 million lbf. The percent contribution to the total force from each component is indicated in parentheses next to its value.

Open Area %	Ram Piston Rod Force (lbs, per ram)				Total Axial Hydrodynamic Force
	Shearing	**Hydrostatic**	**Lateral Hydrodynamic**	**Total Rod Force**	
5	1,177,000 (79.0%)	311,000 (20.9%)	1,127 (0.1%)	1,489,000	23,570
5.8 (max shear)	1,458,000 (82.3%)	311,000 (17.6%)	1,593 (0.1%)	1,771,000	37,800
10	1,166,000 (78.9%)	311,000 (21.0%)	912 (0.1%)	1,478,000	16,120
20	540,000 (63.4%)	311,000 (36.5%)	250 (0.0%)	851,300	7,559
40	0 (0.0%)	311,000 (100.0%)	31 (0.0%)	311,000	902
100	0 (0.0%)	311,000 (100.0%)	≈ 0 (0.0%)	311,000	0

Table 3.17. Force on Rams (lbf) – OEM #1 Geometry with 5.5-inch Diameter Tube Geometry
The hydrostatic and mechanical shearing forces are shown to dominate over the hydrodynamic force.
The maximum total required ram force is computed to be 1.80 million lbf. The percent contribution to the
total force from each component is indicated in parentheses next to its value.

Open Area %	Ram Piston Rod Force (lbs, per ram)				Total Axial Hydrodynamic Force
	Shearing	Hydrostatic	Lateral Hydrodynamic	Total Rod Force	
5	0 (0.0%)	311,000 (99.5%)	1,475 (0.5%)	312,500	26,790
9.7 (max shear)	1,491,000 (82.7%)	311,000 (17.2%)	905 (0.1%)	1,803,000	30,680
10	1,465,000 (82.4%)	311,000 (17.5%)	900 (0.1%)	1,777,000	25,680
20	720,800 (69.8%)	311,000 (30.1%)	254 (0.0%)	1,032,000	9,725
40	0 (0.0%)	311,000 (100.0%)	26 (0.0%)	311,000	828
100	0 (0.0%)	311,000 (100.0%)	≈ 0 (0.0%)	311,000	0

In each case, the axial hydrodynamic force increases up to the point of maximum shear, whereupon a decrease is observed. The axial hydrodynamic force varies about 15% depending on the size of the drill pipe; however, there is no clear trend in the force with respect to the drill pipe diameter. The velocity distributions downstream of the BOP are different for each case, which in turn cause unexpected trends in the changes in the axial hydrodynamic force for different drill pipe sizes.

The lateral hydrodynamic force increases up to the point of maximum shear, whereupon a decrease is observed. This decrease is due to the net effect of the combination of the available surface area and the local pressure results being larger from the hydrodynamic pressure at the maximum shearing position than at the 5% position. This is similar to what was observed during the initial OEM #1 simulations and is described in detail in Section 3.1 in the OEM geometry simulations. When comparing the tubing geometry simulations, the hydrodynamic forces are on the same order of magnitude, but slightly decrease in value as the drill pipe diameter decreases. However, the shearing force is the most dominant force compared to the hydrostatic and hydrodynamic forces, and accounts for 70 to 83% of the total force up to the position of maximum shear. Since the shearing force is the most dominate force and has values on the same order of magnitude for these parametric cases, the change in tubing size, overall, has minimal effect on the total maximum force, which ranges between 1.59 and 1.8 million lbf.

3.7 Summary

A variety of physical parameters were varied from the baseline case, including the ram geometry, shear ram closing time, annular flow rate, annular flowing pressure, annular fluid properties, and tubing geometries. Due to the significant difference observed in mechanical shearing force between the baseline approximated ram geometry with sharp cutting edges and the more blunted OEM geometries, all of the parameter variation simulations were performed using the OEM #1 ram geometry, except for those cases specifically examining the other two OEM ram geometry variations. For all of the cases examined, the mechanical shearing force is the dominant force contributing to the overall total ram piston rod forced. Variations in the tubing geometry resulted in the greatest variation in mechanical and total force requirements. For all cases examined, the lateral hydrodynamic force contribution to the overall force remained under 1% of the total force. For the cases considered here, the maximum axial hydrodynamic force is also small compared to the mechanical shearing force. This force, however, acts to push

the rams into the guiding surfaces for the rams and may be significant for considering the frictional loads on these surfaces and their seals.

4. DATABASE TOOL

A database for organizing the results obtained from simulations of shear ram closure events was developed. The database not only holds the descriptions and the results of the specific cases that were analyzed; it interpolates the results for operational cases that fall between the cases in the database file.

The BOP Shear Ram Simulation Database (BSRSD) is intended to be used as a reference tool for estimating the force required to close blind shear rams when a BOP is activated. The BSRSD was created in Microsoft Access, which must be installed on the user's computer in order to open and use the database. The opening screen and menu of the BSRSD is shown in Figure 4-1.
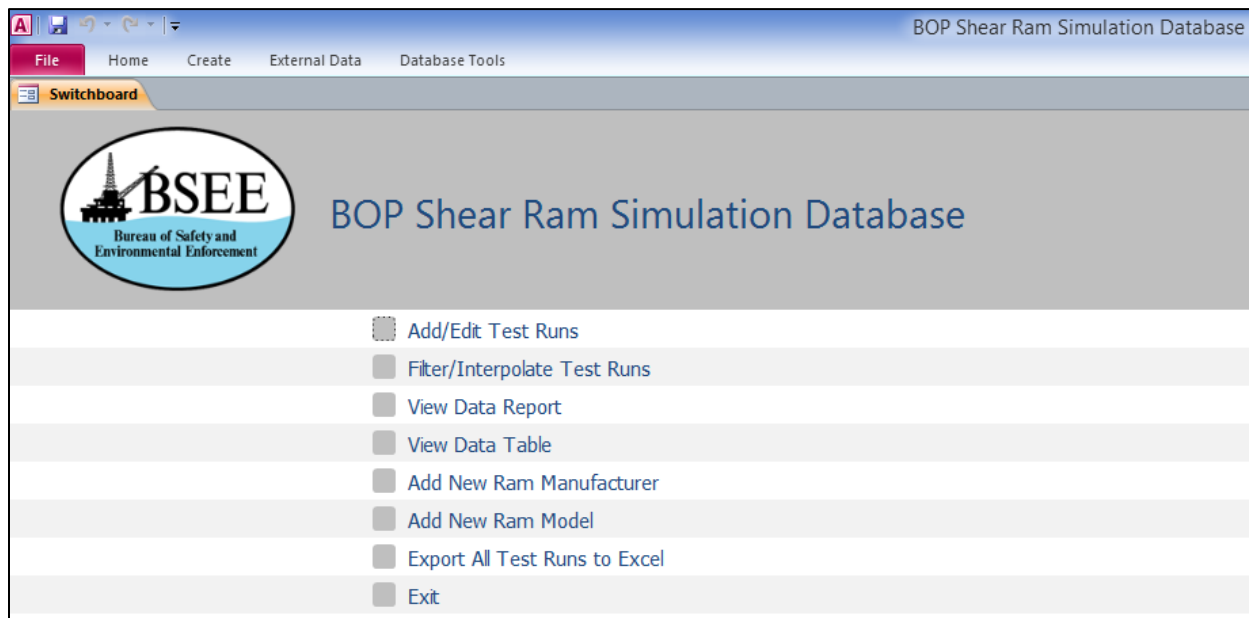
Figure 4-1. The BSRSD Switchboard
Upon launch, the BSRSD default switchboard menu is loaded. The main functions of the database are called through the switchboard.

The database serves to store and organize the simulation results. Results can be compared and interpolated within the database; however, simulations cannot be run directly from the database.

The installation and usage of the database are described in a separate project document, "Database and Resource Documentation." The reader is referred to that document for the complete description of the BSRSD.

5. CONCLUSIONS AND RECOMMENDATIONS

A methodology of combining commercially available FEA and CFD software packages was successfully developed to simulate the structural dynamics of severing a drill pipe in conjunction with concurrent effects of fluid pressure and flow rate acting on BOP shear rams as they close. The methodology was developed using the following scenarios and major assumptions.

- The BOP has a bore diameter of 18.75 inches and the drill pipe has a diameter of 6.625 inches.

- Only S-135 drill pipe was considered in this study. Tool joints and any additional cables or tubing were neglected.

- The study focused on the mechanical, hydrostatic, and hydrodynamic forces exerted on the shear rams while closing on a flowing well; the components and operation of the hydraulic systems that activate the rams were neglected. Both lateral hydrodynamic forces acting in the direction of the piston rod and the axial hydrodynamic forces acting in the flow direction were included here.

- The fluid in the annulus was assumed to be crude oil at the time the BOP blind shear rams are closing, but the analysis procedure was not limited to only crude oils.

- The crude oil properties used in the baseline case were based on API 35 oil with a GOR of 1,397 scf/stb.

- The baseline crude oil flow was 100,000 bpd at 11,000-psi flowing pressure at the BOP stack. A range of flow rates and pressures (30,000 to 100,000 bpd and 3,000 to 11,000 psi) were examined in the parameter variation portion of the study.

- The interior of the drill pipe was at the same pressure as the annulus.

- The rams traveled at constant speed.

- Gas does not break out of the oil prior to reaching the BOP and, thus, no multiphase or potential slugging hydrodynamic effects were modeled.

- The drill pipe was centered in the annulus and was in a neutral state regarding axial load.

- Fluid dynamic forces transverse to the direction of ram motion were neglected in these analyses.

- The additional effects of solid matter suspended in the flow, such as erosion of solid components, were neglected.

- Deformation and/or failure of the blind shear rams was not considered.

- Potential BOP operation and sequencing was not included. Rather, all flow was assumed to travel through the annulus and no other BOP components were considered.

Four tiers of increasing complexity for a combined FEA/CFD fluid-structure simulation methodology were investigated for the baseline conditions.

Tier 1. Transient FEA of the drill pipe as it is acted on by the rams without the hydrodynamic pressure effects. This defines mechanical force required by the ram actuator to sever the drill pipe.

Tier 2. Transient FEA of the drill pipe as in Tier 1. CFD is performed at discrete times of shear ram travel to compute the hydrostatic pressure force and hydrodynamic pressure force on the ram. This is a one-way coupling in which the ram position and pipe deformations can affect the fluid flow field, but the hydrodynamic pressure field is assumed to have no impact on the structural response of the drill pipe.

Tier 3. Transient FEA and CFD are performed in a lock-step fashion. The hydrodynamic forces computed by the CFD analysis at discrete ram travel positions are included in the FEA simulation. The resulting drill pipe deformations and ram positions are used to update the fluid flow simulation conditions. This is a partial two-way coupling of the FEA and CFD simulations.

Tier 4. The FEA and CFD simulations are conducted in a fully coupled mode where the converged solutions for the drill pipe deformations and the fluid flow field are computed at each time step.

The sensitivity of the ram forces to variations in operating conditions was studied with 13 parametric case studies using the Tier 2 methodology.

Finally, the results of all of the simulations were collected into a database tool entitled BOP Shear Ram Simulation Database (BSRSD). These database records include the pertinent operating conditions for each scenario and the components of the total ram actuator force corresponding to the drill pipe shear force, hydrostatic pressure force, and the hydrodynamic pressure force, respectively. The database can interpolate between the operating conditions listed in the records to estimate the shear ram forces for conditions other than those specifically catalogued in the database. The database is user-friendly and can be expanded easily to include coverage of the wide range of BOP shear ram designs and the operating conditions under which they are required to operate.

More specific conclusions and recommendation from this project are listed below.

5.1 Conclusions

This project successfully met all of its stated objectives. A methodology for combining commercial FEA and CFD software packages to simulate the fluid-structure interaction processes that occur during the closure of a well shear ram BOP was developed.

5.1.1 Analysis Methodology

The Tier 2 method has been shown to be the best choice for performing a combined CFD/FEA simulation of BOP shear ram closure for the purpose of evaluating the forces acting on the ram. The Tier 2 results for the baseline case differed only slightly from those obtained by the Tier 3 style of simulation, but the Tier 2 approach is considerably simpler to execute. The Tier 1 approach does not include any hydrodynamic effects, which will be important for future cases where the transverse loads on the rams are considered. The Tier 4 approach is overly complicated and requires inordinate computational time to execute.

It was necessary to make the limiting assumptions listed above to keep the scope of work within a reasonable budget. It is noted that three of the major assumptions are considered to be the most severe limitations of the analyses presented here. Some comments on these assumptions are provided below.

Gas breakout as the flow moves up the wellbore could result in slugging flow at the BOP. There could be large dynamic loads on the rams resulting from liquid slug impacts. These effects are neglected here.

There can be large axial load states on the drill pipe ranging from compression to tension or pressure differentials across the drill pipe walls. These axial and radial loads will affect the fracture process in the drill pipe. Furthermore, a compressive axial load can force the drill pipe against one wall of the annulus, which can affect the operation of the shear rams. The investigation of these scenarios was not within the scope of this project.

If shear rams are closed on a flowing fluid, a large pressure change could occur between the upper and lower faces of the ram transverse to the axis of the ram actuator. The resulting axial hydrodynamic loads will increase the friction in the ram mechanism and could impact other ram actuation processes inherent to a particular design

5.1.2   OEM Geometry Sensitivity

Three BOP manufacturers supplied representative geometric information about specific ram models to this project solely for the purpose of assessing the validity of the analysis methodology developed by the project. The simulation results presented here cannot and should not be used to compare or critically assess the design and operational performance of the different OEM's BOPs, because the vendors provide custom designs tailored to the specific conditions of each application.

The general conclusion here is that any assessment of shear ram loads should be done with simulations that use an accurate ram geometric shape. The unrealistic sharp-edged ram used in the baseline case studies required significantly less force to shear the drill pipe than any of the OEM-provided ram shapes. The OEMs have proprietary ram designs that, for valid reasons, do not include sharp edged surfaces to cut the drill pipe.

5.1.3   Closing Speed Sensitivity

Shear ram speeds of 0.23 in/s to 1.8 in/s (closing times of 45 s to 5.6 s, respectively) were used in the combined FEA/CFD simulations. The magnitude of the shear ram force is slightly sensitive to the ram closing speed. It was seen that as the speed increased, the overall ram force and the peak ram force increased slightly. The effect of ram closing speed may also potentially adversely couple drill pipe metallurgy, where variations in steel properties may result in a material that strain hardens as the rate of pipe deformation increases. That was not observed for the particular S-135 pipe material in this study, but other metals (even other S-135 pipes) may experience different strain hardening effects.

5.1.4   Flow Rate Sensitivity

The oil flow rate was varied between 30,000 and 100,000 bpd. There was a negligible effect of flow rate on the total force required to close the shear rams. The forces transverse to the

rod (i.e., due to differential pressure in the annulus flow direction) are considerable, but still smaller than the BOP closure forces.

5.1.5   Pressure Sensitivity

The hydrostatic flowing pressure at the BOP was varied from 3,000 to 11,000 psi in these simulations. It was assumed here that the back of the shear ram was exposed to the annulus fluid; therefore, the net hydrostatic force on the ram is the product of the ram actuator rod area and the hydrostatic pressure. Consequently, the force on the ram actuator is directly proportional to the hydrostatic pressure. For the range of drill pipes and flowing pressures examined, the hydrostatic force contribution was 6 to 20% of the total maximum force on the rams.

5.1.6   Fluid Sensitivity

Only one oil type, API 26 with GOR = 800 scf/stb, was used in comparison to the fluid used in the baseline case. This alternate crude oil was about 1.15 times denser and three times more viscous than the fluid used in the baseline simulations. The lateral hydrodynamic portion of the force was slightly decreased with the alternate fluid, but the lateral hydrodynamic portion of the total force was small in either case. Similarly, there were only slight changes in the axial hydrodynamic forces with this change in fluid properties.

5.1.7   Drill Pipe Size Sensitivity

Drill pipe sizes of 5.875-inch diameter with 0.938-inch wall thickness and 5.5-inch diameter with 1.125-inch wall thickness were simulated in comparison to the baseline case of 6.625-inch diameter with 0.813-inch wall thickness pipe. Both of these alternate sizes required more force to fracture than the baseline case, but there is not a clear correlation between ram force and pipe size based only on this limited set of simulations.

5.2   Recommendations

With the successful development of a fluid-structure interaction analysis methodology for simulating BOP shear ram closures and the resulting initial database tool for utilizing simulation results, this project will serve as the foundation for future work to expand the coverage of analyses to more BOP shear ram configurations. Some specific recommendations for the possible expansion of this project are listed below.

1. The material specifications of S-135 drill pipe leave room for a wide range of fracture processes when sheared by BOP rams. The allowable variations in the ductility of this material can have a significant impact on the forces required to shear and close the pipe (Levett 2003). The goal of this work was to provide a validated methodology for examining the shearing process and, thus, a single, specific material property definition was used for S-135 pipe where experimental shear data were available. However, a better understanding of the physics that drive the shearing process for the full range of ductile or brittle drill pipes would provide significant improvements in better predicting the required mechanical shearing forces. Also, the effects of fatigue and corrosion may play a secondary role in typical cases, but these factors may be important in high-load conditions requiring long-term service. It is recommended that rigorous investigation of the effect of these allowable variations be undertaken as a means of clarifying this situation for BOP designers and users alike.

2. The SwRI project team, BSEE staff, and the BOP manufacturers engaged in the project noted that the drill pipe axial load state has a significant effect on the concentricity of the drill pipe and the forces required to shear and seal it. A study of this effect should be considered in a future project.

3. This project was limited in its study of the sensitivity of shear rams forces to variations in fluid properties. It is recommended that future projects include the consideration of a wide range of produced fluids and drill fluids and their effects on shear ram closure forces.

4. This project considered the single phase flow of crude oil. It is recommended that a future project include the effects of transient flow and dynamic fluid impact loads that are inherent in bubbly and slugging flows.

5. Drilling fluids can contain potentially abrasive solids from the well and in a high-flow event the BOP components are at risk from erosion by these materials. It is recommended that a future project focus on the effects of flow-induced erosion of shear ram components.

6. The focus of this project was on only shear ram operations in a high-flow, high-pressure scenario. Future projects should include the presence of other equipment in the BOP stack and the effects of flow diverters and riser gas management systems in shear ram operation.

6. REFERENCES

API Specification 5D. (2001). "Specification for Drill Pipe." American Petroleum Institute.

"Estimated Oil and Gas Reserves, Gulf of Mexico OCS Region, December 31, 2013. Available Files for Downloading." *Estimated Oil and Gas Reserves*. BSEE, n.d. Web. 17 Feb. 2016.

Beggs, H. D. (1991). Production Optimization Using Nodal Analysis. Tulsa, OK: OGCI Publications.

Beissel, S. R., Gerlach, C. A., Holmquist, T. J., and Walker, J. D. (2011). "A Comparison of Numerical Methods in the Simulation of Hypervelocity Impact." Proc. of the 11th Hypervelocity Impact Symposium, ed. F. Schaefer and S. Hiermaier. Fraunhofer Verlag, Freiburg, Germany, pp. 787–802.

Bridgman, P. W. (1952). Studies in Large Plastic Flow and Fracture. New York: McGraw-Hill.

Brill, J. P. and Mukherjee, H. (1999). Multiphase Flow in Wells. Society of Petroleum Engineers, SPE Monograph Series Vol. 17. Digital Edition, 1999.

Det Norske Veritas. (2011). "Forensic examination of deepwater horizon blowout preventer." *Washington DC: US DOI, Bureau of Ocean Energy Management, Regulation, and Enforcement. EP030842*.

Dzugan, J., Spaniel, M., Konopik, P., Ruzicka, J., and Kuzelka, J. (2012). "Identification of Ductile Damage Parameters for Austenitic Steel." *International Journal of Mechanical, Aerospace, Industrial, Mechatronic and Manufacturing Engineering.* Vol. 6. No. 5.

Hooputra, H. (2004). "A Comprehensive Failure Model for Crashworthiness Simulation of Aluminum Extrusions." *Int. J. Crashworthiness.* Vol. 9. No. 5. pp. 449–463.

Johnson, G. R. and Cook, W. H. (1985). "Fracture Characteristics of Three Metals Subjected to Various Strains, Strain Rates, Temperatures and Pressures." *Engineering Fracture Mechanics.* Vol. 21 Issue 1, pp. 31–48.

Levett, B. (2003). "The Effects of Improved Drill Pipe Properties on BOP Shearing Capabilities." *IADC World Drilling Conference in Vienna, Austria*.

Martinuzzi, R., & Tropea, C. (1993, March). "The Flow around Surface-Mounted, Prismatic Obstacles Placed in a Fully Developed Channel Flow." Transactions-American Society of Mechanical Engineers Journal of Fluids Engineering. Vol. 115. pp. 85–92.

MCS Kenny (2013). "Assessment of BOP Stack Sequencing, Monitoring, and Kick Detection Technology. Final Report 01 - BOP Stack Sequencing and Shear Ram Design." Report for Bureau of Safety and Environmental Enforcement.

Miscow, G. F., De Miranda, P. E. V., Netto, T. A., and Plácido J. C. R. (2004). "Techniques to characterize fatigue behaviour of full size drill pipes and small scale samples." *Int. J. Fatigue.* Vol. 26. No. 6. pp. 575–584.

Petrosky Jr., G. E., and Farshad, F. F. (1993, January). Pressure-volume-temperature correlations for Gulf of Mexico crude oils. In *SPE Annual Technical Conference And Exhibition*. Society of Petroleum Engineers.

Petrosky Jr., G. E., and Farshad, F. F. (1995, January). Viscosity correlations for Gulf of Mexico crude oils. In *SPE Production Operations Symposium*. Society of Petroleum Engineers.

Pope, S.B., (2000). Turbulent Flows. Cambridge, U.K.: Cambridge University Press.

SINDA/FLUINT, Version 5.5 (2011). Cullimore and Ring Technologies, Inc., Littleton, Colorado.

Wylie, E. B. and Streeter V.L. (1983). , Fluid Transients, Corrected Edition, Ann Arbor, Michigan: FEB Press.